



**CENTRO DE INVESTIGACIÓN Y DE ESTUDIOS AVANZADOS
DEL INSTITUTO POLITÉCNICO NACIONAL**

UNIDAD ZACATENCO

DEPARTAMENTO DE BIOTECNOLOGÍA Y BIOINGENIERÍA

**“Caracterización del ciclo del metano en ecosistemas
de agua salobre y dulce”**

Tesis que presenta

María Teresa Aguirrezabala Cámpano

Para obtener el grado de

DOCTOR EN CIENCIAS

EN LA ESPECIALIDAD DE BIOTECNOLOGÍA

Director de la tesis: **Dr. Frédéric Thalasso**

Ciudad de México

Marzo 2021

Agradecimientos

Agradezco al Consejo Nacional de Ciencia y Tecnología por su apoyo financiero a través del proyecto #255704, la beca de manutención y beca de movilidad al extranjero #531383, así como al fondo SEP-Cinvestav a través del proyecto #203.

Gracias a mis asesores por su tiempo y consejo para mejorar este trabajo.

Gracias a Francisco Silva por su absoluto apoyo logístico y técnico para la realización de las campañas de muestreo. Siempre buscando hacer más allá de lo que era necesario.

Gracias a mis compañeros de laboratorio Cinvestav por su compañía y apoyo, por los buenos momentos que pasamos, desde la cotidiana convivencia a la hora de la comida hasta aventurarse a realizar trabajo de campo conmigo. Gracias en especial a Oscar y Rodrigo, que con paciencia resolvían mis dudas, que fueron muchísimas, pero gracias a su apertura logré aprender mucho más de lo que hubiera podido por mí misma. Además de gases de efecto invernadero y lagos, siempre tuvieron una buena plática para compartir.

Gracias a las nuevas amistades que conocí en estos cuatro años en Ciudad de México, Mérida, Sao Paulo y Montreal, y a las viejas amistades por seguir cerca, aunque estemos lejos.

Gracias a mi director de tesis, Frédéric Thalasso, por su guía y consejo. Me siento particularmente afortunada por haberlo tenido como supervisor porque a través de su ejemplo enseña grandes lecciones. Espero que conforme pase el tiempo pueda lograr adquirir sus cualidades como su trato amable, excelente forma de enseñar, su pasión y creatividad científica. Agradezco su sinceridad cuando requería saber que podía hacer un mejor trabajo, la confianza que depositó en mí y su apoyo para ampliar mis horizontes a través de cursos, estancias, etcétera.

Gracias a mi familia Aguirrezzabala Cámpano y a mi familia extendida Martínez Biro. Gracias a mi papá por sembrar una semilla de curiosidad científica. Gracias a mi hermana del alma, a mi sobrina y, sobre todo, a mi mamá por siempre estar ahí para mí. Gracias a mi mamá, quien, al darme los medios para desarrollar mi formación inicial, impulsó mi carrera académica. Mi mamá también es una gran maestra de la previsión, la perseverancia y la entrega. No cabe duda de que sin ti nada de esto hubiera sido posible.

Finalmente, quiero agradecer a mi compañero de vida, David, quien estuvo en este largo camino en los días buenos, los malos y los peores. Siempre listo para empujarme a lo desconocido, para darme palabras de aliento, para escucharme. Nunca dejo de aprender cosas de tí, quizás la más importante que me enseñaste en estos cuatro años es que debo creer en mí misma.

Doy gracias por las cosas buenas y malas, al final éstas son las que me han puesto donde estoy. Gracias a la vida.

Contenido

Índice de figuras y tablas	5
1. Resumen.....	8
2. Abstract	11
3. Introducción	14
4. Justificación	25
5. Objetivos generales y específicos	26
6. Materiales y métodos	27
7. Resultados y discusión.....	30
7.1 Dinámica el metano en las pozas subsalinas del Desierto Chihuahuense: Una primera evaluación	30
7.1.1 Introduction.....	32
7.1.2 Materials and methods.....	34
7.1.3 Results and discussion.....	42
7.1.4 Conclusions.....	53
7.1.5 References.....	54
7.2 Dinámica espaciotemporal global de la dinámica de gases de efecto invernadero y oxígeno de dos reservorios subtropicales con estados tróficos contrastantes.....	41
7.2.1 Introduction.....	43
7.2.2 Materials and methods	45

7.2.3	Results and discussion	53
7.2.4	Conclusion	65
7.2.5	References.....	66
7.3	Dinámica estacional de gases de efecto invernadero y oxígeno sobre un gradiente de salinidad de una laguna costera tropical	73
7.3.1	Introduction.....	75
7.3.2	Materials and methods	77
7.3.3	Results and discussion	84
7.3.4	Conclusions.....	104
7.3.5	References.....	104
8.	Conclusiones globales.....	112
9.	Recomendaciones y perspectivas.....	114
10.	Bibliografía	117
11.	Anexos	122
11.1	Anexo 1: Material suplementario del capítulo 7.1	122
11.2	Anexo 2: Material suplementario del capítulo 7.2	127
11.3	Anexo 3 : Artículo publicado en Science of the Total Environment.....	136

Índice de figuras y tablas

Figura 4.1. Esquema simplificado de los componentes principales del ciclo del CH₄. Se presentan los bioprocesos más relevantes para el ciclo del CH₄ en ecosistemas acuáticos. Del lado derecho se presentan, con fines ilustrativos, los perfiles de concentración de CH₄, CO₂ y O₂ disueltos de un cuerpo de agua típico. PAR: radiación fotosintéticamente activa.....16

Figure 7.1.1. Cuatro Cienegas Valley. The valley is in the Northeast of Mexico as shown in the yellow rectangle. The colored golden area represents the valley, while the delineated mountain is the Sierra de San Marcos which divides the basin in east and west sub-basins. The ponds have been numbered as 1: Poza Becerra (PB), 2: Poza Manantial (PM), 3: Poza Churince (PCH), 4: Poza Azul (PA), and 5: Poza Los Hundidos (LH). (For interpretation of the references to color in this figure legend, the reader is referred to the web version of this article.).....35

Figure 7.1.2. Contour maps obtained from bathymetric data collected in: PA, Poza Azul; PM, Poza Manantial; PCH, Poza Churince; LH, Los Hundidos; PB, Poza Becerra. The scale varies as shown by the scale bar next to the ponds acronym (in m). The dotted line indicates the selected longitudinal transects.....43

Figure 7.1.3. Longitudinal transect of C_{CH₄} profile for PB, Poza Becerra, during winter. Lines A and B indicate zone of high CH₄ concentration. A is the location of a resurgence, while no resurgence was observed in B. The maximum depth and transect length correspond to the values reported in Table 145

Figure 7.1.4. CH₄ fluxes contour maps for all the ponds and seasons, means are shown in brackets. The ponds are indicated as follows: PA, Poza Azul; PM, Poza Manantial; PCH, Poza Churince; LH, Los Hundidos; PB, Poza Becerra. The letters indicate the season of the campaign: spring, SP, in April 2016; winter, W, in January 2017; or summer, S, in August 2017.....49

Figure 7.1.5. CO₂ fluxes contour maps for all the ponds and seasons, means are shown in brackets. The ponds are indicated as follows: PA, Poza Azul; PM, Poza Manantial; PCH, Poza Churince; LH, Los Hundidos; PB, Poza Becerra. The letters indicate the season of the campaign: spring, SP, in April 2016; winter, W, in January 2017; or summer, S, in August 2017.....50

Figure 7.2.1. Satellite images of the studied reservoirs and locations of the monitoring and sampling stations: A. “Lago de Guadalupe” (LG), and B. “Lago el Llano” (LL). Created in ArcGIS 10.7.1.....54

Figure 7.2.2. Contour maps of (A) C_{CH₄}, (B) C_{CO₂}, and (C) C_{O₂} over the three distinct seasons in LG and LL. MSS references are displayed as inverted triangles at the top of the maps. To improve readability, lengths are scaled differently in each reservoir (scale shown at the top left). The thermoclines are represented as a dashed line. Water level changes are shown as dotted areas...55

Figure 7.2.3. Graphical representation of the carbon mass balance components in LG and LL. Grey picture is for explanatory and scaling purposes. Each quarter-pie chart, where areas are scaled to magnitude, represents the proportional share of each process: MG, methanogenesis; MT, methanotrophy; F, flux; R, respiration; GPP, and gross primary production, for CH₄, CO₂ and O₂.

Rates located on the left side are positive (input/production) and those on the right side are negative (output/uptake). Inferior solid-color circles represent the scaled total mass of the compound (M_x ; mmole m⁻²) and the circle arrows represent the scaled turnover time (θ_x). The superior circle represents the homogeneity factor of dissolved gases distribution (h) and the anisotropic factor (ω).....63

Figure 7.3.1. Bathymetric map of La Mancha during the northern season referenced for each sampling station, longitudinal transect from the river (T1, red dashed line), and longitudinal transect from the mangrove to the opening of the lagoon (T2, beige dashed line).....86

Figure 7.3.2. GHG concentration in sediment along a longitudinal transect and across seasons..87

Figure 7.3.3. Seasonal continuous measurement of surface water concentration of dissolved gases (A) and physicochemical parameters (B).....89

Figure 7.3.4. Contour maps of seasonal CH₄ (top) and CO₂ (bottom) fluxes for the three sampled seasons. A close-up of the river to lagoon zone is shown to the right of each map for ease of visualization. Cross symbol (×) indicates flux sampling stations.....95

Table 7.1.1. Morphometric parameters of the selected Cuatro Cienegas Valley ponds. Aw: surface area; Zm: mean depth; Zmax: maximum depth; V: total volume.....36

Table 7.1.2. Physicochemical parameters of the selected ponds (mean values over the entire water column at 1-m intervals). T: temperature; DO: Dissolved Oxygen; SO₄²⁻: sulfates; Cond: conductivity; ORP: oxidation-reduction potential; C_{CH4}: mean dissolved CH₄ concentration; C_{CO2}: mean dissolved CO₂ concentration. NM: Not Measured. Standard deviations are shown in parentheses. Difference in superscript letters indicates significative differences between means (Tukey-Kramer test; p<0.05).....46

Table 7.1.3. Comparative methane emissions from aquatic ecosystems.....49

Table 7.1.4. Methane production rates in the ponds during summer. R² indicates the coefficient of determination.....50

Table 7.2.1. Seasonal and mean parameters (A); metabolic rates and mass balance summary (B) for LG and LL. CV is the coefficient of variation (%). * indicates a significant difference between the means of the reservoirs (p<0.05).....60

Table 7.3.1. Mean concentrations of the measured physicochemical parameters across seasons.86

Table 7.3.2. Mean dissolved gas concentrations of the entire water column for the sampled seasons. *Median values are shown.....90

Table 7.3.3. Methanotrophic and respiration rates measured in our incubation assays. Non-significant rates are labeled as n.s. (p>0.05), whereas not sampled stations in certain seasons are labeled as -963

Table 7.3.4. Greenhouse gas flux statistics; min: minimum, max: maximum, SD: standard deviation, VC: variation coefficient..... 97

1. Resumen

La reducción de emisiones de los gases de efecto invernadero tiene un lugar primordial en la agenda del cambio climático. El metano destaca por ser el segundo gas de efecto invernadero más abundante en la atmósfera y tener un potencial de calentamiento 28 veces mayor al del dióxido de carbono en un lapso de 100 años. Este gas es liberado a la atmósfera a través de diversos procesos antropogénicos y naturales. La emisión total global anual de metano se encuentra alrededor de los 550 Tg, siendo los procesos naturales responsables del 37 al 51% de las emisiones. Entre los principales productores naturales de metano están los ecosistemas acuáticos que representan el 23% de las emisiones de metano. La variabilidad espacial y temporal de las emisiones de metano de estos ecosistemas es tal que se requieren métodos de alta variabilidad espaciotemporal para su apropiada caracterización. Además, existe una subrepresentación de la caracterización de ecosistemas acuáticos salobres y de latitudes bajas en la literatura e inventarios globales de gases de efecto invernadero. El ciclo del metano se puede caracterizar en ecosistemas acuáticos mediante la cuantificación de los procesos de producción (metanogénesis), consumo (metanotrofía) y emisión del metano. La disponibilidad de oxígeno disuelto en la columna de agua es determinante en el ciclo del metano, ya que puede limitar o potenciar la metanogénesis y metanotrofía.

En este trabajo se complementaron métodos de alta resolución espaciotemporal, previamente desarrollados para la medición de metano y dióxido de carbono, para incluir la medición de oxígeno disuelto en los componentes del ciclo del metano. Se seleccionaron sensores ópticos de oxígeno debido a su alta resolución, precisión y tiempo de respuesta corto. Por otra parte, los ensayos de actividad metanotrófica fueron complementados con un sensor de oxígeno disuelto tipo parche adherido a la parte interior de la jeringa donde se realizan las incubaciones para poder

determinar el consumo de oxígeno durante los ensayos. Ambos métodos son no invasivos, por lo que no modifican las condiciones propias del ecosistema.

Los métodos antes mencionados fueron utilizados para la caracterización de tres tipos de ecosistemas escasamente reportados en la literatura e inventarios globales: aguas interiores salobres, reservorios subtropicales y una laguna costera tropical. Esta tesis presenta evidencia de que los ecosistemas salobres (las pozas de Cuatro Ciénegas, Coahuila), a pesar de presentar condiciones adversas para la metanogénesis, pueden ser fuentes significativas de metano. Además de su salinidad presentan concentraciones relativamente altas de sulfatos, sin embargo, se encontraron emisiones de 0.12 a $0.98 \text{ mg m}^{-2} \text{ d}^{-1}$, equivalentes a lo observado en ecosistemas salobres costeros. El área de los lagos salinos y subsalinos del mundo representan el 23% del área global total, por lo que las emisiones acumuladas de estos ecosistemas podrían ser significativa a nivel mundial.

En los reservorios subtropicales se observaron emisiones superiores a las correspondientes a su estado trófico, confirmando el potencial de emisión superior de los ecosistemas subtropicales. Se seleccionaron dos ecosistemas, ubicados en el Estado de México y pertenecientes a la misma cuenca hidrológica, con estados tróficos contrastantes. En este sentido, se evaluó el impacto de la eutrofización cultural en el ciclo del carbono en estos ecosistemas. Los datos obtenidos alimentaron un modelo de balance de masa, del cual se determinaron parámetros globales relevantes para el ciclo del metano. A partir de los parámetros determinados se creó una representación gráfica que facilita la apreciación global y contrastante del ciclo del carbono. El impacto de la eutrofización cultural fue profundo y resultó en una completa redistribución de los diversos bioprocessos que participan en el ciclo del metano.

Finalmente, esta tesis presenta la caracterización exhaustiva de la dinámica de metano, dióxido de carbono y oxígeno en los sedimentos y columna de agua, así como las emisiones de la laguna costera tropical “La Mancha”, Veracruz, en tres estaciones características. El ciclo del metano fue caracterizado en dos transectos, uno longitudinal y uno transversal. El primero abarcó el gradiente de salinidad ocasionado por el mezclado de agua dulce, proveniente de un río (Caño Grande) en el extremo sur de la laguna, y agua marina, en el lado opuesto. El segundo transecto, abarcó desde una zona dominada por manglar hasta la salida de La Mancha al mar. Se observó una fuerte regulación estacional que a su vez influyó sobre la entrada de agua dulce a La Mancha. En particular, la temporada de lluvias, en la que aumenta la descarga del río, la materia orgánica y la entrada de agua del mar, se observó la mayor variabilidad y magnitud de emisiones. Los resultados presentados resaltan la importancia de realizar estudios que caractericen con alta resolución espaciotemporal los cuerpos de agua costeros.

2. Abstract

Reducing greenhouse gas emissions is at the top of the climate change agenda. Methane stands out as the second most abundant greenhouse gas in the atmosphere and has a warming potential 28 times greater than carbon dioxide in a 100-year horizon. This gas is released into the atmosphere through various anthropogenic and natural processes. The total annual global emission of methane is around 550 Tg, with natural processes accounting for 37 to 51% of the emissions. Among the main natural producers of methane are aquatic ecosystems, which represent 23% of methane emissions. The spatial and temporal variability of methane emissions from these ecosystems is such that high spatial-temporal methods are required for their appropriate characterization. In addition, there is an under-representation of the characterization of brackish and low-latitude aquatic ecosystems in the literature and global greenhouse gas inventories. The methane cycle can be characterized in aquatic ecosystems by quantifying the processes of production (methanogenesis), consumption (methanotrophy), and emission of methane. The availability of dissolved oxygen in the water column is a determining factor in the methane cycle, since it can limit or enhance methanogenesis and methanotrophy.

In this work, high resolution spatial-temporal methods, previously developed for the measurement of methane and carbon dioxide, were complemented to include the measurement of dissolved oxygen in the components of the methane cycle. Optical oxygen sensors were selected due to their high resolution, accuracy, and short response time. In addition, the methane activity tests were complemented with a dissolved oxygen patch sensor attached to the inside of the syringe where incubations take place in order to determine the oxygen consumption during the tests. Both methods are non-invasive, so they do not modify the conditions of the ecosystem.

The above-mentioned methods were used for the characterization of three types of ecosystems scarcely reported in the literature and global inventories: brackish inland waters, subtropical reservoirs, and a tropical coastal lagoon. This thesis presents evidence that brackish ecosystems (the Cuatro Cienegas pools, Coahuila), despite presenting adverse conditions for methanogenesis, can be significant sources of methane. In addition to their salinity, they present relatively high concentrations of sulfates, however, emissions of 0.12 to $0.98 \text{ mg m}^{-2} \text{ d}^{-1}$ were found, equivalent to what has been observed in coastal brackish ecosystems. The area of the world's saline and sub-saline lakes represents 23% of the total global area, so accumulated emissions from these ecosystems could be significant worldwide.

Emissions in subtropical reservoirs were higher than those corresponding to their trophic state, confirming the superior emission potential of subtropical ecosystems. Two ecosystems were selected, located in the State of Mexico and belonging to the same hydrological basin, with contrasting trophic states. In this sense, the impact of cultural eutrophication on the carbon cycle was evaluated in these ecosystems. The obtained data fed a mass balance model, from which relevant global parameters for the methane cycle were determined. From the determined parameters a graphic representation was created, facilitating the contrast and appraisal of the global carbon cycle. The impact of cultural eutrophication was profound and resulted in a complete redistribution of the various bioprocesses involved in the methane cycle.

Finally, this thesis presents the exhaustive characterization of the dynamics of methane, carbon dioxide and oxygen in sediments and water column, as well as the emissions of the tropical coastal lagoon "La Mancha", Veracruz, in three characteristic stations. The methane cycle was characterized in two transects, one longitudinal and one transversal. The first one covered the

salinity gradient caused by the mixing of fresh water, coming from a river (Caño Grande) in the southern end of the lagoon, and seawater, in the opposite side. The second transect covered an area dominated by mangroves up to the exit of La Mancha to the sea. A strong seasonal regulation was observed which in turn influenced the entrance of freshwater to La Mancha. In particular, the rainy season, in which the river discharge, organic matter and sea water input increase, the greatest variability and magnitude of emissions was observed. The results presented in this work highlight the importance of carrying out studies that characterize with high spatiotemporal resolution coastal water bodies.

3. Introducción

La reducción de emisiones de los gases de efecto invernadero (GEI) tiene un lugar primordial en la agenda del cambio climático. El metano (CH_4) destaca por ser el segundo gas de efecto invernadero más abundante en la atmósfera y tener un potencial de calentamiento 28 veces superior al del dióxido de carbono (CO_2 ; Saunois et al., 2019). Este gas es liberado a la atmósfera a través de diversos procesos antropogénicos y naturales, sin embargo, se estima que el 37% de las emisiones, aproximadamente 210 Tg- CH_4 por año, provienen de fuentes naturales. Entre éstas, sobresalen los cuerpos de agua situados hacia adentro de la zona costera, también conocidos como aguas interiores, que incluyen lagos, ríos, lagunas, reservorios y humedales. Se caracterizan por ser sitios de intenso intercambio de carbono (C; Cole et al., 2007), provocando que sean fuentes desproporcionadas de GEI. A pesar de cubrir aproximadamente el 2.4% de área terrestre se estima que contribuyen 23% de las emisiones globales totales (Bastin et al., 2019; Bastviken, Tranvik, Downing, Crill, & Enrich-Prast, 2011; Saunois et al., 2019).

En los cuerpos de agua existe una gran diversidad de microorganismos que, como parte de su metabolismo, producen y consumen GEI. Los procesos que se desarrollan en el agua y los sedimentos dependen del estado redox, mismo que se ve determinado por la concentración de los aceptores terminales de electrones disponibles. Esto quiere decir que los procesos asociados a la reducción de cierto acceptor de electrones más favorable energéticamente serán priorizados sobre otros. La sucesión ecológica de los aceptores terminales de electrones ordena de manera decreciente la energía libre que resulta de la reducción de cierto acceptor de electrones como: oxígeno (O_2) > nitrato (NO_3^{-2}) > manganeso (Mn) (IV) > hierro (Fe) (III) > sulfato (SO_4^{-2}) > CO_2 (McMahon & Chapelle, 2008). Este ordenamiento indica que los procesos aerobios, aquellos

asociados al O₂, serán los más favorables, mientras que aquellos asociados a la reducción de CO₂ serán los menos favorables.

El agua entre la superficie y los sedimentos, o columna de agua, tendrá una cierta distribución profunda de aceptores y donadores de electrones regida por procesos de producción y consumo. Adicionalmente, en el caso de los gases disueltos, la columna de agua puede recibirlos o emitirlos hacia la atmósfera dependiendo si el gas se encuentra en insaturación o sobresaturación. El grado de saturación se verá determinado a su vez principalmente por el balance entre las tasas de producción y consumo. En el caso del O₂, su producción se lleva a cabo a través de la fotosíntesis, en la zona fótica del lago (capa superior de la columna de agua que recibe luz, mientras que se consume por la respiración heterótrofa, comúnmente presente en toda la columna de agua. El O₂ producido o capturado en la superficie se difunde hacia los sedimentos por diferencia de concentración. Por lo tanto, es común observar que la concentración de O₂ es alta en la superficie y disminuye conforme se aumenta la profundidad. En el caso del CO₂, producido por la respiración heterótrofa y consumido por la fotosíntesis, suele mostrar el comportamiento contrario al O₂ en el sentido de que se encuentra usualmente en concentraciones relativamente mayores en las capas inferiores de la columna de agua, comparado con las aguas superficiales.

Por otra parte, la producción de CH₄, o metanogénesis, por ser un proceso con bajo rendimiento energético, ocurre en ambientes donde otros aceptores de electrones más favorables son limitantes. De ahí que en condiciones óxicas, la metanogénesis no ocurre. Las concentraciones a lo largo de la columna de agua, también conocidos como perfiles de concentración, reflejan este mismo fenómeno. Así como la concentración de O₂ disminuye conforme aumenta la profundidad, la

concentración de CH₄ tiene el comportamiento contrario, alta concentración en los sedimentos que disminuye conforme se acerca a la agua superficial.

La Figura 1, además de mostrar los perfiles de concentración de CH₄ y O₂, ilustra las relaciones que se establecen entre los diversos bioprocessos involucrados en la producción de consumo de los gases mencionados. La metanogénesis, el consumo de CH₄, o metanotrofía, y la respiración se encuentran parcialmente reguladas por el O₂. La metanogénesis es realizada por arqueas metanógenas que se encuentran en los sedimentos anaerobios. Los procesos anaerobios de mineralización que ocurren en los sedimentos producen sustratos que son consumidos por las arqueas metanógenas para producir CH₄. Actualmente se sabe que existen tres rutas metabólicas anaerobias principales a través de las cuales se lleva a cabo la metanogénesis en los cuerpos de agua: (i) la ruta metilotrófica, que utiliza compuestos metilados; (ii) la acetoclástica, cuyo sustrato para la producción de CH₄ es el acetato (CH₃OH); y (iii) la hidrogenotrófica, a través de la cual se reduce CO₂ utilizando H₂ como donador de electrones (Thauer, 1998). En contraste a la metanogénesis, la metanotrofía puede ser aerobia o anaerobia y puede ocurrir tanto en los sedimentos como en la columna de agua. La metanotrofía aerobia procede con el uso de O₂ como acceptor electrones, sin embargo, altas concentraciones de O₂ pueden ser inhibitorias, ya que el rango óptimo de concentración de O₂ es relativamente bajo (7.8 – 31.3 umol L⁻¹; Thottathil et al., 2018). La metanotrofía anaerobia presenta una mayor variedad de aceptores de electrones como sustancias húmicas, nitrato, sulfato, óxidos de hierro, manganeso y, posiblemente, otros metales (Egger et al., 2015; Ettwig et al., 2016; Timmers et al., 2017; Valenzuela et al., 2020, 2017).

La disponibilidad de la materia orgánica, la temperatura y la salinidad del ecosistema acuático juegan un rol importante en la actividad metanógena y metanótrofa (Blake, Tveit, Øvreås, Head,

& Gray, 2015; Cui et al., 2015; Osudar, Matoušů, Alawi, Wagner, & Bussmann, 2015; Yuan, Conrad, & Lu, 2009; Zeikus & Winfrey, 1976). Los ecosistemas acuáticos son clasificados de acuerdo con su productividad primaria fotosintética, es decir, la producción de materia orgánica a

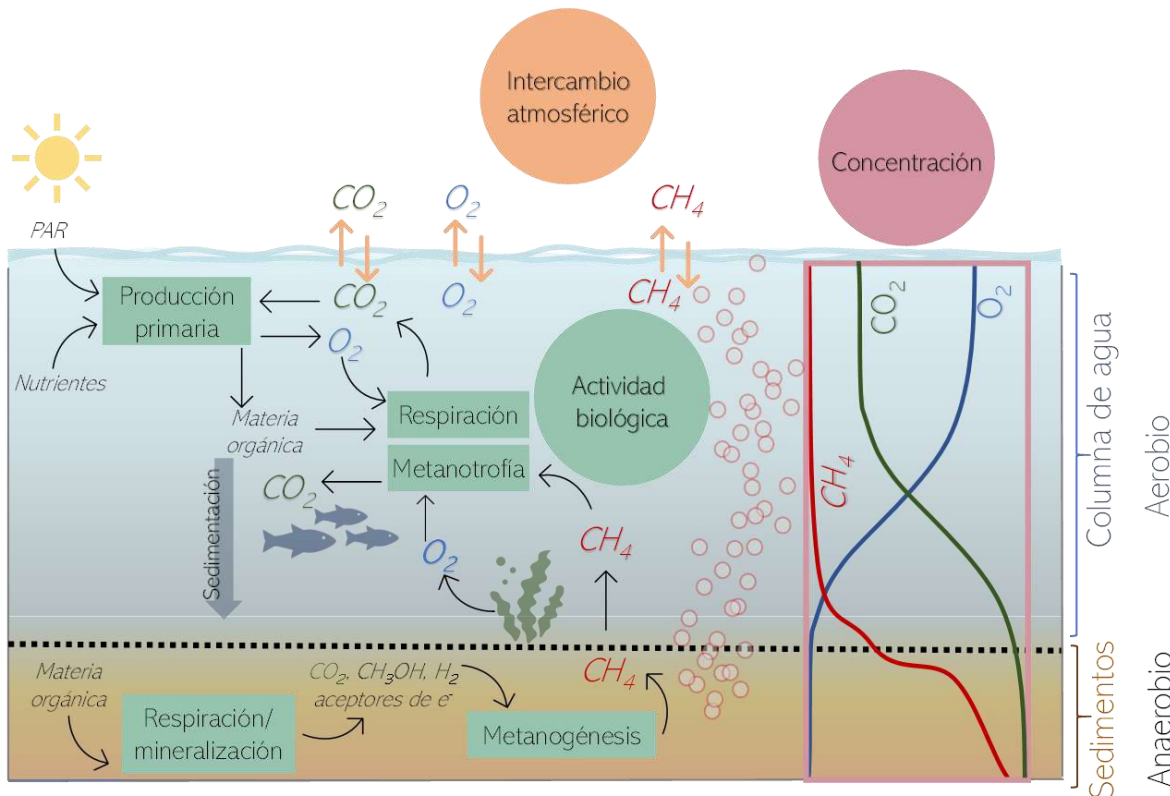


Figura 4.2. Esquema simplificado de los componentes principales del ciclo del CH_4 . Se presentan los bioprocesos más relevantes para el ciclo del CH_4 en ecosistemas acuáticos. Del lado derecho se presentan, con fines ilustrativos, los perfiles de concentración de CH_4 , CO_2 y O_2 disueltos de un cuerpo de agua típico. PAR: radiación fotosintéticamente activa.

partir de la energía solar. Se clasifican en estados tróficos de manera creciente como oligotróficos, mesotróficos, eutróficos e hipereutróficos. Los ecosistemas eutrofizados presentan una alta productividad y se caracterizan por tener bajos niveles de O_2 , ya que la materia orgánica producida en exceso es respirada de manera aerobia agotando el O_2 (Wetzel, 2001). Dichas condiciones son favorables para la metanogénesis, de tal forma que existe una relación positiva entre el estado

trófico y las emisiones de CH₄ (Deemer et al., 2016; DelSontro, Beaulieu, & Downing, 2018; Gonzalez-Valencia, Sepulveda-Jauregui, et al., 2014). La tendencia actual es que los ecosistemas acuáticos son impactados de forma creciente por descargas de contaminantes antropogénicos que ocasionan eutrofización cultural (Istvánovics, 2009; Y. Wen, Schoups, & Van De Giesen, 2017). En ese contexto, se espera que los ecosistemas acuáticos eventualmente emitan cantidades cada vez mayores de GEI (Sepulveda-Jauregui et al., 2018).

La temperatura ha sido identificada como un agente de control sobre la composición de las comunidades microbianas ligadas al ciclo del CH₄ (X. Wen et al., 2017), ya que tanto la metanogénesis como la metanotrofía son procesos biológicos realizados principalmente por organismos mesófilos, con una temperatura óptima alrededor de los 20 a 40 °C (Serrano-Silva, Sarria-Guzmán, Dendooven, & Luna-Guido, 2014). En contraste, la salinidad impacta negativamente a la metanotrofía y metanogénesis por ser un agente de estrés debido al desbalance osmótico (Osudar et al., 2015). En su metaanálisis, Wen et al. (2017) determinan que el nivel de salinidad regula fuertemente la composición de arqueas metanogénicas. Las arqueas metanógenas de lagos alcalinos, ambientes marinos y humedales se agrupan, en contraste con metanógenas de ecosistemas terrestres o de agua dulce. Existe una variedad de osmorreguladores metilados que confiere una ventaja a las metanógenas metilotróficas del género *Metanosarcina* que se han encontrado en ambientes hipersalinos (Ferry, 2012, Liu et al., 2016). A pesar de que se ha encontrado una correlación negativa entre producción de CH₄ y salinidad en algunos ambientes y que la salinidad inhibe la metanogénesis hidrogenotrófica, también existe evidencia de que la salinidad favorece la metanotrofía acetoclástica (Liu et al., 2016).

Los ecosistemas acuáticos costeros, como los manglares, estuarios y lagunas costeras, suelen presentar gradientes de salinidad que van desde agua dulce, con niveles inferiores a 0.5‰ de salinidad, hasta agua salina, con >30‰ de salinidad. Estos ecosistemas son un enlace vital para el intercambio de carbono entre el ecosistema marino y terrestre. Además, se caracterizan por tener alta productividad primaria y alta variación espaciotemporal debido a que tienen topografía y mareas variables. La alta variabilidad de estos ecosistemas es tal que en algunos sitios no se encuentra actividad metanogénica y la concentración de CH₄ se encuentra por debajo del nivel de saturación, mientras que otros llegan a tener concentraciones similares a la de los ecosistemas de agua dulce (Bridgham, Cadillo-Quiroz, Keller, & Zhuang, 2013; P.-C. Chuang et al., 2017; P. C. Chuang et al., 2016; dos Santos Furtado, Casper, & Esteves, 2002; Fonseca, Minello, Marinho, & Esteves, 2004; Verma, Subramanian, & Ramesh, 2002). Cabe destacar que la dinámica del CH₄ en estos ecosistemas no está bien documentada y, al igual que los ecosistemas de agua dulce, existe una subrepresentación de los ecosistemas tropicales (Bridgham et al., 2013; Deborde et al., 2010).

Los factores hasta ahora mencionados impactan el balance entre la metanogénesis y la metanotrofía, y por extensión juegan un papel importante sobre la magnitud de las emisiones de CH₄. Sin embargo, existen aspectos adicionales que regulan el intercambio gaseoso entre el agua y la atmósfera. Las emisiones de CH₄ de los ecosistemas acuáticos pueden ocurrir por dos mecanismos principales: difusión y ebullición. El primero se refiere a la emisión que se da por el gradiente de concentración que surge entre los sedimentos, la columna de agua y la atmósfera, mientras que el segundo se refiere a la liberación de burbujas de CH₄ formadas en los sedimentos, que escapan rápidamente hacia la atmósfera. Las emisiones ebullitivas son más difíciles de caracterizar dado que se trata de un fenómeno estocástico y que ocurre de manera heterogénea en

los cuerpos de agua (Casper, Maberly, & Hall, 2000). En general, las emisiones están sujetas a variaciones espaciales y temporales que son problemáticas para su estimación dentro de un mismo cuerpo de agua, ya que las mediciones con alta resolución temporal y espacial son escasas (Natchimuthu et al., 2016). Asimismo, las estimaciones de emisiones acopladas a modelos de velocidad de viento tienen un rango de error alto (Schilder et al., 2013). Hasta hace relativamente poco, este tipo de mediciones predominaban en la literatura, pero actualmente la recomendación es realizar mediciones de fluxes a lo largo de transectos espaciales. Algunos factores que contribuyen directamente a la variabilidad de las emisiones en un mismo lago se describen brevemente a continuación.

Schilder et al. (2013) encontraron que había un efecto de la morfología del lago sobre la relación entre el coeficiente de intercambio gaseoso (k) y la velocidad del viento. Las concentraciones de CH_4 superficiales son mayores en zonas de baja profundidad en lagos o zonas que reciben un flujo externo (Murase, Sakai, Sugimoto, Okubo, & Sakamoto, 2003; Schilder et al., 2013), una mayor concentración de CH_4 se traduce a una mayor emisión. Adicionalmente, la variabilidad temporal en las condiciones climáticas tiene un gran impacto en las emisiones. Los lagos suelen separarse en dos capas durante el verano a través de un fenómeno conocido como estratificación. El calentamiento de la capa superior del lago, o epilimnio, produce una separación por diferencia de densidad respecto a la capa inferior, o hipolimnio, ya que ésta última se encuentra a una menor temperatura que impide el mezclado de ambas capas. Conforme se acerca el invierno, la capa superior se enfriá y permite el mezclado de las capas. Sin embargo, en la capa inferior puede llegar a almacenarse una masa importante de CH_4 durante la estratificación, y el mezclado ocasiona su liberación a la atmósfera (Gerardo-Nieto, Astorga-España, Mansilla, & Thalasso, 2017). Estos

factores, en conjunto con las corrientes de aire, precipitaciones y cambio de presión, contribuyen a la variabilidad de las emisiones de CH₄. Finalmente, la ubicación de un ecosistema acuático dado en cierta zona geográfica, regulará la dinámica de los GEI y el O₂ de acuerdo a las características propias del sitio y las condiciones climáticas. Desafortunadamente, la mayoría de los trabajos de investigación se limitan a cierta zona geográfica/climática, lo cual resulta problemático dado que existen variaciones regionales que no deben ser generalizadas.

Con gran razón la emisión total de CH₄ derivado de ecosistemas acuáticos es uno de los aspectos con mayor incertidumbre dentro del inventario global de CH₄ (Saunois et al., 2019). Esta incertidumbre se debe a la alta variabilidad espacial y temporal de estos ecosistemas, por ello es necesario realizar campañas de muestreo que permitan: (i) representar las variaciones espacio-temporales dentro de un mismo lago y (ii) evitar el sesgo en las estimaciones globales por la sobrerrepresentación de ciertos ecosistemas acuáticos o latitudes. De este último punto los ecosistemas subtropicales, tropicales, salinos y costeros son algunos ecosistemas con poca representación en la literatura (Aguirrezabala-Campano, Gerardo-Nieto, Gonzalez-Valencia, Souza, & Thalasso, 2019; Camacho et al., 2017; Deborde et al., 2010; Gonzalez-Valencia, Sepulveda-Jauregui, et al., 2014). Este trabajo de investigación está enfocado al desarrollo y uso de métodos de alta resolución espaciotemporal para la caracterización de la dinámica de CH₄, CO₂ y O₂ en ecosistemas escasamente estudiados.

Antecedentes directos

La caracterización del ciclo de los GEI (CH₄ y CO₂) y O₂ en lagos debe contemplar la medición de las emisiones hacia/desde la atmósfera y la caracterización de los principales bioprocessos involucrados; producción primaria, respiración, metanogénesis y metanotrofía. Tal como lo

describiremos en la sección de materiales y métodos, así como en la sección de resultados, se pueden cuantificar dichos procesos mediante tres grupos de métodos;

1. Medición de las emisiones: Las técnicas actuales se basan en la colocación de cámaras estáticas en la superficie del agua. Esas cámaras colectan los gases emitidos y mediante la toma de muestras y su posterior análisis en laboratorio, permiten cuantificar las emisiones. Estas técnicas son relativamente fáciles de implementar pero; (i) requieren transferir las muestras del ecosistema al laboratorio y (ii) requieren de largos periodos de mediciones (de 4 a 8 horas por punto de muestreo). Por estos inconvenientes, la cuantificación de las emisiones se basa comúnmente en un número limitado de mediciones. Por ejemplo, mediante una revisión de la literatura, Martinez-Cruz, (2011) mostró que la cuantificación de las emisiones se limita en general de 3 a 20 mediciones por ecosistema. Dada la alta variabilidad espacial y temporal de las emisiones (Ortiz-Llorente y Alvarez-Cobelas, 2012), un número tan limitado de mediciones resulta estadísticamente poco representativo. No obstante, cabe destacar que en la literatura se reporta cada vez más el uso de detectores conectados a las cámaras, lo cual permite reducir considerablemente el tiempo de estudio.

2. Medición de gases disueltos en agua: La medición del oxígeno disuelto (OD) se realiza tradicionalmente con un sensor polarográfico o galvanométrico que se sumerge a la profundidad deseada y permite obtener perfiles discretos de concentración. el OD se puede determinar *in situ* con electrodos que, no obstante, tienen el inconveniente de tener tiempos de respuesta relativamente lentos, haciendo necesaria la espera de varios minutos para la medición de OD en un punto específico. Por otra parte, las técnicas actuales para la determinación de CH₄, y CO₂ se basan en la toma de muestras discretas de agua que son colocadas en viales que contienen un

espacio de cabeza de un gas inerte, libre del gas que se desea medir. Después del establecimiento de un equilibrio gas/líquido por agitación a temperatura controlada, se mide la concentración del gas de interés en el espacio de cabeza por cromatografía u otra técnica, y se determina la concentración en la muestra mediante el cálculo del equilibrio gas/líquido (ley de Henry). Al igual que las técnicas de medición de fluxes, esta técnica es relativamente sencilla, pero requiere de largos tiempos de medición, limitando el número de mediciones que se pueden realizar para la caracterización del ecosistema.

3. Medición de las actividades microbianas mediante incubaciones: La determinación de la actividad metanotrófica se basa usualmente en la incubación de muestras de agua del sitio de interés en viales con espacio de cabeza enriquecido con CH₄ y O₂. A tiempos regulares, se toma una muestra del espacio de cabeza en la cual se determina la concentración de CH₄. Esta estrategia permite determinar la disminución de la concentración del CH₄ en el tiempo, pero modifica sustancialmente la cinética de la reacción debido a la adición de CH₄ y O₂. Por lo tanto, el resultado no corresponde a las condiciones reales del ecosistema del cual proviene la muestra.

Como fue descrito anteriormente, los métodos actualmente utilizados para caracterizar el ciclo de los GEI tienen serias limitantes, que impiden su caracterización con alta resolución espaciotemporal y/o bajo las condiciones prevalentes en los ecosistemas. Es por esa razón que el grupo de trabajo en el cual se realizó la presente tesis ha desarrollado recientemente varios métodos de alta resolución, incluyendo pero no limitado a (i) la medición de emisiones de GEI (Gerardo-Nieto et al., 2017; Gerardo-Nieto, Vega-Peñaanda, Gonzalez-Valencia, Alfano-Ojeda, & Thalasso, 2019; Frederic Thalasso et al., 2020), (ii) la determinación de la concentración de gases disueltos con alta resolución espacial (Gonzalez-Valencia, Magana-Rodriguez, et al., 2014;

Frédéric Thalasso et al., 2020), y (iii) la determinación de las actividades metanotróficas (Martinez-Cruz et al., 2018). Esos métodos, que forman la base metodológica del presente trabajo, no contemplan la medición de las emisiones de oxígeno a/desde la atmósfera, la determinación del consumo/producción de oxígeno durante los ensayos de incubación y la determinación con alta resolución espacial de la concentración de oxígeno disuelto.

4. Justificación

El aumento de los GEI en la atmósfera causa el cambio climático. El CH₄ es un importante GEI, es el segundo más abundante y tiene una fuerza radiativa 28 veces superior a la del CO₂. Los ecosistemas acuáticos son fuentes naturales importantes de CH₄ con alta variabilidad espaciotemporal. Dado que algunas zonas geográficas se encuentran subrepresentadas en la literatura y que los métodos tradicionales no permiten describir adecuadamente la dinámica del CH₄, existe una incertidumbre considerable asociada a las estimaciones de CH₄ de ecosistemas acuáticos. Por lo tanto, existe una creciente necesidad por caracterizar ecosistemas escasamente estudiados y desarrollar métodos con mejor desempeño, precisión y frecuencia de mediciones.

5. Objetivos generales y específicos

- 1) Completar el paquete de métodos de alta resolución para la caracterización del ciclo del metano en ecosistemas acuáticos (emisiones, concentración y actividad) con el desarrollo de un método para la determinación de (i) gases disueltos (CH_4 , CO_2 , y O_2) en la columna de agua con alta resolución espacial y temporal, y (ii) actividad biológica (metanotrofía, metanogénesis y sulfatorreducción)
 - a) Acoplar la medición de OD con alta sensibilidad y frecuencia de lectura al actual método de medición M-ICOS
 - b) Acoplar la medición de OD en los ensayos de actividad metanotrófica
 - c) Desarrollar un método para cuantificar actividad metanogénica en columna de agua
 - d) Desarrollar un método para cuantificar la actividad metanogénica y sulfatorreductora en sedimentos
- 2) Aplicar los métodos desarrollados para caracterizar el ciclo del CH_4 en ecosistemas acuáticos de agua dulce y salobre escasamente estudiados
 - a) Manantiales de Cuatro Ciénegas
 - b) Reservorios subtropicales
 - c) Ecosistemas costeros

6. Materiales y métodos

El ciclo del CH₄ está compuesto por tres procesos principales: producción, consumo y emisiones. Existen diversas tecnologías para realizar la caracterización de los procesos involucrados en el ciclo del metano; sin embargo, se describirán a continuación los métodos más relevantes para este trabajo.

La espectroscopía de láser de cavidad integrada (Off-Axis Integrated-Cavity Output Spectroscopy, OA-ICOS) es la plataforma tecnológica que se eligió para la detección de GEI en este trabajo. La integración de la cavidad óptica en espectroscopía provoca un aumento considerable en la longitud efectiva de interacción entre el láser y la muestra. El sistema Analizador de Gases de Efecto Invernadero Ultraportátil (UGGA) que se utilizó en este trabajo cuenta con tecnología desarrollada por Los Gatos Research, Inc. de Mountain View (CA). En éste, la intensidad del láser de onda es registrada a la salida de la cavidad de OA-ICOS. La excitación fuera del eje fue implementada como medida para mejorar el desempeño de la espectroscopía láser de cavidad integrada. Esta herramienta de análisis permite tener alta resolución temporal, precisión de partes por billón (ppb; Los Gatos Research, 2017), alta exactitud y presenta notables ventajas sobre otros instrumentos por su robustez y portabilidad que permite realizar mediciones *in situ* (Romanini, Ventrillard, Méjean, Morville, & Kerstel, 2014). El cálculo de la concentración de los GEI se determina a partir de la absorción registrada, haciendo uso de la ley Beer-Lambert. En este grupo de trabajo, OA-ICOS fue acoplado a la cuantificación de emisiones, actividad metanotrófica real y gases disueltos en la columna de agua. Las ventajas de este método sobre cromatografía de gases (CG) es que es más rápido, no es invasivo y se puede realizar en el sitio.

La determinación de la actividad metanotrófica real se realizó a través de un método modificado de Kankaala et al. (2006). En éste, se contiene la muestra de agua de cierta profundidad en una jeringa de vidrio que es impermeable a CH₄, CO₂ y O₂. Se toman submuestras de volumen conocido en otra jeringa, sin contacto con la atmósfera, a la que se le agrega un volumen conocido de nitrógeno (N₂) libre de CH₄ y CO₂. Se realiza el monitoreo de la concentración de CH₄ y CO₂ en el tiempo y, a partir de las concentraciones, se estima el consumo de CH₄ en la muestra. Este método tiene la ventaja de minimizar el cambio de las condiciones reales y, al estar acoplado a OA-ICOS, a tener una mayor sensibilidad (1 ppb). Una contribución importante de esta investigación fue el acoplamiento de la medición simultánea de OD en conjunto con CH₄ y CO₂. Para lograrlo, se colocaron sensores ópticos en el interior de las jeringas, permitiendo la medición no invasiva de la concentración de DO (Sensor Spots PSt3 y PSt6, PreSens, Alemania). Por lo tanto, se puede monitorear el consumo de O₂ (respiración aerobia) conforme se mide la actividad metanotrófica. Este desarrollo permite además discernir entre metanotrofía aerobia y anaerobia.

La medición in situ del CH₄ disuelto en la columna de agua utilizando una membrana de intercambio (M-ICOS) fue desarrollado en el trabajo de Gonzalez-Valencia et al. (2014). M-ICOS consiste en una membrana de intercambio gas-líquido en la que la fase gaseosa fluye por dentro de fibras de silicona con un área de intercambio de 1000 cm². El agua extraída continuamente del lago con una bomba peristáltica fluye a contracorriente por fuera de las fibras de silicona de la membrana. Debido a las fuerzas difusivas, el CH₄ y CO₂ contenidos en el líquido se transfieren a la fase gaseosa que está conectada a la entrada del UGGA. Utilizando este método se pueden obtener tantos datos puntuales como se deseé, pero normalmente se registran entre 60-100 por metro de profundidad de la columna de agua. De manera similar a la metanotrofía, se acopló un

medidor óptico de oxígeno al sistema M-ICOS (FTC-PSt3, PreSens, Alemania), permitiendo la determinación simultánea de perfiles de concentración de CH₄, CO₂ y O₂.

Finalmente, para la medición de fluxes de CH₄ emitidos de los lagos hacia la atmósfera se utiliza el método de la cámara flotante estática. En contraste con métodos de micrometeorología, la cámara estática es un método de bajo costo que puede ser utilizado y transportado con facilidad, además de requerir periodos más cortos para obtener resultados (Duchemin, Lucotte, & Canuel, 1999). Además, dado que su manejo es sencillo puede cubrir amplias áreas de muestreo y permite observar variaciones espaciales de escala menor. El principio se basa en el método de Rolston (1986), originalmente utilizado en suelo, pero fácilmente adaptable para realizar mediciones en cuerpos de agua. Consiste en colocar una cámara que se cierre herméticamente con el agua y permitir la acumulación de gas dentro de la misma por un periodo de tiempo determinado. En este trabajo, se conectó una salida de dicha cámara en circuito cerrado al UGGA para observar la acumulación de gases en tiempo real con alta precisión y resolución temporal.

7. Resultados y discusión

7.1 Dinámica el metano en las pozas subsalinas del Desierto Chihuahuense: Una primera evaluación

Artículo publicado en Science of the Total Environment

Resumen

La Cuenca de Cuatro Ciénegas en el desierto de Chihuahua se caracteriza por la presencia de más de 500 pozas ubicadas en una cuenca endorreica. Estas pozas son ecosistemas subsalinos caracterizados por una concentración de sulfato particularmente alta, comparable con ecosistemas marinos. Este estudio se enfocó a evaluar los parámetros fisicoquímicos principales en estas pozas, junto con la caracterización de la dinámica del metano a través de la determinación de fluxes, concentración de metano disuelto y actividad neta metanotrófica y metanogénica. A pesar de una concentración de sulfato que van desde 1.06 a 4.73 g L⁻¹, las pozas estudiadas mostraron una producción y emisión moderada pero evidente, lo cual sugiere que la metanogénesis no es completamente superada por la reducción de sulfato. Los fluxes de metano fueron desde 0.12 a 0.98 mg m⁻² d⁻¹, los cuales caen en el rango superior de emisiones de las emisiones marinas y en el rango inferior reportado para ecosistemas costeros y pozas salinas. Durante el verano, fue observada una producción de metano significativa en la columna de agua bajo condiciones óxicas. Aparte de los fluxes de metano, se determinaron fluxes de dióxido de carbono en niveles entre 0.20 y 0.53 mg m⁻² d⁻¹, que está en el rango reportado para lagos salinos del mundo. Nuestros resultados representan evidencia adicional de que los ecosistemas salinos y subsalinos juegan un papel importante en la emisión de gases de efecto invernadero a la atmósfera.

Methane cycling in the brackish ponds of the Chihuahuan Desert: a first assessment

Teresa Aguirrezabala-Campano¹, Oscar Gerardo-Nieto¹, Rodrigo Gonzalez-Valencia¹, Valeria Souza², Frederic Thalasso¹.

¹ Cinvestav, Department of Biotechnology and Bioengineering, Mexico City, Mexico.

² Universidad Nacional Autónoma de México, Departamento de Ecología Evolutiva , Mexico City, Mexico.

Abstract

The Cuatro Cienegas Basin (CCB) in the Chihuahuan desert is characterized by the presence of over 500 ponds located in an endorheic basin. These ponds are subsaline ecosystems characterized by a low productivity and a particularly high sulfate concentration, comparable to marine environments. This study focused on assessing the main physicochemical parameters in these ponds along with the characterization of the CH₄ dynamics through the determination of fluxes, dissolved CH₄ concentrations, and net methanotrophic and methanogenic activity. Despite a sulfate concentration ranging from 1.06 to 4.73 g L⁻¹, the studied ponds showed moderate but clear CH₄ production and emission, which suggests that methanogenesis is not completely outcompeted by sulfate reduction. CH₄ fluxes ranged from 0.12 to 0.98 mg m⁻² d⁻¹, which falls within the higher range of marine emissions and within the lower range reported for coastal saline lagoons and saline ponds. During summer, significant CH₄ production in the oxic water column was observed. In addition to CH₄, CO₂ fluxes were determined at levels from 0.2 to 53 g m⁻² d⁻¹, which is within the range recorded for saline lakes in other parts of the world. Our results provide additional evidence

that subsaline/saline aquatic ecosystems play an important role in the emission of greenhouse gases to the atmosphere.

7.1.1 Introduction

Methane (CH_4) is a major greenhouse gas (GHG) released to the atmosphere through diverse anthropogenic and natural processes. Total global emission of CH_4 is estimated to 550 Tg per year, including natural processes, which account to 51% (Kirschke et al., 2013). Aquatic environments have been identified as a major natural source of CH_4 . In particular, lakes and reservoirs represent only 3.7% of the total continental area (Verpoorter et al., 2014) but account for 16% of the global CH_4 emissions (Bastviken et al., 2011; Saunois et al., 2016). Methane emissions from aquatic ecosystems have been well described since the early 1960s (Koyama, 1963) and have been the subject of a growing interest since the early 1980s (Harriss and Sebacher, 1981). However, relatively little attention has been given to ponds, which represent a large fraction of land area (Verpoorter et al., 2014). Indeed, 7% of the total lake area is covered by lakes with an area from 0.001 to 0.01 km^2 (Downing and Duarte, 2006), which contribute approximately 18% of the global CH_4 diffusive emissions (Holgerson and Raymond, 2016). Similarly, our current knowledge on the CH_4 cycling is mostly limited to freshwater systems, while inland subsaline/saline aquatic ecosystems have been generally undervalued (Alcocer and Hammer, 1998; Cole et al., 2007; Stenger-Kovács et al., 2014; Williams, 2002). Since CH_4 production is negatively correlated to salinity and sulfate concentration (Wen et al., 2017), potentially low methanogenic rates are expected from these saline ecosystems. However, the low methane production might be compensated, in terms of emissions, by

the large fraction they represent to the total continental aquatic ecosystems; i.e., 23% of the total area and 48% of the total water volume (Babkin et al., 2003; Wurtsbaugh et al., 2017).

Brackish and saline aquatic ecosystems are found in a diversity of environments wherever an endorheic basin is subject to a balance between hydrological inputs and outputs (Williams, 2002). These conditions are found in the Cuatro Cienegas Basin (CCB), which is located at the northwestern edge of the Sierra Madre Oriental, a mountain range that delineates the Chihuahuan Desert to the east (Figure 7.1.1). The valley is set on a complex geological structure and is composed of endorheic and generally well-preserved basins resulting on the existence of over 500 ponds. CCB is the product of desertification of a marine environment that existed in the area between the Late Triassic and the Early Cretaceous (Souza et al., 2012), which became part of the western seaway that connected the Gulf of Mexico with Canada. The ponds of the valley are subsaline aquatic ecosystems; i.e. salinity from 0.5 to 3‰ (Hammer, 1986), dominated by sulfate (SO_4^{2-}), carbonate, calcium, and magnesium ions (Minckley and Cole, 1968). Moreover, the ponds are characterized by the presence of ancient and living microbialites, and by a high level of endemism (Alcaraz et al., 2008; Kornfield et al., 1982; Minckley and Cole, 1968; Taboada et al., 2018; Taylor, 1966).

The ponds of the CCB have been well-studied in the fields of biodiversity and evolutionary ecology, while relatively little attention has been paid to the biogeochemical functioning of these aquatic ecosystems. To the best of our knowledge, CH_4 dynamics in Cuatro Cienegas ponds has never been reported before. An assessment of CH_4 dynamics and emissions in these ponds is therefore of major importance, not only to address the knowledge-gap previously described, but also to serve as a baseline condition for pristine subsaline/saline environments with which to compare other chronically polluted ecosystems. In this context, the objective of this study was to characterize, for the first time, CH_4 cycling and emissions in five ponds of the CCB, in different seasons. Our study

included the determination of CH₄ emissions, dissolved CH₄ concentrations within the water column, and CH₄ production/oxidation rates. To complement data on CH₄ cycling, carbon dioxide (CO₂) flux and dissolved CO₂ concentrations, dissolved oxygen (DO) concentrations, and several other physicochemical parameters were also measured.

7.1.2 Materials and methods

7.1.2.1 Site description

In CCB, the Sierra de San Marcos divides the valley into east and west sub-basins (Wolaver, 2008; Figure 7.1.1). Depending on the ⁴ sub-basin in which they are located, the physicochemical characteristics of the ponds are likely to differ. Eastern ponds have generally lower discharge, temperature, and total dissolved solids relative to the western ponds (Wolaver et al., 2008). In both sub-basins, the ponds are recharged by groundwater flowing from the mountain ranges (Johannesson et al., 2004; Wolaver et al., 2013, 2008), although on the western side, a significant water input comes from the 91,000 km² carbonate aquifer located underneath the region (Wolaver et al., 2008). This deep water has a magmatic influence that maintains the water cycle in the wetland and explains the high sulfur concentrations in the water (Wolaver et al., 2013). For example, the Cuatro Cienegas ponds have SO₄²⁻ concentrations comparable to marine environments (>1 g L⁻¹; Holmer and Storkholm, 2001; Escalante et al., 2008; Minckley and Cole, 1968). It has also been suggested that the microbes and viruses in the ponds still contain the genetic signatures of the ancient marine ecosystems that once prevailed in the region (Desnues et al., 2008; Souza et al., 2018; Souza et al., 2006). Moreover, the ponds are characterized by the presence of ancient and living microbialites, and by a high level of endemism (Alcaraz et al., 2008; Kornfield et al., 1982; Minckley and Cole, 1968; Taboada et al., 2018; Taylor, 1966) including fishes (e.g.,

Herichthys minckleyi), turtles (e.g., *Terrapene Coahuila*), crustaceans (e.g., *Leptocaris stromatolicolus*), mollusks, and gastropods. These exceptional and unique characteristics have led to the CCB being granted the status of a Federal Natural Protected Area, and it is considered the most important wetland in the Chihuahuan Desert, also recognized as a Ramsar site; i.e., wetland of international importance.

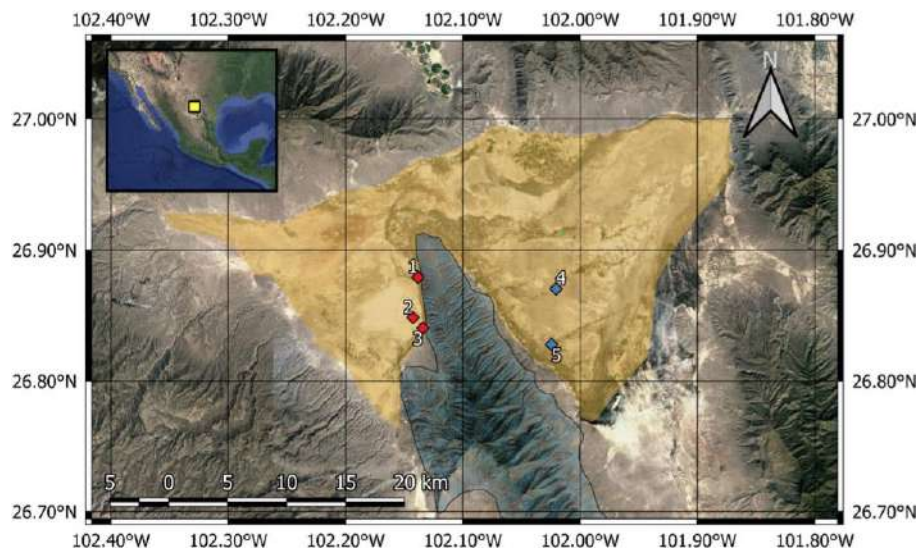


Figure 7.1.1. Cuatro Cienegas Valley. The valley is in the Northeast of Mexico as shown in the yellow rectangle. The colored golden area represents the valley, while the delineated mountain is the Sierra de San Marcos which divides the basin in east and west sub-basins. The ponds have been numbered as 1: Poza Becerra (PB), 2: Poza Manantial (PM), 3: Poza Churince (PCH), 4: Poza Azul (PA), and 5: Poza Los Hundidos (LH).

A total of five ponds were selected, which according to their local names were: Poza Azul (PA), Los Hundidos (LH), Poza Becerra (PB), Poza Manantial (PM), and Poza Churince (PCH, also described in other studies as intermedia lagoon; Table 7.1.1). An initial field campaign was performed in April 2016, at PA, PM, and PCH. During a second campaign, we observed that PM and PCH, both part of the same hydrological system (Cerritos et al., 2011), were desiccated, probably due to mismanagement of groundwater resources by agriculture (Leal Nares et al., 2018; Souza et al., 2018). Thus, an alternative strategy was selected in which we opted for the characterization

of the three permanent ponds (PA, LH, and PB) over two contrasting seasons; measurements were made in January and August 2017, the months with the greatest thermal contrast, with a mean temperature of 12.8 and 28.7 °C, respectively (SMN; Sistema Meteorológico Nacional, 2011). Despite the fact that precipitation is highly variable from year to year, historical records show that January corresponds to the dry season and August corresponds to the wet season, with average monthly precipitation rates of 12.3 and 29.4 mm, respectively (SMN; Sistema Meteorológico Nacional, 2011).

Table 7.1.1. Morphometric parameters of the selected Cuatro Cienegas Valley ponds. Aw: surface area; Zm: mean depth; Zmax: maximum depth; V: total volume.

Pond	Poza Azul	Poza Becerra	Los Hundidos		Manantial	Churince
Season	All seasons	All seasons	Winter	Summer	Spring	Spring
Latitude	26°49'39"N	26°52'42"N	26°52'13"N	26°50'25"N	26°50'54"N	
Longitude	102° 1'27"W	102° 8'17"W	102° 1'13"W	102° 8'3"W	102° 8'29"W	
Aw (m ²)	1,800	3,000	1,200	1,200	1,100	10,900
Z _m (m)	3.52	1.18	1.56	1.06	0.96	0.3
Z _{max} (m)	9.5	3.3	4.89	4.21	2.1	0.5
V (m ³)	6,500	3,500	1,900	1,300	1,000	3,200
Transect length (m)	45	140	75	75	45	210

7.1.2.2 Limnological characteristics

Water depth was measured in over 20 locations in each pond with a portable sounder (Depthmate Portable Sounder, Speedtech, USA). A global positioning system (eTrex 20, Garmin, USA) was used to determine the location of each measurement in the ponds. The pond surface area (Aw) was obtained through image analysis of aerial photographs obtained from Google Earth Pro (v. 7.3). Pond volumes (V) were determined from depth and area measurements. The average depth (Z_m) of each pond was obtained by dividing the total volume by the total area.

Physicochemical measurements were made at sampling sites along the longest section of each pond, referred to as the longitudinal transect (Table 7.1.1; Figure 7.1.2). Along each transect, from 7 to 15 locations were selected, depending on the size of the pond, for physicochemical measurements. Temperature, conductivity, oxidation-reduction potential (ORP), pH, salinity, and dissolved oxygen were measured with a multiparametric probe (HI 9828, Hanna Instruments, Mexico, and YSI 556 MPS, Xylem Analytics, USA). These measurements were made from the surface of the water to the sediment at the bottom of each pond at depth intervals of 1 m, or 0.3 m when depth was b1 m. Chlorophyll-a concentrations were determined in August 2017 using a Hydrolab MS5 (OTT Hydromet, USA), calibrated according to the operating manual which included a chlorophyll standard. For the determination of SO_4^{2-} concentrations in surface and bottom water (0.2 m depth and just above sediments, respectively), samples were taken with a horizontal 2.2-L Van Dorn bottle (Wildco, Mexico) and analyzed according to standard methods (APHA, 2012).

7.1.2.3 Greenhouse gases fluxes

CH_4 and CO_2 fluxes were determined with a floating static chamber (SC) connected to an ultraportable greenhouse gas analyzer (UGGA, Los Gatos Research, USA) in a closed circuit. Fluxes were determined according to Eq. (1):

$$F = \frac{\Delta C}{\Delta t} \cdot \frac{V_{sc}}{A_{sc}} \quad (1)$$

where F is the flux ($\text{mg m}^{-2} \text{ d}^{-1}$); ΔC is the change in CH_4 or CO_2 concentrations observed in the SC over the measured time interval Δt ; V_{sc} is the SC volume (7.8L); and A_{sc} is the area of the SC in contact with the water surface (0.096 m^2).

The SC method measures the total flux at the surface of the ecosystem and includes both diffusive and ebullitive fluxes. Since the method includes a continuous measurement of CH_4 and CO_2

concentration with a frequency of 1 Hz, it allows for a clear distinction between both emission modes. Indeed, any ebullitive event would be observed as an abrupt step increase in the concentration, while diffusive flux would be observed as a linear concentration increase. Thus, prior to the flux measurements and to determine if ebullitive fluxes were present, visual observations of the area were performed and long-term (15 min) flux measurements were taken in the littoral zones of the ponds; i.e., where ebullition is more frequently observed (Natchimuthu et al., 2016). As it will be described in the Results and Discussion section, no ebullitive event was observed over a total of 40 h of continuous flux measurement. Thus, only diffusive fluxes were considered, and two criteria were used to validate measurements, as reported by Duchemin et al. (1999): first, the initial concentrations were close to ambient atmospheric concentrations, and second, the linear correlation coefficient (R^2) of the regression analysis exceeded 0.75. Triplicate flux measurements were done at 10–20 positions, covering the entire surface area of the ponds, including the littoral zones. In each case, fluxes measurements were started 30 s after positioning the SC on the water surface and sustained over 3 min. All fluxes were measured under maximum daylight conditions; i.e., from 10 am to 5 pm.

7.1.2.4 Dissolved greenhouse gas concentrations

Dissolved CH₄ (C_{CH4}) and CO₂ (C_{CO2}) concentrations in the water column were determined according to the M-ICOS method previously developed and reported by Gonzalez-Valencia et al. (2014a). Briefly, this method consisted of a gas-liquid exchange membrane (PDMSXA- 1000, Medarray Inc., USA) composed of an array of silicone hollow fibers, with a total exchange area of 1000 cm². The water extracted from the pond constantly flowed around the hollow fibers, while CH₄- and CO₂-free nitrogen flowed inside the hollow fibers at a constant rate. Due to diffusive

forces, the dissolved CH₄ and CO₂ contained in the water were transferred to the gas phase, where they were detected by the UGGA. The water was continuously extracted at the desired depth with a peristaltic pump (12 V, Solinst, Mexico) at a flow rate of 1.2 L min⁻¹, while the CH₄- and CO₂-free nitrogen was flowing at a constant flow rate of 0.75 L min⁻¹, controlled by a mass flow controller (GFC 17, Aalborg, Mexico). According to the M-ICOS method, the setup was calibrated at the beginning and at the end of each measurement day using a standard headspace equilibration technique (Gonzalez-Valencia et al., 2014a). In order to obtain the C_{CH₄} and C_{CO₂} profiles, the extraction probe was maintained just below the water surface for about 60 s, the probe was then allowed to descend steadily at a rate of 1 m min⁻¹ until it reached the bottom of the pond, where it was kept for an additional 30 s. Using this procedure, about 60 data points for dissolved gases were acquired for each meter of water column depth. This method has been reported to have a lower limit of detection of 4.4 ng L⁻¹ for CH₄ and 6.6 µg L⁻¹ for CO₂ (Gonzalez-Valencia et al., 2014a).

In all estimations, water solubility of CH₄ and CO₂ were calculated from the Bunsen coefficient, β , defined as the volume of gas absorbed by a volume of solvent at a partial pressure of 1 atm (with units L L⁻¹ atm⁻¹ for CH₄ and mol kg⁻¹ atm⁻¹ for CO₂) as detailed by Liotta and Martelli (2012) and in accordance with Eq. (2):

$$\ln \beta = A_1 + A_2 \left(\frac{100}{T} \right) + A_3 \ln \left(\frac{T}{100} \right) + S \left[B_1 + B_2 \left(\frac{T}{100} \right) + B_3 \left(\frac{T}{100} \right)^2 \right] \quad (2)$$

where A_n and B_n are constants for each gas; T is the water temperature (K); and S is the salinity (PSU). Bunsen coefficients were subsequently corrected for the partial pressure of the gases at each site.

7.1.2.5 Methane production/oxidation rates in water

In order to measure the net CH₄ production/oxidation rates, water samples were taken from the surface (ca. 0.2 m depth) or the bottom (ca. 0.1 m above sediments) of the ponds using a Van Dorn

bottle. After sampling, the Van Dorn bottle was carefully turned to a vertical position and the top rubber lid was fully opened. Then, 10-mL glass syringes were dismantled, fully submerged into the water sample, filled and assembled again. This procedure ensured the absence of any bubble in the syringes. These syringes were transferred to the laboratory as soon as possible (typically within one to 3 h) for incubation in the dark at a constant temperature similar to the temperature of the ponds. Then, at set time intervals, 2 mL sub-samples were transferred from each sample into 5-mL plastic syringes, to which 3 mL of CH₄- and CO₂-free nitrogen were added. The syringes containing the subsamples were then vigorously shaken for 30 s, to allow for gas/liquid equilibration. The liquid volume in each sub-sample syringe was then evacuated, and the 3 mL gas content was injected through a septum into a continuous flow of nitrogen passing through the UGGA open circuit. The presence of CH₄ in each injected sample was detected as a peak response that was integrated after full calibration with known volumes of CH₄. The CH₄ concentrations in the original samples were determined according to the Bunsen coefficient (Eq. (2)). These incubations were sustained from five to seven days, during which a total of five triplicate measurements of C_{CH₄} were performed to establish the net CH₄ production/oxidation rates. Sterile water samples (autoclaved for 15 min at 121 °C) were used as controls and were measured following the same procedures. This protocol allowed for the determination of net CH₄ production/oxidation rates from incubation with no headspace, thus without addition of DO and CH₄, and therefore under the conditions prevailing in the water column of the ponds. This is the reason why these CH₄ production/oxidation rates can be referred as actual rates (Kankaala et al., 2006), in opposition to potential rates determined in vials with headspace or spiked with CH₄ or DO, as often reported in the literature.

7.1.2.6 Sediment characterization in Poza Becerra

A sediment sample was taken from the center of PB, using an Ekman dredge (Wildco, Mexico) immediately placed in a Ziploc bag and carefully sealed under water to avoid further contact with air. The sample was used for the determination of SO_4^{2-} concentration, as well as methanogenic and sulfate reduction rates through incubation assays. For the determination of SO_4^{2-} concentration, the sediment was mixed with water and filtrated through a $0.2 \mu\text{m}$ membrane (Millipore, USA). Then, the resulting water was used to determine SO_4^{2-} according to standard methods (APHA, 2012). The sediment sample used to determine methanogenic and sulfate reduction rates was transferred as soon as possible (typically within one to 3 h) to an inflatable anaerobic chamber (AtmosBag, Sigma-Aldrich, Mexico) under constant N_2 flow. 130 g of sediments were diluted with 130 g of PB bottom water, sampled with a Van Dorn bottle. 15 mL of the resulting slurry were transferred, under constant agitation and N_2 flushing, to 120 mL serum bottles, which were then sealed with rubber stoppers (Bellco, USA) and aluminum crimp caps. A total of 48 vials were prepared for triplicate determination of methanogenic and sulfate reduction rates. At time intervals, over a 25-day period, three vials were sacrificed for CH_4 and sulfide (S^{-2}) measurements, according to the following procedure; (i) 3 mL of ZnAc (40%) were added to each closed vial to precipitate S^{-2} as ZnS using a syringe, (ii) 2 mL of the headspace was taken and measured in the UGGA, as described in Section 2.6, (iii) the vials were opened and S^{-2} concentration was determined by the methylene blue method (APHA, 2012) using 1 mL samples of the slurry. Methanogenesis and sulfate reduction were quantified as the change of concentration of CH_4 and S^{-2} per unit of wet sediment (WS) volume and time.

7.1.2.7 Data treatment and statistics

Data collected during the campaigns were used to generate contour maps for bathymetry, and CH₄ and CO₂ fluxes. A contour map of the C_{CH4} profile along the longitudinal transect of pond PB was also created. The contour maps were generated by data interpolation using Surfer 11.0 software (Golden Software, USA). Surfer provides 10 interpolation methods, from which the best method was chosen based on two criteria (the mean absolute error and the mean bias error), following Willmott and Matsuura (2006).

Data were tested for normality using the Shapiro-Wilk test. The physicochemical parameters were compared among all ponds and seasons using a one-way analysis of variance (ANOVA) in conjunction with the Tukey-Kramer test. Fluxes were compared on the basis of their medians using a sign test. Bonferroni corrections were applied to avoid type I errors. All statistical analyses were performed in MATLAB Statistics Toolbox (R2015a, Mathworks Inc.).

7.1.3 Results and discussion

7.1.3.1 Pond descriptions and physicochemical characteristics

The morphometry and transect length of the ponds are presented in Table 7.1.1. Pond area ranged from 1100 to 3000 m², except PCH, which had a considerably larger area of 10,900 m². Maximum pond depth ranged from 0.5 m (PCH) to 9.5 m (PA), while volume ranged from 1000 m³ (PM) to 6500 m³ (PA). Bathymetric maps of the ponds are presented in Figure 7.1.2. The depths of PA and PB remained unchanged throughout the field campaigns, while LH showed a reduction in depth of about 0.7 m between January and August 2017. PCH and PM were both desiccated after April 2016. With the exception of PCH, aquatic life was observed in all ponds. This was minimal in PA but abundant in LH and PB, as shown in Video S1 (link provided in supplementary material).

Stromatolites were only observed in PA, while strong underwater resurgences; i.e., groundwater input, were observed in PM and PB, having distinctive columns of resuspended sediments.

The key physicochemical parameters of the ponds are summarized in Table 7.1.2. A significant water temperature difference was observed between winter and summer in PA and LH, but not in PB ($p < 0.05$). This was probably due to the observed water resurgences, which may explain the significantly higher water temperature of PB. A slight thermocline was observed during the summer only in PA, where a temperature gradient of 1.3°C was observed between the surface and a depth of 3 m.

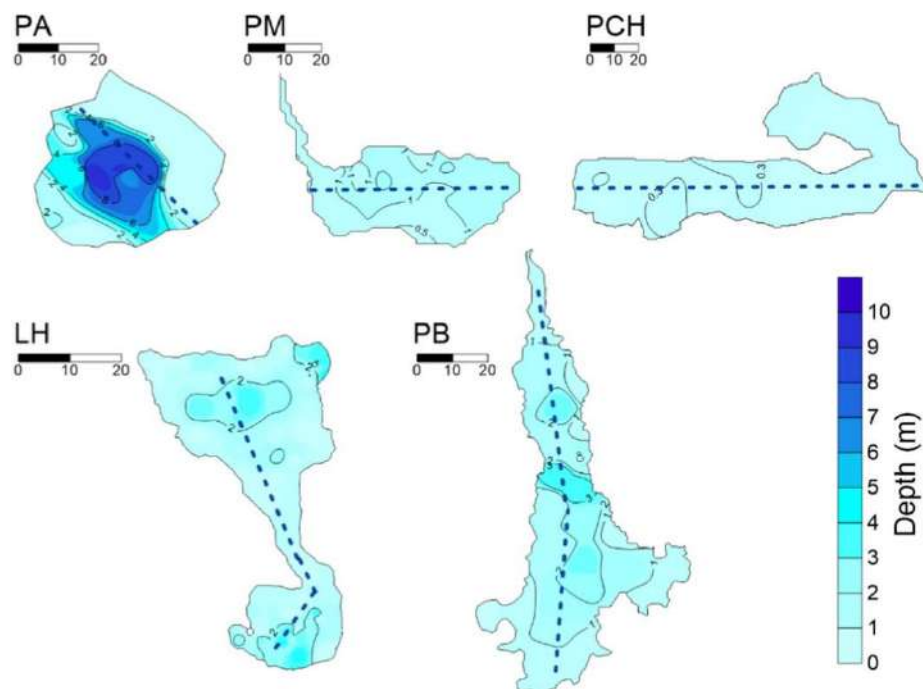


Figure 7.1.2. Contour maps obtained from bathymetric data collected in: PA, Poza Azul; PM, Poza Manantial; PCH, Poza Churince; LH, Los Hundidos; PB, Poza Becerra. The scale varies as shown by the scale bar next to the ponds acronym (in m). The dotted line indicates the selected longitudinal transects.

Overall, the water columns of the ponds were well-mixed and under oxic conditions, with DO ranging from 3.0 to 6.6 mg L^{-1} depending on the pond and the season. A near neutral pH was found

in most of the ponds, except in PCH where a pH of 8.3 was observed. Chlorophyll-a concentrations were below the detection limit of the Hydrolab ($<0.1 \mu\text{g L}^{-1}$) at all depths in every pond, except at the bottom of PA where a concentration of up to $2 \mu\text{g L}^{-1}$ was measured during the summer. The absence of chlorophyll is a clear indicator of low productivity, as it has been previously reported for the Cuatro Cienegas ponds (Alcaraz et al., 2010; Elser et al., 2005; Escalante et al., 2008; Souza et al., 2018). SO_4^{2-} concentrations similar to marine environments were observed, ranging from 1.06 to 4.73 g L^{-1} , which is in agreement with previous reports (Corman et al., 2016; Escalante et al., 2008; Johannesson et al., 2004; Minckley and Cole, 1968). In PB, SO_4^{2-} concentrations measured in the surface sediments ($1.23 \pm 0.12 \text{ g L}^{-1}$) were lower than those measured at the bottom of the water column, above the sediment ($1.75 \pm 0.06 \text{ g L}^{-1}$). This suggests active SO_4^{2-} reduction in the surface sediments, which was confirmed during sulfate reduction assays, described in the next section.

7.1.3.2 *Dissolved greenhouse gases*

Mean C_{CH_4} values observed in the ponds are shown in Table 7.12. With the exception of PB, where longitudinal and profundal gradients were observed (Figure 7.1.3), C_{CH_4} was homogeneously distributed. In all ponds except PCH, C_{CH_4} was between 4 and 92 times above the atmospheric equilibrium, taking into account the salinity and the temperature of the ponds (Eq. (2)). In PCH, C_{CH_4} was $30 \pm 3 \text{ ng L}^{-1}$, which was close to the C_{CH_4} in equilibrium with the atmosphere, i.e. 31 ng L^{-1} . These results indicate that the ponds, except PCH, are net CH_4 producers, which combined with relatively high concentration of SO_4^{2-} , suggest the coexistence of methanogenesis and SO_4^{2-} reduction processes as previously reported for other subsaline/saline environments (Dupraz et al., 2009; Oremland and Polcin, 1983; Schink and Stams, 2013; Sela-Adler et al., 2017). The latter was confirmed experimentally, through incubation of surface sediment samples obtained from PB

(Figure 7.1.S2). During these assays, a net CH_4 production of $16.7 \pm 5.25 \times 10^3 \mu\text{g m}^{-3} \text{ d}^{-1}$ and a net SO_4^{2-} reduction rate of $1.80 \pm 0.7 \times 10^6 \mu\text{g-S}^{-2} \text{ m}^{-3} \text{ d}^{-1}$ were observed. These rates correspond to $1.04 \pm 0.33 \times 10^3$ and $56.4 \pm 21.9 \times 10^3 \mu\text{mol m}^{-3} \text{ d}^{-1}$, for methanogenesis and SO_4^{2-} reduction, respectively. It can be concluded that both processes coexisted, being SO_4^{2-} reduction dominant over methanogenesis, which is in agreement to the ecological succession of electron acceptors (McMahon and Chapelle, 2008). Although the substrate used by both processes in CCB ponds is unidentified, assuming acetoclastic processes, the observed rates would correspond stoichiometrically (Okabe and Characklis, 1992; Whitman et al., 2006) to an acetate uptake of 98.2% through the sulfate reduction pathway.

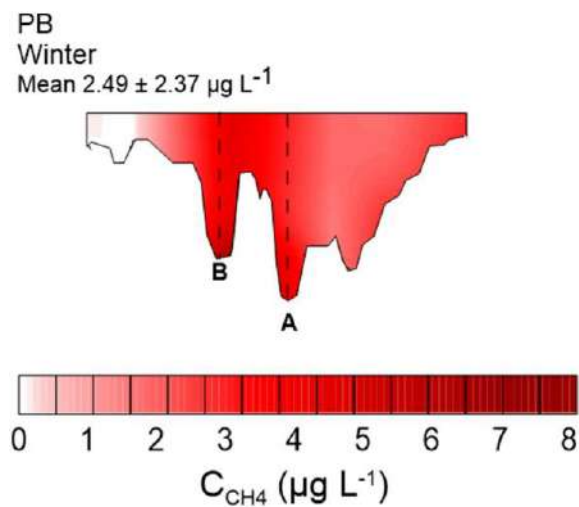


Figure 7.1.3. Longitudinal transect of C_{CH_4} profile for PB, Poza Becerra, during winter. Lines A and B indicate zone of high CH_4 concentration. A is the location of a resurgence, while no resurgence was observed in B. The maximum depth and transect length correspond to the values reported in Table 7.1.1.

During winter, a C_{CH_4} profundal gradient was observed in PB, which is an additional evidence of net CH_4 production in the sediments of the ponds, as opposed to possible lateral transport. A longitudinal gradient was also observed in PB, with higher concentrations found at the center of the pond,

Table 7.1.2. Physicochemical parameters of the selected ponds (mean values over the entire water column at 1-m intervals). T: temperature; DO: Dissolved Oxygen; TOC, total organic carbon; TN, total nitrogen; SO₄²⁻: sulfates; PO₄³⁻: ortho-phosphates; Cond: conductivity; ORP: oxidation-reduction potential; C_{CH4}: mean dissolved CH₄ concentration; C_{CO2}: mean dissolved CO₂ concentration. NM: Not Measured. Standard deviations are shown in parentheses. Difference in superscript letters indicate significative differences between means (Tukey-Kramer test; p < 0.05).

Pond (ID)	Poza Azul (PA)			Poza Becerra (PB)		Los Hundidos (LH)		Manantial (PM)	Churince (PCH)
Season	Winter	Spring	Summer	Winter	Summer	Winter	Summer	Spring	Spring
T (°C)	21.55 ^b (0.08)	27.30 ^d (0.70)	30.40 ^e (0.80)	32.31 ^f (0.62)	33.19 ^f (0.67)	17.02 ^a (0.73)	25.36 ^c (1.20)	26 ^c (0.30)	25.5 ^c (1.10)
DO (mg L ⁻¹)	5.44 ^c (0.43)	4.79 ^b (0.40)	6.32 ^b (0.11)	2.97 ^a (0.79)	3.11 ^a (0.52)	6.59 ^c (1.44)	3.08 ^a (1.71)	3.68 ^a (0.52)	6.60 ^c (0.39)
pH	7.53 ^{d,e} (0.03)	7.60 ^e (0.10)	7.56 ^d (0.11)	7.09 ^b (0.26)	6.70 ^a (0.18)	7.53 ^{c,d,e} (0.08)	7.37 ^{c,e} (0.046)	7.45 ^{c,d,e} (0.14)	8.31 ^f (0.52)
SO ₄ ²⁻ (g L ⁻¹)	1.06 ^a (0.04)	NM	1.83 ^a (0.05)	1.25 ^a (0.01)	1.75 ^a (0.06)	1.25 ^a (0.05)	4.73 ^b (0.1)	1.77 ^a (0.04)	3.35 ^b (0.04)
Cond (μS cm ⁻¹)	2672 ^a (6)	2,666 ^a (140)	2,614 ^a (68)	2,598 ^a (53)	2,303 ^a (363)	4,688 ^b (33)	5,391 ^c (14)	2,526 ^a (29)	36,000 ^d (1000)
Salinity (‰)	NM	1.37 ^a (0.07)	1.42 ^a (0.006)	NM	1.17 ^a (0.19)	NM	2.97 ^c (0.007)	1.30 ^a (0.01)	19.1 ^d (0.6)
ORP (mV)	203 ^d (9)	66 ^{a,b} (7.40)	NM	96 ^b (12)	138 ^c (39)	124 ^{b,c} (7)	230 ^d (23)	44 ^a (15)	69 ^{a,b} (5.40)
C _{CH4} (μg L ⁻¹)	0.20 ^b (0.026)	0.15 ^b (0.039)	0.49 ^{b,c} (0.18)	3.50 ^e (2.28)	0.12 ^b (0.11)	1.22 ^d (0.11)	0.62 ^c (0.20)	0.70 ^c (0.093)	0.03 ^a (0.003)
C _{CO2} (mg L ⁻¹)	11.19 ^f (1.23)	9.7 ^{b,c} (2.51)	10.7 ^{b,c} (1.35)	15.81 ^d (1.03)	23.21 ^g (1.50)	10.7 ^c (1.35)	9.37 ^c (3.49)	9.44 ^b (1.21)	1.70 ^a (0.76)

corresponding to its deepest section and the region where resurgences were observed (marked as line A in Figure 7.1.3). The possible input of exogenous CH₄ through resurgences was investigated and discarded, as similar C_{CH₄} values were observed in a separate, deep section of the pond where no resurgence was observed (marked as line B in Figure 7.1.3). There are scarce data regarding C_{CH₄} in endorheic subsaline/saline lakes and, to the best of our knowledge, they have been reported only for Lake Issyk-Kul, Kyrgyzstan, which is an ultraoligotrophic lake, with a reported salinity of approximately 6 g L⁻¹ (Savvaitova and Petr, 1992). In that lake, Zavialov et al. (2016) reported C_{CH₄} ranging from 0.35 to 2.78 µg L⁻¹, similar to those measured in the CCB ponds. Compared to other aquatic ecosystems, the C_{CH₄} found in the CCB ponds were below (PCH) or within the lower range previously reported for oligotrophic boreal lakes (Bastviken et al., 2004).

Mean C_{CO₂} values for the ponds are displayed in Table 7.1.2. In all cases, C_{CO₂} was homogeneously distributed. The lowest and highest mean C_{CO₂} values were found in PCH and in PB during the summer (1.7 ± 0.8 and 23.0 ± 1.5 mg L⁻¹, respectively). These C_{CO₂} values were 3.2 and 51 times above the atmospheric equilibrium values of 0.535 and 0.459 mg L⁻¹, respectively. The levels of C_{CO₂} found in the ponds might result from weathering of carbonates; high levels of carbonates are present in the soil of the Cuatro Cienegas Valley (Escalante et al., 2008; INE-SEMARNAP, 1999; Minckley and Cole, 1968), and inputs from weathering of carbonates have been observed in other saline lakes (Duarte et al., 2008). Furthermore, Marcé et al. (2015) positively correlated CO₂ supersaturation with the weathering of carbonate in lakes with alkalinity above 1 meq L⁻¹, which is the case for the Cuatro Cienegas ponds (2–4 meq L⁻¹; Escalante et al., 2008). From chemical equilibrium (see Section S1.1) the dissolved CO₂ concentration was estimated to 24.4, 11.8, and 1.5 mg L⁻¹, in PB, LH and PCH, respectively (Section S2; Table 7.S2), while C_{CO₂} experimentally

measured was 23.2, 10.7 and 1.7 mg L⁻¹, in these same ponds. Therefore, the dissolved CO₂ found in the Cuatro Cienegas ponds might be of chemical origin as well as resulting from microbial heterotrophic activity, especially given the low primary production as suggested by low chlorophyll-a concentrations.

7.1.3.3 Greenhouse gas emissions

Both CH₄ and CO₂ emissions were determined in the ponds. Over the three campaigns, we determined a total of 700 flux, which corresponded to 40 h of measurements, during which no ebullitive event was observed. Although ebullitive flux is not thoroughly discarded, diffusive flux was considered as the main emission mode. All the ponds emitted CH₄, except PCH, from which no flux was observed. The minimum and maximum CH₄ fluxes in the ponds were zero (PCH during spring) and 2.37 mg m⁻² d⁻¹ (PM during spring), while the mean CH₄ fluxes ranged from 0 to 1.22 mg m⁻² d⁻¹, respectively (Figure 7.1.4). The pond with the least change in flux among seasons was PB, which is also the only pond for which no temperature change was observed.

The observed mean CH₄ fluxes are within the higher range of marine emissions and within the lower range reported for coastal saline wetlands and saline ponds (Table 7.1.3). Camacho et al. (2017) observed lower CH₄ emissions together with higher salinity in endorheic saline ponds. The latter coincides with our observation of zero CH₄ flux from PCH —the pond with the highest salinity (Table 7.1.2). Salinity has been identified as an important factor for methane cycling since it decreases both the methanogenic activity, and the composition and diversity of archaea populations (Liu et al., 2016; Wen et al., 2017).

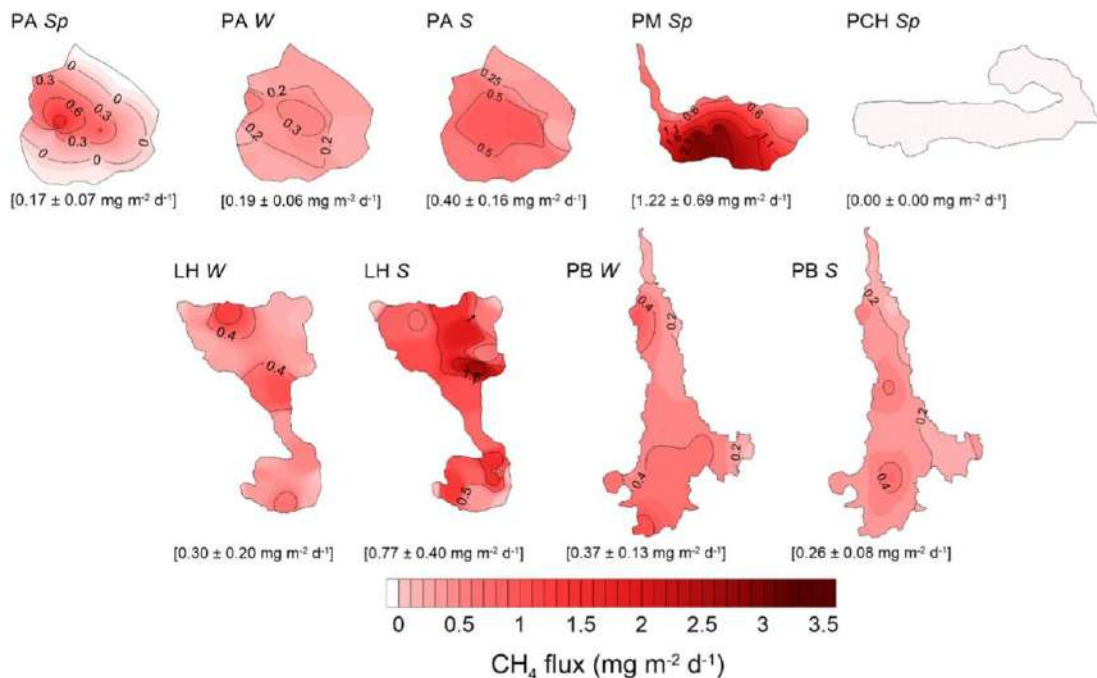


Figure 7.1.4. CH₄ fluxes contour maps for all the ponds and seasons, means are shown in brackets. The ponds are indicated as follows: PA, Poza Azul; PM, Poza Manantial; PCH, Poza Churince; LH, Los Hundidos; PB, Poza Becerra. The letters indicate the season of the campaign: spring, SP, in April 2016; winter, W, in January 2017; or summer, S, in August 2017.

Table 7.1.3. Comparative methane emissions from aquatic ecosystems.

Ecosystem	CH ₄ emission range (mg m ⁻² d ⁻¹)	Reference
Cuatro Cienegas	-0.009 – 1.04	This study
Spanish saline lakes		Camacho et al., 2017
Hypersaline	0.1 – 2.00	
Hyposaline		
Eutrophic	0.1 – 14	
Mesotrophic	0.1 – 110	
Marine	0.013 – 0.22	Bange et al., 1994
Coastal lagoons	0.01 – 240	(Chuang et al., 2017; Deborde et al., 2010; Dos Santos Fonseca et al., 2004; Hirota et al., 2007; Verma et al., 2002)
Freshwater ponds (area 0.001 – 0.01 km ²)	10.4 ± 2.6	(Holgerson and Raymond, 2016)
Oligotrophic lakes	1.08 – 4.73	Bastviken et al., 2004

The studied ponds had a mean CH₄ flux below that reported for oligotrophic boreal lakes (Bastviken et al., 2004; Rasilo et al., 2015) and arid lakes (Wen et al., 2016), but was similar to observations of both concentration and flux from an alpine lake in Colorado (Smith and Lewis, 1992). The measured CH₄ fluxes from the ponds are also well below those estimated for small lakes (0.001–0.01 km²; 10.4 ± 2.6 mg m⁻² d⁻¹; Holgerson and Raymond, 2016), a category that corresponds to the studied ponds, which is an additional evidence that salinity was a major governing parameter on CH₄ emissions. Trophic state is well-known to have a major influence on methanogenesis and CH₄ fluxes (Gonzalez-Valencia et al., 2014b; DelSontro et al., 2018), thus the relatively low CH₄ fluxes observed in the Cuatro Cienegas ponds might be a result of the combined low productivity conditions and salinity.

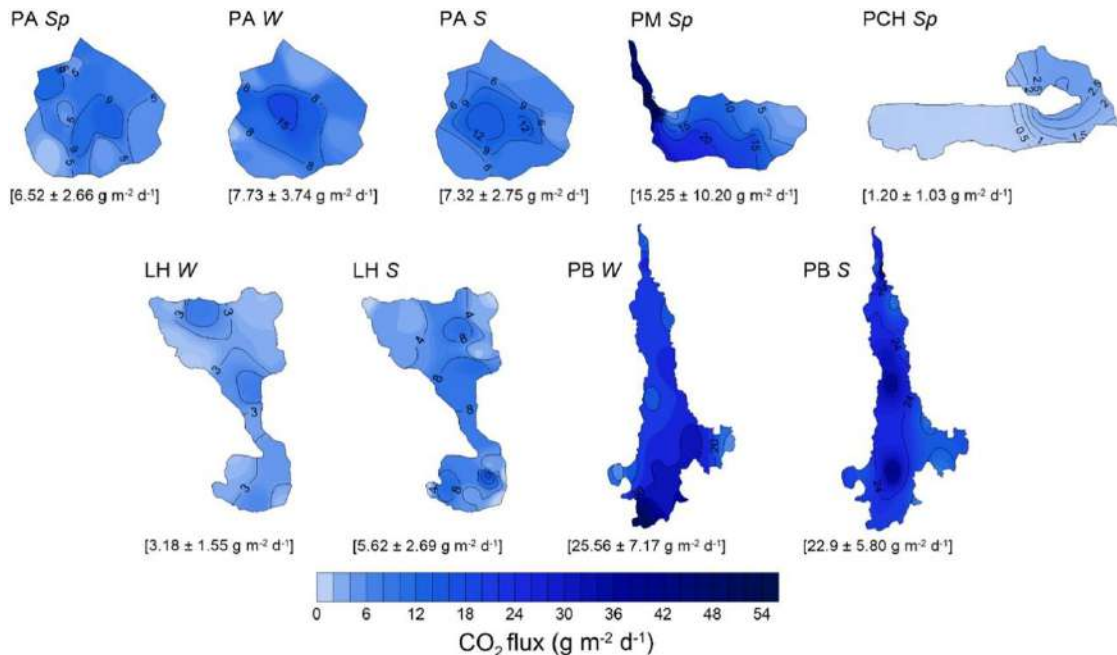


Figure 7.1.5. CO₂ fluxes contour maps for all the ponds and seasons, means are shown in brackets. The ponds are indicated as follows: PA, Poza Azul; PM, Poza Manantial; PCH, Poza Churince; LH, Los Hundidos; PB, Poza Becerra. The letters indicate the season of the campaign: spring, SP, in April 2016; winter, W, in January 2017; or summer, S, in August 2017.

All ponds showed CO₂ fluxes, with mean values ranging from 1.20 g m⁻² d⁻¹ (PCH during spring) to 25.56 g m⁻² d⁻¹ (PB during winter; Figure 7.1.5) and a range of 0.2 to 53 g m⁻² d⁻¹. No significant differences were observed among ponds when PCH was excluded ($p < 0.05$). The observed CO₂ emission rates are within the higher range of CO₂ fluxes reported for boreal lakes (2.9 to 15 g m⁻² d⁻¹; Rasilo et al., 2015) and semi-arid lakes in Northeastern China (-0.7 to 8 g m⁻² d⁻¹; Wen et al., 2016). The measured CO₂ fluxes from the Cuatro Cienegas ponds are also up to 10 times higher than those estimated for small lakes (0.001–0.01 km²; 0.93 ± 0.25 g m⁻² d⁻¹; Holgerson and Raymond, 2016). Notwithstanding, the CO₂ fluxes reported in this work are within the range previously observed in saline lakes by Duarte et al. (2008) (-12 to 137 g m⁻² d⁻¹) who suggested that saline lakes possess chemical processes that enhance CO₂ emission; via carbonate dissolution and enhanced CO₂ exchange rates at the air/water interface. Thus, compared to freshwater ecosystems, the relatively high CO₂ emissions observed in the ponds of CCB might be explained by a combined effect of high carbonate concentration and relatively high salinity. In CO₂ equivalent units, using a 34-times conversion factor for a 100-yr time-scale (Myhre et al., 2013), the mean CO₂ emissions observed in the five ponds, represents 99.87% of global GHG emissions, while CH₄ represents 0.13%.

7.1.3.4 Methane production/oxidation rates in water

The net CH₄ production/oxidation rates in water were measured in PA, LH, and PB during both seasons (Table 7.1.4). During the summer, all results indicated a net CH₄ production in the oxic water column. Several arguments support the validity of this observation: a significant difference was observed between the control samples and all of the assays ($p < 0.05$); the mean coefficient of determination (R^2) of the linear regression of CH₄ concentration was 0.92 ± 0.06 ($n = 10$, $p < 0.05$); and the mean coefficient of variation among replicates was $9.6 \pm 0.05\%$ ($n = 3$, $p < 0.05$). During winter, no

clear tendency was observed and lower R^2 values were obtained (data not shown). The difference between summer and winter might be due to differences in hydrological regimes, or any other seasonal variation in the functioning of the ponds.

Table 7.1.4. Methane production rates in the ponds during summer. R^2 indicates the coefficient of determination, which was highest for the untreated samples, evidencing biogenic CH₄ production.

Ecosystem	Sample depth	Mean net CH ₄ production ($\mu\text{g m}^{-3} \text{d}^{-1}$)	R^2
Poza Azul	Top	178 ± 9	0.95
	Bottom	177 ± 30	0.82
	Abiotic control	6 ± 2.26	0.79
Los Hundidos	Top	196 ± 16	0.92
	Bottom	196 ± 4	0.99
	Abiotic control	1.90 ± 1.50	0.56
Poza Becerra	Top	119 ± 9	0.93
	Abiotic control	-2.20 ± 2.84	0.18

Oxic CH₄ production has been previously reported in the water column of freshwater ecosystems (Bogard et al., 2014; Tang et al., 2014) but never in subsaline inland ecosystems. In terms of rates, an oxic methane production rate of $3680 \mu\text{g m}^{-3} \text{d}^{-1}$ was found in Lake Cromwell (Bogard et al., 2014), which is about twenty times higher than the average observed in the present work; i.e., $173 \mu\text{g m}^{-3} \text{d}^{-1}$. Regarding the potential mechanism of that process, Repeta et al. (2016), have shown that CH₄ supersaturation in marine oxic waters is due to the demethylation of methylphosphonate (MPn), a component found in dissolved organic matter (DOM), through the cleavage of the C:P bond, by bacteria that utilize DOM as the sole source of phosphorus. A previous report on the metagenome of microbialites present in PA has shown their metabolic capacity to produce and utilize phosphonates (Breitbart et al., 2009), as observed in marine environments. The latter suggests that the mechanism for CH₄ production found in marine oxic water may also be occurring in the ponds

of Cuatro Cienegas, although we acknowledge that a more detailed approach involving a higher spatial and temporal resolution would be required to confirm the oxic methanogenesis observed.

7.1.4 Conclusions

We reported, for the first time, the main indicators of the CH₄ cycle in ponds of the Cuatro Cienegas valley. These ecosystems showed moderate but clear CH₄ production and emission, which suggests that despite high SO₄²⁻ concentrations, methanogenesis was not completely outcompeted by sulfate reduction. Our findings along with others' (Avrahamov et al., 2015; Camacho et al., 2017; Dong et al., 2006; Zavialov et al., 2016) confirm that CH₄ production does occur in these environments, although at low rates. In contrast, CO₂ emissions were relatively higher than those usually reported for freshwater ecosystems, but within the range previously reported for saline lakes. Thus, the salinity conditions and the sulfate concentration found in CCB ponds are likely the dominant factors explaining lower CH₄ emissions and higher CO₂ emissions, compared to freshwater ponds (Duarte et al., 2008; Holgerson and Raymond, 2016; Wen et al., 2017). Saline and subsaline lakes constitute a significant proportion of the world's total lake area (around 23% or 600 × 10³ km²; Messager et al., 2016; Wurtsbaugh et al., 2017), still underrepresented in previous GHG flux estimations. Our results provide therefore additional evidence that subsaline aquatic ecosystems may play a significant role in the global emission of greenhouse gases, being CH₄ a minor component, compared to CO₂ that represented 99.8% of the total greenhouse gas emitted, expressed in CO₂ equivalent units. Finally, evidence of oxic methanogenesis was found for the first time in these subsaline environments, which may substantially modify our current understanding of CH₄ cycling. Further research adopting sampling at a high spatial resolution is required to obtain conclusive evidence of said oxic methanogenesis.

Supplementary data to this article can be found online at <https://doi.org/10.1016/j.scitotenv.2019.02.163>.

7.1.5 References

- Alcaraz, L.D., Olmedo, G., Bonilla, G., Cerritos, R., Hernández, G., Cruz, A., Ramírez, E., Putonti, C., Jiménez, B., Martínez, E., López, V., Arvizu, J.L., Ayala, F., Razo, F., Caballero, J., Siefert, J., Eguiarte, L., Vielle, J.-P., Martínez, O., Souza, V., Herrera- Estrella, A., Herrera- Estrella, L., 2008. The genome of *Bacillus coahuilensis* reveals adaptations essential for survival in the relic of an ancient marine environment. Proc. Natl. Acad. Sci. U. S. A. 105, 5803–5808. <https://doi.org/10.1073/pnas.0800981105>.
- Alcaraz, L., Moreno-Hagelsieb, G., Eguiarte, L.E., Souza, V., Herrera-Estrella, L., Olmedo, G., 2010. Understanding the evolutionary relationships and major traits of *Bacillus*; through comparative genomics. BMC Genomics 11, 1–17. <https://doi.org/10.1186/1471-2164-11-332>.
- Alcocer, J., Hammer, U.T., 1998. Saline lake ecosystems of Mexico. Aquat. Ecosyst. Health Manag. 1, 291–315. <https://doi.org/10.1080/14634989808656925>.
- APHA, AWWA, WEF, 2012. Standard methods for the examination of water and wastewater. 22nd ed. American Public Health Association, Washington, D.C.
- Avrahamov, N., Gelman, F., Yechieli, Y., Aizenshtat, Z., Nissenbaum, A., Sivan, O., 2015. Proposed sources of methane along the Dead Sea Transform. Chem. Geol. 395, 165–175. <https://doi.org/10.1016/j.chemgeo.2014.11.026>.

Babkin, V.I., Klige, R.K., Vuglinsky, V.S., 2003. The Earth and its physical features. In: Shiklomanov, I.A., Rodda, J. (Eds.), *World Water Resources at the Beginning of the Twenty-First Century*. Cambridge University Press, Cambridge, pp. 1–18.

Bange, H.W., Bartell, U.H., Rapsomanikis, S., Andreae, M.O., 1994. Methane in the Baltic and North Seas and a reassessment of the marine emissions of methane. *Glob. Biogeochem. Cycles* 8, 465–480. <https://doi.org/10.1029/94gb02181>.

Bastviken, D., Cole, J., Pace, M., Tranvik, L., 2004. Methane emissions from lakes: dependence of lake characteristics, two regional assessments, and a global estimate. *Glob. Biogeochem. Cycles* 18, 1–12. <https://doi.org/10.1029/2004GB002238>.

Bastviken, D., Tranvik, L.J., Downing, J.A., Crill, P.M., Enrich-Prast, A., 2011. Freshwater methane emissions offset the continental carbon sink. *Science* 6031, 331, 50. <https://doi.org/10.1126/science.1196808>.

Bogard, M.J., del Giorgio, P.A., Boutet, L., Chaves, M.C.G., Prairie, Y.T., Merante, A., Derry, A.M., 2014. Oxic water column methanogenesis as a major component of aquatic CH₄ fluxes. *Nat. Commun.* 5, 5350. <https://doi.org/10.1038/ncomms6350>.

Breitbart, M., Hoare, A., Nitti, A., Siefert, J., Haynes, M., Dinsdale, E., Edwards, R., Souza, V., Rohwer, F., Hollander, D., 2009. Metagenomic and stable isotopic analyses of modern freshwater microbialites in Cuatro Ciénegas, Mexico. *Environ. Microbiol.* 11, 16–34. <https://doi.org/10.1111/j.1462-2920.2008.01725.x>.

Camacho, A., Picazo, A., Rochera, C., Santamans, A.C., Morant, D., Miralles-Lorenzo, J., Castillo-Escrivà, A., 2017. Methane emissions in Spanish Saline Lakes: current rates, temperature

and salinity responses, and evolution under different climate change scenarios. *Water* 9, 659. <https://doi.org/10.3390/w9090659>.

Cerritos, R., Eguiarte, L.E., Avitia, M., Siefert, J., Travisano, M., Rodríguez-Verdugo, A., Souza, V., 2011. Diversity of culturable thermo-resistant aquatic bacteria along an environmental gradient in Cuatro Ciénegas, Coahuila, México. *Antonie Van Leeuwenhoek* 99, 303–318. <https://doi.org/10.1007/s10482-010-9490-9>.

Chuang, P.-C., Young, M.B., Dale, A.W., Miller, L.G., Herrera-Silveira, J.A., Paytan, A., 2017. Methane fluxes from tropical coastal lagoons surrounded by mangroves, Yucatán, Mexico. *J. Geophys. Res. Biogeosci.* 122, 1156–1174. <https://doi.org/10.1002/2017JG003761>.

Cole, J.J., Prairie, Y.T., Caraco, N.F., McDowell, W.H., Tranvik, L.J., Striegl, R.G., Duarte, C.M., Kortelainen, P., Downing, J.A., Middelburg, J.J., Melack, J., 2007. Plumbing the global carbon cycle: integrating inland waters into the terrestrial carbon budget. *Ecosystems* 10, 172–185. <https://doi.org/10.1007/s10021-006-9013-8>.

Corman, J.R., Poret-Peterson, A.T., Uchitel, A., Elser, J.J., 2016. Interaction between lithification and resource availability in the microbialites of Río Mesquites, Cuatro Ciénegas, México. *Geobiology* 14, 176–189. <https://doi.org/10.1111/gbi.12168>.

Deborde, J., Anschutz, P., Guérin, F., Poirier, D., Marty, D., Boucher, G., Thouzeau, G., Canton, M., Abril, G., 2010. Methane sources, sinks and fluxes in a temperate tidal Lagoon: the Arcachon lagoon (SW France). *Estuar. Coast. Shelf Sci.* 89, 256–266. <https://doi.org/10.1016/j.ecss.2010.07.013>.

DelSontro, T., Beaulieu, J.J., Downing, J.A., 2018. Greenhouse gas emissions from lakes and impoundments: upscaling in the face of global change. *Limnol. Oceanogr. Lett.* 3, 64–75. <https://doi.org/10.1002/lol2.10073>.

Desnues, C., Rodriguez-Brito, B., Rayhawk, S., Kelley, S., Tran, T., Haynes, M., Liu, H., Furlan, M., Wegley, L., Chau, B., Ruan, Y., Hall, D., Angly, F.E., Edwards, R.A., Li, L., Thurber, R.V., Reid, R.P., Siefert, J., Souza, V., Valentine, D.L., Swan, B.K., Breitbart, M., Rohwer, F., 2008. Biodiversity and biogeography of phages in modern stromatolites and thrombolites. *Nature* 452, 340–343. <https://doi.org/10.1038/nature06735>.

Dong, H., Zhang, G., Jiang, H., Yu, B., Chapman, L.R., Lucas, C.R., Fields, M.W., 2006. Microbial diversity in sediments of Saline Qinghai Lake, China: linking geochemical controls to microbial ecology. *Microb. Ecol.* 51, 65–82. <https://doi.org/10.1007/s00248-005-0228-6>.

Dos Santos Fonseca, A.L., Minello, M., Marinho, C.C., Esteves, F. de A., 2004. Methane concentration in water column and in pore water of a coastal lagoon (Cabiúnas lagoon, Macaé, RJ, Brazil). *Braz. Arch. Biol. Technol.* 47, 301–308. <https://doi.org/10.1590/S1516-89132004000200018>.

Downing, J.A., Duarte, C.M., 2006. Abundance and size distribution of lakes, ponds and impoundments. *Limnol. Oceanogr.* 51, 2388–2397. <https://doi.org/10.1016/B978-0-12-409548-9.03867-7>.

Duarte, C.M., Prairie, Y.T., Montes, C., Cole, J.J., Striegl, R., Melack, J., Downing, J.A., 2008. CO₂ emissions from saline lakes: a global estimate of a surprisingly large flux. *J. Geophys. Res. Biogeosci.* 113, 1–7. <https://doi.org/10.1029/2007JG000637>.

Duchemin, E., Lucotte, M., Canuel, R., 1999. Comparison of static chamber and thin boundary layer equation methods for measuring greenhouse gas emissions from large water bodies. Environ. Sci. Technol. 33, 350–357. <https://doi.org/10.1021/es9800840>.

Dupraz, C., Reid, R.P., Braissant, O., Decho, A.W., Norman, R.S., Visscher, P.T., 2009. Processes of carbonate precipitation in modern microbial mats. Earth Sci. Rev. 96, 141–162. <https://doi.org/10.1016/j.earscirev.2008.10.005>.

Elser, J.J., Schampel, J.H., Garcia-Pichel, F., Wade, B.D., Souza, V., Eguiarte, L., Escalante, A., Farmer, J.D., 2005. Effects of phosphorus enrichment and grazing snails on modern stromatolitic microbial communities. Freshw. Biol. 50, 1808–1825. <https://doi.org/10.1111/j.1365-2427.2005.01451.x>.

Escalante, A.E., Eguiarte, L.E., Espinosa-Asuar, L., Forney, L.J., Noguez, A.M., Souza Saldivar, V., 2008. Diversity of aquatic prokaryotic communities in the Cuatro Cienegas basin. FEMS Microbiol. Ecol. 65, 50–60. <https://doi.org/10.1111/j.1574-6941.2008.00496.x>.

Gonzalez-Valencia, R., Magana-Rodriguez, F., Gerardo-Nieto, O., Sepulveda-Jauregui, A., Martinez-Cruz, K., Walter Anthony, K., Baer, D., Thalasso, F., 2014a. In situ measurement of dissolved methane and carbon dioxide in freshwater ecosystems by off-axis integrated cavity output spectroscopy. Environ. Sci. Technol. 48, 11421–11428. <https://doi.org/10.1021/es500987j>.

Gonzalez-Valencia, R., Sepulveda-Jauregui, A., Martinez-Cruz, K., Hoyos-Santillan, J., Dendooven, L., Thalasso, F., 2014b. Methane emissions from Mexican freshwater bodies: correlations with water pollution. Hydrobiologia 721, 9–22. <https://doi.org/10.1007/s10750-013-1632-4>.

Hammer, U.T., 1986. Classification of inland saline waters. In: Dumont, H.J. (Ed.), Saline Lake Ecosystems of the World. Dr. W Junk Publishers, Dordrecht, Boston, Lancaster, pp. 9–15.

Harriss, R.C., Sebacher, D.I., 1981. Methane flux in forested freshwater swamps of the southeastern United States. *Geophys. Res. Lett.* 8 (9), 1002–1004.

Hirota, M., Senga, Y., Seike, Y., Nohara, S., Kunii, H., 2007. Fluxes of carbon dioxide, methane and nitrous oxide in two contrastive fringing zones of coastal lagoon, Lake Nakumi, Japan. *Chemosphere* 68, 597–603. <https://doi.org/10.1016/j.chemosphere.2007.01.002>. Holgerson, M.A., Raymond, P.A., 2016. Large contribution to inland water CO₂ and CH₄ emissions from very small ponds. *Nat. Geosci.* 9, 222–226. <https://doi.org/10.1038/ngeo2654>.

Holmer, M., Storkholm, P., 2001. Sulphate reduction and sulphur cycling in lake sediments: a review. *Freshw. Biol.* 46, 431–451. <https://doi.org/10.1046/j.1365-2427.2001.00687.x>.

INE-SEMARNAP, 1999. Programa de Manejo del Área de Protección de Flora y Fauna Cuatrociénegas.

Johannesson, K.H., Cortés, A., Kilroy, K.C., 2004. Reconnaissance isotopic and hydrochemical study of Cuatro Ciénegas groundwater, Coahuila, México. *J. S. Am. Earth Sci.* 17, 171–180. <https://doi.org/10.1016/j.jsames.2004.01.002>.

Kankaala, P., Huotari, J., Peltomaa, E., Saloranta, T., Ojala, A., 2006. Methanotrophic activity in relation to methane efflux and total heterotrophic bacterial production in a stratified, humic, boreal lake. *Limnol. Oceanogr.* 51, 1195–1204. <https://doi.org/10.4319/lo.2006.51.2.1195>.

Kirschke, S., Bousquet, P., Ciais, P., Saunois, M., Canadell, J.G., Dlugokencky, E.J., Bergamaschi, P., Bergmann, D., Blake, D.R., Bruhwiler, L., Cameron-Smith, P., Castaldi, S., Chevallier, F., Feng, L., Fraser, A., Heimann, M., Hodson, E.L., Houweling, S., Josse, B., Fraser, P.J., Krummel, P.B., Lamarque, J.F., Langenfelds, R.L., Le Quéré, C., Naik, V., O'doherty, S., Palmer, P.I., Pison, I., Plummer, D., Poulter, B., Prinn, R.G., Rigby, M., Ringeval, B., Santini, M., Schmidt, M., Shindell, D.T., Simpson, I.J., Spahni, R., Steele, L.P., Strode, S.A., Sudo, K., Szopa, S., Van Der Werf, G.R., Voulgarakis, A., Van Weele, M., Weiss, R.F., Williams, J.E., Zeng, G., 2013. Three decades of global methane sources and sinks. *Nat. Geosci.* 6, 813–823. <https://doi.org/10.1038/ngeo1955>.

Kornfield, I., Smith, D.C., Gagnon, P.S., Taylor, J.N., 1982. The cichlid fish of Cuatro Cienegas, Mexico: direct evidence of conspecificity among distinct trophic morphs. *Evolution* 36, 658. <https://doi.org/10.2307/2407880> N. Y.

Koyama, T., 1963. Gaseous metabolism in lakes sediments and paddy soils and the production of atmospheric methane and hydrogen. *J. Geophys. Res.* 68 (13), 3971–3973. Leal Nares, A., Rendón Herrera, G., Carrillo Buentello, V.P., de la Maza Benignos, M., 2018. Seguridad Hídrica del Valle de Cuatro Ciénegas: Un Análisis de las Concesiones Subterráneas, Volúmenes y usos del Agua de Cuatro Ciénegas, Coahuila, México (Coahuila).

Liotta, M., Martelli, M., 2012. Dissolved gases in brackish thermal waters: an improved analytical method. *Geofluids* 12, 236–244. <https://doi.org/10.1111/j.1468-8123.2012.00365.x>.

Liu, Y., Priscu, J.C., Xiong, J., Conrad, R., Vick-Majors, T., Chu, H., Hou, J., 2016. Salinity drives archaeal distribution patterns in high altitude lake sediments on the Tibetan Plateau. *FEMS Microbiol. Ecol.* 92, 1–10. <https://doi.org/10.1093/femsec/fiw033>.

Marcé, R., Obrador, B., Morguí, J.A., Lluís Riera, J., López, P., Armengol, J., 2015. Carbonate weathering as a driver of CO₂ supersaturation in lakes. *Nat. Geosci.* 8, 107–111. <https://doi.org/10.1038/ngeo2341>.

McMahon, P.B., Chapelle, F.H., 2008. Redox processes and water quality of selected principal aquifer systems. *Ground Water* 46, 259–271. <https://doi.org/10.1111/j.1745-6584.2007.00385.x>.

Messager, M.L., Lehner, B., Grill, G., Nedeva, I., Schmitt, O., 2016. Estimating the volume and age of water stored in global lakes using a geo-statistical approach. *Nat. Commun.* 7, 13603. <https://doi.org/10.1038/ncomms13603>.

Minckley, W.L., Cole, G.A., 1968. Preliminary limnologic information on waters of the Cuatro Cienegas Basin, Coahuila, Mexico. Southwest. *Nat.* 421–431.

Myhre, G., Shindell, D., Bréon, F.-M., Collins, W., Fuglestvedt, J., Huang, J., Koch, D., Lamarque, J.F., Lee, D., Mendoza, B., Nakajima, T., Robock, A., Stephens, G., Takemura, T., Zhang, H., 2013. Climate Change 2013 - The Physical Science Basis. Cambridge University Press, Cambridge <https://doi.org/10.1017/CBO9781107415324>.

Natchimuthu, S., Sundgren, I., Gålfalk, M., Klemedtsson, L., Crill, P., Danielsson, Å., Bastviken, D., 2016. Spatio-temporal variability of lake CH₄fluxes and its influence on annual whole lake emission estimates. *Limnol. Oceanogr.* 61, S13–S26. <https://doi.org/10.1002/lno.10222>.

Okabe, S., Characklis, W.G., 1992. Effects of temperature and phosphorous concentration on microbial sulfate reduction by *Desulfovibrio desulfuricans*. *Biotechnol. Bioeng.* 39, 1031–1042. <https://doi.org/10.1002/bit.260391007>.

Oremland, R.S., Polcin, S., 1983. Methanogenesis and sulfate reduction: competitive and noncompetitive substrates in estuarine sediments. *Deep Sea Res. Part B. Oceanogr. Lit. Rev.* 30, 470. [https://doi.org/10.1016/0198-0254\(83\)90262-5](https://doi.org/10.1016/0198-0254(83)90262-5).

Rasilo, T., Prairie, Y.T., del Giorgio, P.A., 2015. Large-scale patterns in summer diffusive CH₄ fluxes across boreal lakes, and contribution to diffusive C emissions. *Glob. Chang. Biol.* 21, 1124–1139. <https://doi.org/10.1111/gcb.12741>.

Repeta, D.J., Ferrón, S., Sosa, O.A., Johnson, C.G., Repeta, L.D., Acker, M., DeLong, E.F., Karl, D.M., 2016. Marine methane paradox explained by bacterial degradation of dissolved organic matter. *Nat. Geosci.* 9, 884–887. <https://doi.org/10.1038/ngeo2837>.

Saunois, M., Bousquet, P., Poulter, B., Peregon, A., Ciais, P., Canadell, J.G., Dlugokencky, E.J., Etiope, G., Bastviken, D., Houweling, S., Janssens-Maenhout, G., Tubiello, F.N., Castaldi, S., Jackson, R.B., Alexe, M., Arora, V.K., Beerling, D.J., Bergamaschi, P., Blake, D.R., Brailsford, G., Brovkin, V., Bruhwiler, L., Crevoisier, C., Crill, P., Covey, K., Curry, C., Frankenberg, C., Gedney, N., Höglund-Isaksson, L., Ishizawa, M., Ito, A., Joos, F., Kim, H.S., Kleinen, T., Krummel, P., Lamarque, J.F., Langenfelds, R., Locatelli, R., Machida, T., Maksyutov, S., McDonald, K.C., Marshall, J., Melton, J.R., Morino, I., Naik, V., O'Doherty, S., Parmentier, F.J.W., Patra, P.K., Peng, C., Peng, S., Peters, G.P., Pison, I., Prigent, C., Prinn, R., Ramonet, M., Riley, W.J., Saito, M., Santini, M., Schroeder, R., Simpson, I.J.,

Spahni, R., Steele, P., Takizawa, A., Thornton, B.F., Tian, H., Tohjima, Y., Viovy, N., Voulgarakis, A., Van Weele, M., Van Der Werf, G.R., Weiss, R., Wiedinmyer, C., Wilton, D.J., Wiltshire, A., Worthy, D., Wunch, D., Xu, X., Yoshida, Y., Zhang, B., Zhang, Z., Zhu, Q., 2016. The global methane budget 2000–2012. *Earth Syst. Sci. Data* 8, 697–751. <https://doi.org/10.5194/essd-8-697-2016>.

Savvaitova, K., Petr, T., 1992. Lake Issyk-kul, Kirgizia. *Int. J. Salt Lake Res.* 1, 21–46. <https://doi.org/10.1007/BF02904361>.

Schink, B., Stams, A.J.M., 2013. Syntrophism among prokaryotes. In: Rosenberg, E., DeLong, E.F., Lory, S., Stackebrandt, E., Thompson, F. (Eds.), *The Prokaryotes*. Springer Berlin Heidelberg, Berlin, Heidelberg, pp. 471–493 https://doi.org/10.1007/978-3-642-30123-0_59.

Sela-Adler, M., Ronen, Z., Herut, B., Antler, G., Vigderovich, H., Eckert, W., Sivan, O., 2017. Co-existence of methanogenesis and sulfate reduction with common substrates in sulfate-rich estuarine sediments. *Front. Microbiol.* 8, 1–11. <https://doi.org/10.3389/fmicb.2017.00766>.

Sistema Meteorológico Nacional, 2011. Información Climatológica por Estado [WWW Document]. URL <http://smn.cna.gob.mx/es/informacion-climatologica-ver-estado?estado=coah> (accessed 7.30.18).

Smith, L.K., Lewis, W.M., 1992. Seasonality of methane emissions from five lakes and associated wetlands of the Colorado Rockies. *Glob. Biogeochem. Cycles* 6, 323–338. <https://doi.org/10.1029/92GB02016>.

Souza, V., Espinosa-Asuar, L., Escalante, A.E., Eguiarte, L.E., Farmer, J., Forney, L., Lloret, L., Rodriguez-Martinez, J.M., Soberon, X., Dirzo, R., Elser, J.J., 2006. An endangered oasis of aquatic

microbial biodiversity in the Chihuahuan desert. Proc. Natl. Acad. Sci. 103, 6565–6570. <https://doi.org/10.1073/pnas.0601434103>.

Souza, V., Siefert, J.L., Escalante, A.E., Elser, J.J., Eguiarte, L.E., 2012. The Cuatro Ciénegas Basin in Coahuila, Mexico: an astrobiological Precambrian park. Astrobiology 12, 641–647. <https://doi.org/10.1089/ast.2011.0675>.

Souza, V., Moreno-Letelier, A., Travisano, M., Alcaraz, L.D., Olmedo, G., Eguiarte, L.E., 2018. The lost world of Cuatro Ciénegas Basin, a relictual bacterial niche in a desert oasis. eLife 7. <https://doi.org/10.7554/eLife.38278>.

Stenger-Kovács, C., Lengyel, E., Buczkó, K., Tóth, F., Crossetti, L., Pellinger, A., Zámbóné Doma, Z., Padisák, J., 2014. Vanishing world: alkaline, saline lakes in Central Europe and their diatom assemblages. Inl. Waters 4, 383–396. <https://doi.org/10.5268/IW- 4.4.722>.

Taboada, B., Isa, P., Gutiérrez-Escobano, A.L., del Ángel, R.M., Ludert, J.E., Vázquez, N., Tapia-Palacios, M.A., Chávez, P., Garrido, E., Espinosa, A.C., Eguiarte, L.E., López, S., Souza, V., Arias, C.F., 2018. The geographic structure of viruses in the Cuatro Ciénegas Basin, a unique oasis in northern Mexico, reveals a highly diverse population on a small geographic scale. Appl. Environ. Microbiol. 84. <https://doi.org/10.1128/AEM.00465-18>.

Tang, K.W., McGinnis, D.F., Frindte, K., Brüchert, V., Grossart, H.-P., 2014. Paradox reconsidered: methane oversaturation in well-oxygenated lake waters. Limnol. Oceanogr. 59, 275–284. <https://doi.org/10.4319/lo.2014.59.1.0275>.

Taylor, D.W., 1966. A remarkable snail fauna from Coahuila, Mexico, The veliger.

Verma, A., Subramanian, V., Ramesh, R., 2002. Methane emissions from a coastal lagoon: Vembanad Lake, West Coast, India. *Chemosphere* 47, 883–889.

Verpoorter, C., Kutser, T., Seekell, D.A., Tranvik, L.J., 2014. A global inventory of lakes based on high-resolution satellite imagery. *Geophys. Res. Lett.* 41, 6396–6402. <https://doi.org/10.1002/2014GL060641>.

Wen, Z., Song, K., Zhao, Y., Jin, X., 2016. Carbon dioxide and methane supersaturation in lakes of semi-humid/semi-arid region, Northeastern China. *Atmos. Environ.* 138, 65–73. <https://doi.org/10.1016/j.atmosenv.2016.05.009>.

Wen, X., Yang, S., Horn, F., Winkel, M., Wagner, D., Liebner, S., 2017. Global biogeographic analysis of methanogenic archaea identifies community-shaping environmental factors of natural environments. *Front. Microbiol.* 8, 1–13. <https://doi.org/10.3389/fmicb.2017.01339>.

Whitman, W.B., Bowen, T.L., Boone, D.R., 2006. The methanogenic bacteria. In: Dworkin, M., Falkow, S., Rosenberg, E., Schleifer, K.-H., Stackebrandt, E. (Eds.), *Prokaryotes*. Springer New York, New York, NY, pp. 165–207 <https://doi.org/10.1007/0-387-30742-7>.

Williams, W.D., 2002. Environmental threats to salt lakes and the likely status of inland saline ecosystems in 2025. *Environ. Conserv.* 29, 154–167. <https://doi.org/10.1017/S0376892902000103>.

Willmott, C.J., Matsuura, K., 2006. On the use of dimensioned measures of error to evaluate the performance of spatial interpolators. *Int. J. Geogr. Inf. Sci.* 20, 89–102. <https://doi.org/10.1080/13658810500286976>.

Wolaver, B., 2008. Hydrogeology of the Cuatrocienegas Basin, Coahuila, Mexico: An Integrative Approach to Arid Karst Aquifer Delineation. The University of Texas at Austin. Wolaver, B.D., Sharp, J.M., Rodriguez, J.M., Ibarra Flores, J.C., 2008. Delineation of regional arid karstic aquifers: an integrative data approach. *Ground Water* 46, 396–413.

<https://doi.org/10.1111/j.1745-6584.2007.00405.x>.

Wolaver, B.D., Crossey, L.J., Karlstrom, K.E., Banner, J.L., Cardenas, M.B., Ojeda, C.G., Sharp, J.M., 2013. Identifying origins of and pathways for spring waters in a semiarid basin using He, Sr, and C isotopes: Cuatrocienegas Basin, Mexico. *Geosphere* 9, 113–125.

<https://doi.org/10.1130/GES00849.1>.

Wurtsbaugh, W.A., Miller, C., Null, S.E., DeRose, R.J., Wilcock, P., Hahnenberger, M., Howe, F., Moore, J., 2017. Decline of the world's saline lakes. *Nat. Geosci.* 10, 816–821.

<https://doi.org/10.1038/ngeo3052>.

Zavialov, P., Makkaveev, P., Rimskiy-Korsakov, N., Alymkulov, S., Izhitskiy, A., 2016. Hydrophysical and hydrochemical features of Lake Issyk-Kul (Kyrgyzstan) as revealed by field survey of June, 2015, in: EGU General Assembly Conference Abstracts. p. 4697.

7.2 Dinámica espaciotemporal global de la dinámica de gases de efecto invernadero y oxígeno de dos reservorios subtropicales con estados tróficos contrastantes

Artículo sometido a Water Research

Resumen

Se evaluó el impacto de la eutrofización cultural en el ciclo del carbono en reservorios subtropicales utilizando mediciones de alta resolución de concentración de gases disueltos, intercambio atmosférico y tasas de consumo/producción de metano, dióxido de carbono y oxígeno. Se realizaron mediciones estacionales en dos reservorios que pertenecen a la misma cuenca hidrológica, pero que son drásticamente diferentes en cuanto al carbono alóctono que reciben.

Estos resultados fueron utilizados para alimentar un modelo de balance de masa, del cual un gran número de parámetros globales fueron determinados. Se seleccionaron 22 de estos parámetros por su potencial para describir explícitamente la dinámica y atributos espaciales del ciclo del carbono en los reservorios. Se creó una representación gráfica para facilitar la apreciación global y contraste del ciclo del carbono. El impacto de la eutrofización cultural fue profundo y resultó en una completa redistribución de los diversos bioprocesos que participan en los ciclos del metano, dióxido de carbono y oxígeno. Dentro de los diferentes impactos de la eutrofización, se observó que el efecto sobre el ciclo del metano fue compensado por un aumento relativamente moderado en las emisiones de metano y las tasas de metanotrofía, mientras que la producción primaria fue limitada.

Overall spatiotemporal dynamics of greenhouse gases and oxygen in two subtropical reservoirs with contrasting trophic states

Teresa Aguirrezabala-Campano¹, Rodrigo Gonzalez-Valencia¹, Francisco J. Cervantes², and Frédéric Thalasso¹

¹ Department of Biotechnology and Bioengineering, Cinvestav, Avenida IPN 2508, Mexico City, San Pedro Zacatenco, 07360, Mexico.

² Laboratory for Research on Advanced Processes for Water Treatment, Engineering Institute, Campus Juriquilla, Universidad Nacional Autónoma de México, Blvd. Juriquilla 3001, Querétaro, 76230, Mexico

Abstract

The impact of cultural eutrophication on carbon cycling in subtropical reservoirs was assessed using high-resolution measurements of dissolved gas concentration, atmospheric exchange, and uptake/production rates of methane, carbon dioxide, and oxygen. Seasonal measurements were performed in two reservoirs that pertain to the same hydrological basin but are drastically different in terms of allochthonous carbon input. These results were used to feed a mass balance model, from which a large number of overall parameters were determined. A total of 22 of these parameters were selected for their potential to explicitly describe the dynamics and spatial attributes of the carbon cycle in the reservoirs. A single graphical representation of each reservoir was created to facilitate an overall appraisal and contrast of the carbon cycle. The impact of cultural eutrophication was profound and resulted in a complete redistribution of how the various bioprocesses participated in the methane, carbon dioxide, and oxygen cycles. Among

several identified impacts of eutrophication, it was observed that the trigger effect on the methane cycle was compensated by a relatively moderate increase in methane emissions and methanotrophic rates, while gross primary production was depleted.

7.2.1 Introduction

Despite their relatively small contribution to the global landscape, freshwater ecosystems have been identified as an important natural source of methane (CH_4) and carbon dioxide (CO_2), which act as greenhouse gases (GHG) when released into the atmosphere (Tranvik et al., 2009). Many processes are involved in the carbon cycle, and they directly impact the GHG emissions from lakes and reservoirs. Among these, CH_4 production (methanogenesis) and CH_4 oxidation (methanotrophy) are the dominant bioprocesses involved in CH_4 emissions, while primary production and heterotrophic respiration are those most closely related to CO_2 emissions. These processes interact and create a complex metabolic network that is regulated, to a great extent, by the availability of oxygen (O_2), CH_4 , and CO_2 , together with nutrient and organic carbon concentrations as well as physicochemical conditions. The complexity of carbon cycling explains the high variability usually observed, not only among water bodies but also within a given ecosystem.

The characterization and comparison of aquatic ecosystems is therefore a difficult task, often simplified through mass balances and/or the use of overall parameters that numerically describe a given feature of the studied ecosystem. The mass balance approach consists of describing the overall carbon cycle in an ecosystem by a grey model fed with a limited number of interconnected processes. By closing the mass balance, some individual processes, which could otherwise not be determined experimentally, can be derived. An example of this approach has

been given by Santoso et al. (2020), who determined the dynamics of CH₄ and CO₂ storage in a eutrophic, monomictic lake. In the same context, overall parameters usually link several components of the studied cycles that are relevant to a given feature. Among these, some examples are: (i) the trophic state index (TSI); (ii) the net ecosystem productivity (NEP), which indicates whether the ecosystem is predominantly autotrophic or heterotrophic (Lovett et al., 2006); (iii) the proportion of gross primary production (GPP) or NEP that is lost as GHG (Whiting and Chanton, 1993); (iv) the mean oxidation-reduction potential, which defines whether oxidative or reductive processes predominate in the ecosystem (McMahon and Chapelle, 2008); (v) the sestonic C:N:P proportion that provides insights into the biological processes; and (vi) the homogeneity and anisotropic factors that describe the spatiotemporal distribution of a given parameter (Gonzalez-Valencia et al., 2019).

However, despite an extensive literature on carbon cycling in lakes and reservoirs, most of the reports present an in-depth analysis of either a single component or a reduced number of the carbon cycle components (Li et al., 2020; Santoso et al., 2020). In this context, the objective of the present work was to perform a comprehensive spatiotemporal analysis of the carbon cycle in subtropical reservoirs, including as many overall parameters as possible, all of them determined from high resolution measurements of CH₄, CO₂, and O₂. For each of these molecules, a global mass balance was established, including emissions to/from the atmosphere, primary production, methanogenesis, methanotrophy, and heterotrophic respiration. Finally, the overall parameters and the mass balances were coupled with spatiotemporal attributes into a single graphical representation. This strategy was used to assess the impact of anthropogenic pollution on the carbon cycle in two reservoirs that pertain to the same hydrological basin but are drastically different in terms of allochthonous carbon input. One reservoir is in a natural

protected area, while the other is located in an urban area and has a high input of untreated wastewater.

7.2.2 Materials and methods

7.2.2.1 Site description and sampling campaigns

Two subtropical reservoirs that belong to the same hydrological basin located close to Mexico City were selected: “Lago de Guadalupe” (LG; 19.6333, -99.2602) and “Lago El Llano” (LL; 19.6582, -99.5071). The former is a dendritic reservoir with an area of 450 ha and is located 2300 m above sea level. LG receives an estimated flow of $0.5 \text{ m}^3 \text{ s}^{-1}$ of untreated wastewater from the surrounding densely populated urban areas (Sepulveda-Jauregui et al., 2013). Contrastingly, LL is a U-shaped 6 ha reservoir situated 2840 m above sea level in a protected area that receives water from springs and a pristine tributary river. Both reservoirs have a subtropical climate of warm summers and mild winters with an average annual air temperature of 17°C and 15°C for LG and LL, respectively. Six monitoring and sampling stations (MSS) were established in LG, and five were set up in LL (Figure 7.2.1). Since LG is characterized by a clear longitudinal zonation, the MSS locations were selected to cover the fluvial and lacustrine zones, i.e. southwest to northeast. In LL, the MSS were distributed to cover both arms of the U-shape. Both reservoirs were monitored in August 2018, January 2019, and May 2019, which correspond to the three annual seasons of the area, i.e. mild and rainy (wet), cold and dry (dry cold), and warm and dry (dry hot), respectively.

7.2.2.2 Limnological characteristics

Temperature, pH, and oxidation-reduction potential (ORP) were measured at each MSS with a multi-parametric probe (HI 9828, Hanna Instruments, Mexico) from the surface to the sediments at depth intervals of 0.25 m. Surface water samples were taken from each MSS; additional water samples were taken at 1-m depth intervals from the surface to the bottom at LG-6 (Figure 7.2.1A) and LL-4 (Figure 7.2.1B). The water samples were collected with a horizontal 2.2-L Van Dorn bottle (Wildco, Mexico) and handled according to standard methods (APHA et al., 2012); they were used to determine the total organic carbon (TOC), total nitrogen (TN), and orthophosphate (PO_4^{3-}) concentrations. TOC and TN were determined using a Shimadzu TOC Analyzer equipped with a total nitrogen module (Model TOC-Vcn + TNM), whereas PO_4^{3-} concentrations were determined with a colorimetric standard method (APHA et al., 2012). Secchi depth (SD) was determined with a 0.2 m Secchi disk at each MSS.

These measurements were used to establish the trophic state of each lake, according to Wetzel (2001) and Carlson (1977). The thermocline depth and the Schmidt stability, which indicates the resistance to mechanical mixing due to stratification, were obtained from temperature profiles, using the *rLakeAnalyzer* package (Winslow et al., 2019) of R software version 3.6.2 (R Core Team, 2019).

7.2.2.3 Fluxes of greenhouse gases

We used the floating static chamber (SC) method to measure CH_4 and CO_2 fluxes. The SC was connected to an ultraportable greenhouse gas analyzer (UGGA, Los Gatos Research, USA) in a closed circuit. A continuous five-minute measurement was used to determine diffusive fluxes from CH_4 and CO_2 concentrations; the first 30 s after positioning the SC on the water surface

were discarded. Each flux determination was done in triplicate with a measurement/data logging frequency of 1 Hz. In some cases, ebullitive events occurred while measuring fluxes. In order to filter these, a threshold was set to differentiate diffusive and ebullitive emissions; i.e. an abrupt increase of concentration at least five times higher than the linear slope observed during diffusive fluxes and for five seconds or more. The total flux was defined as the mean concentration slope of the entire measurement, whereas the ebullitive flux was defined as the difference between the total flux and the diffusive flux.

The O₂ flux was determined theoretically by using an approach similar to Jähne et al. (1987) and Wanninkhof (2014); here, measured CO₂ fluxes ($F_{CO_2}^*$) were used to determine the O₂ mass transfer coefficient of the boundary layer. In this approach, CO₂ fluxes were preferred over CH₄ given that CO₂ was emitted only via diffusion. Briefly, O₂ fluxes (F_{O_2}) were calculated as follows:

$$F_{O_2} = k_{O_2} \cdot H_{O_2} \cdot (p_{O_2,w} - p_{O_2,air}) \quad (1)$$

where k_{O_2} is the O₂ mass transfer coefficient (m h⁻¹, see below), H_{O_2} is the Henry constant for O₂ (mole m⁻³ atm; Sander, 2017), $p_{O_2,w}$ and $p_{O_2,air}$ are the partial pressure of dissolved oxygen (DO) measured in the surface water and in the atmosphere (atm), respectively.

To determine k_{O_2} , the $F_{CO_2}^*$ was first used to determine the CO₂ mass transfer coefficient (k_{CO_2}), as per Eq. 2, which is equivalent to Eq. 1;

$$k_{CO_2} = F_{CO_2}^* / (H_{CO_2} \cdot (p_{CO_2,w} - p_{CO_2,air})) \quad (2)$$

Once k_{CO_2} was determined, k_{O_2} was obtained as follows:

$$k_{O_2} = k_{CO_2} \cdot (0.851)^{-0.5} = 1.084 \cdot k_{CO_2} \quad (3)$$

where 0.851 is the ratio between the Schmidt numbers of O₂ and CO₂, as recommended by Wanninkhof (2014), and 0.5 is an adjustment parameter recommended by Cole et al. (2010) for low wind conditions.

7.2.2.4 Dissolved gas concentration

The dissolved CH₄ (C_{CH₄}) and CO₂ (C_{CO₂}) concentrations in the water column were determined onsite with a previously reported M-ICOS method (Gonzalez-Valencia et al., 2014). Briefly, this method consists of a gas-liquid exchange module (PDMSXA-1000, Medarray Inc., USA) through which water extracted from the reservoir flows constantly on the shell side of the gas exchange module while a CH₄- and CO₂-free nitrogen counterflows inside the silicone fibers; i.e. exchange area of 1000 cm². Diffusive forces from the concentration gradient promote transfer of the dissolved CH₄ and CO₂ contained in the water to the gas phase, where they are quantified by the UGGA. In the present study, the water was continuously extracted at the desired depth with a peristaltic pump (12 V, Solinst, Mexico) at a flow rate of 1.2 L min⁻¹, while the CH₄- and CO₂-free nitrogen was flowing at a constant flow rate of 0.75 L min⁻¹, controlled by a mass flow controller (GFC 17, Aalborg, Mexico). The setup was calibrated as specified in the method, at the beginning and at the end of each measurement day, with a standard headspace equilibration technique (Gonzalez-Valencia et al., 2014). The C_{CH₄} and C_{CO₂} profiles were

obtained by placing the extraction probe just below the water surface for about 60 s. Afterwards, the probe was allowed to descend steadily at a rate of approximately 1 m min^{-1} until it reached the bottom, where it was kept for an additional 30 s. Additionally, a flow-through oxygen optode (FTC-PSt3, PreSens, Germany) was included in the water extraction line, allowing the simultaneous determination of dissolved oxygen concentration (C_{DO}). Using this procedure, about 60 data points of dissolved gases were acquired for each meter of water column depth. The lower detection limit of the M-ICOS method coupled with the DO sensor under the present configuration was 0.005 mmol m^{-3} for C_{CH_4} , 4 mmol m^{-3} for C_{CO_2} , and 0.625 mmol m^{-3} for C_{DO} .

7.2.2.5 *Methane production and oxidation rates*

Water samples were taken with a Van Dorn bottle, usually guided by C_{CH_4} and C_{DO} profiles, to measure the CH_4 production and oxidation rates at several characteristic water depths. The samples were immediately and carefully transferred to 50–mL glass syringes that included an optical oxygen Sensor Spot (PSt3 or PSt6, PreSens, Germany) previously fixed to the inside wall, close to the syringe output. The difference between PSt-3 or PSt-6 sensors is their lower detection limits and ranges (expressed in air saturation percentage) of 0.03–100% and 0.002–5%, respectively. Thus, PSt-6 sensors were preferred for low DO and anaerobic samples. Once the samples had been collected, the syringes were taken to the laboratory for incubation under dark conditions at a constant temperature similar to that of the reservoirs. Then, at time intervals, C_{DO} was determined and 2 mL sub-samples were transferred into 5–mL plastic syringes, to which 3 mL of CH_4 - and CO_2 -free nitrogen were added. The sub-sample syringes were vigorously shaken for 30 s to allow for equilibration, the liquid volume was evacuated, and the 3 mL gas content of the syringe was injected through a septum into a continuous flow

of nitrogen passing through an open circuit into the UGGA. The presence of CH₄ and CO₂ in the sample was detected as a peak response, that was integrated, after proper calibration. Lastly, C_{CH4} and C_{CO2} in the liquid sub-samples were derived from Henry's solubility constant (Sander, 2017). These incubations were sustained for five to seven days, during which a total of five to six triplicate measurements of C_{CH4}, C_{CO2}, and C_{DO} were done to ascertain the CH₄, CO₂, and DO production/uptake rates. It is worth noting that this protocol allowed for the determination of the production/uptake rates without headspace addition; thus, the laboratory conditions matched those prevalent in the reservoirs.

7.2.2.6 Mass balance and gas transfer velocity

The full mass balance calculations and assumptions are described in detail in the Supplementary Material (Section S1.1). Briefly, assuming steady state, the CH₄ balance over the entire water column and sediments was considered as a three-compartment system: (i) methanogenesis (MG), described by the methanogenic rate (r_{CH4}^{MG}); (ii) methanotrophy (MT), described by the methanotrophic rate (r_{CH4}^{*MT}); and (iii) emissions to/from the atmosphere (F_{CH4}^*). Of these, two were measured (r_{CH4}^{*MT} and F_{CH4}^*), which then allowed r_{CH4}^{MG} to be calculated. The DO balance consisted of three compartments: (i) respiration (R), described by the respiratory rate (r_{O2}^{*R}); (ii) oxygen production, described by the gross primary production (GPP; r_{O2}^{GPP}); and (iii) atmospheric exchange (F_{O2}). The rates r_{O2}^{*R} and F_{O2} were measured, which in turn allowed r_{O2}^{GPP} to be determined. The CO₂ balance was considered as a four-compartment model: (i) MG, described by r_{CO2}^{MG} and that can result in CO₂ production (acetoclastic pathway) or uptake (hydrogenotrophic pathway); (ii) R in the water column, described by r_{CO2}^R ; (iii) the GPP in the photic zone of the water column, described by r_{CO2}^{GPP} ; and (iv) emission to/from the atmosphere

($F_{CO_2}^*$). In this case, only two of these four compartments were measured ($r_{CO_2}^{*R}$ and $F_{CO_2}^*$). Thus, $r_{CO_2}^{GPP}$ was determined from $r_{O_2}^{GPP}$, assuming a constant $r_{CO_2}^{GPP}$ to $r_{O_2}^{GPP}$ ratio of 1.2 (Wetzel et al., 2000). Once $r_{CO_2}^{GPP}$ was determined, $r_{CO_2}^{MG}$ was estimated by closing the mass balance. In these mass balance equations, negative rate values indicate uptake or efflux of a given molecule, while positive values indicate production or influx. The steady-state assumption used in this mass balance model will be discussed in the results and discussion section.

In addition to process rates, for each compound x (CH₄, O₂, and CO₂), the total mass of x in the water column was determined according to:

$$M_x = \sum_{i=1}^n C_x \cdot \delta_i \quad (4)$$

where δ_i is the depth section of the water column corresponding to each concentration measurement (C_x).

Finally, the turnover time (θ_x), which is the mean time that M_x remains within the water column, was defined. To that end, a total rate was defined for each compound (r_x^{TOT}), which is the sum of all positive rates involved in the compound mass balance:

$$\theta_x = M_x / r_x^{TOT} \quad (5)$$

7.2.2.7 Numerical Homogeneity Model

The numerical homogeneity model (NHM; Gonzalez-Valencia et al., 2019) was implemented to explore the spatial distribution of the dissolved gas concentrations and to assign a numerical

value to the distribution. Briefly, this model includes a homogeneity index (h_p , %), which represents the homogeneity of the parameter P, along two dimensions (x, y); in our case, longitudinal distance along the reservoir transect and depth. The significance of this quantity is that for a nonhomogeneous distribution, $0 \leq h_p < 100\%$, while for a homogeneous distribution, $h_p = 100\%$. Furthermore, to establish in which dimension heterogeneities are dominant, the NHM also defines an anisotropic factor (ω_p) that indicates the angle of the heterogeneities in the two-dimensional space; this value ranges from -45° when heterogeneities are observed only in the x dimension (length), to 45° for heterogeneities observed only in the y dimension (depth).

7.2.2.8 Data treatment and statistics

The *dplyr* package was used in R software to determine the mean and standard deviation of the physicochemical parameters (Wickham et al., 2020). Data collected during the campaigns were smoothed by weighted linear least squares and a Savitzky-Golay filter using MATLAB (version 2015a, MathWorks, USA); the smoothed data were then used to generate contour maps of dissolved gas concentration. The contour maps were generated by interpolation of the high-resolution data using Surfer 11.0 software (Golden Software, USA). The Surfer Software provides 10 interpolation methods, from which the best was chosen, according to Willmott and Matsuura (2006), using the mean absolute error (MAE) and the mean bias error (MBE) as selection criteria. We log-transformed our data in order to compare means between reservoirs given that aquatic ecosystems usually show log normal distribution (St-Pierre et al., 2018). Welch's t-test was used in MATLAB to compare the annual means from the log-transformed data of the reservoirs.

7.2.3 Results and discussion

7.2.3.1 Physicochemical characterization

Clear differences were observed in the water physicochemical parameters measured in both reservoirs, as expected based on the urban vs. natural ecosystems surrounding LG and LL, respectively. The wastewater discharged into LG resulted in mean seasonal TOC ranging from 0.82 to 2.55 mmol L⁻¹; meanwhile, the values observed in LL ranged from 0.23 to 0.56 mmol L⁻¹. In LG, the seasonal mean TN ranged from 0.95 to 1.28 mmol L⁻¹, whereas in LL it ranged from 0.011 to 0.015 mmol L⁻¹. The mean seasonal PO₄⁻³ concentration ranged from 0.017 to 0.022 mmol L⁻¹ in LG, while in LL, the concentration was between 0.7 and 2 µmol L⁻¹. Differences in terms of element balance were also observed between the reservoirs, as reflected by the stoichiometric C:N:P molar ratio, which was on average 171:53:1 in LG and 582:10:1 in LL. These ratios revealed no nutrient limitation in LG, whereas a moderate to severe N and P limitation was observed in LL (Wetzel, 2001). A significant difference in terms of water transparency was also observed with a mean SD in LG of 0.75 ± 0.42 m, while in LL the mean SD was 2.71 ± 0.93 m ($p < 0.01$). Reductive processes predominated in LG, as shown by a mean ORP of -124.36 ± 488 mV, while in LL oxidation prevailed with mean ORP of 94.32 ± 97.07 mV (McMahon and Chapelle, 2008). According to Wetzel (2001), the physicochemical parameters of LG were in line with those commonly found in eutrophic/hypereutrophic ecosystems, while LL corresponded to an oligotrophic/mesotrophic site.

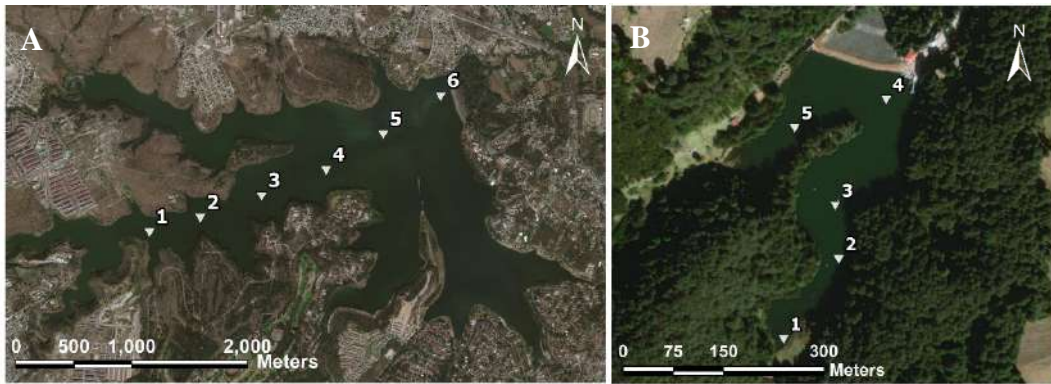


Figure 7.2.1. Satellite images of the studied reservoirs and locations of the monitoring and sampling stations: A. “Lago de Guadalupe” (LG), and B. “Lago el Llano” (LL). Created in ArcGIS 10.7.1.

7.2.3.2 Dissolved gases and gas emission

The C_{CH4} was subject to a large spatial variability, as shown in the contour maps (Figure 7.2.2A).

The C_{CH4} concentration in LL was, on average, 50 times lower than that of LG. In all cases, these concentrations corresponded to an oversaturation relative to the atmospheric CH₄ by four to five orders of magnitude in LG and three orders of magnitude in LL, which indicate that both reservoirs are sources of atmospheric CH₄. Surface C_{CH4} observed in LL and LG was generally higher than in other subtropical reservoirs (Table 7.2.S2) and world lakes of the same class size (Holgerson and Raymond, 2016). Contrastingly, bottom C_{CH4} was in the lower range of reported values for tropical and subtropical ecosystems (Table 7.2.S2) in LL and within the range in LG. Together, higher surface C_{CH4} and similar or lower bottom C_{CH4} suggest a lower CH₄ oxidation and/or a better CH₄ transfer from the bottom to the surface water, than is usually seen in other lakes. The latter is further supported by relatively low Schmidt numbers ranging from 13.8–55.1 J m⁻² in LG and 38.9–96.6 J m⁻² in LL, which reflects a relatively weak thermal stratification for both reservoirs, considering that Schmidt numbers as high as 1×10^4 J m⁻² have been reported (Wetzel, 2001).

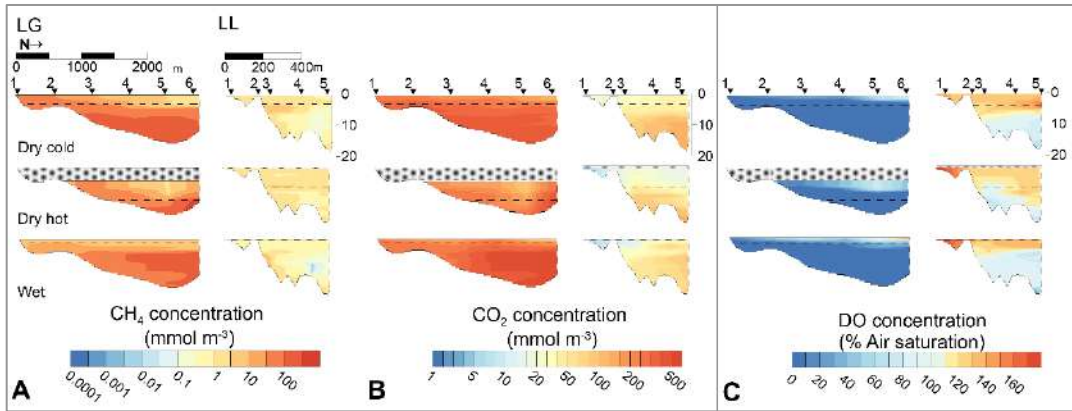


Figure 7.2.2. Contour maps of (A) C_{CH_4} , (B) C_{CO_2} , and (C) DO over the three distinct seasons in LG and LL. MSS references are displayed as inverted triangles at the top of the maps. To improve readability, lengths are scaled differently in each reservoir (scale shown at the top left). The thermoclines are represented as a dashed line. Water level changes are shown as dotted areas.

As expected from the large variability of C_{CH_4} , CH_4 fluxes were also highly variable (Figs. S2A and S2B). Mean total fluxes were $128.5 \pm 222.6 \text{ mmol m}^{-2} \text{ d}^{-1}$ and $62.0 \pm 155.7 \text{ mmol m}^{-2} \text{ d}^{-1}$ in LG and LL, respectively. Ebullition was a major emission mode in LG, accounting for $54.70 \pm 38.83\%$ of the total flux. In LL, ebullition was sporadic and represented $21.62 \pm 40.41\%$ of the total emission. CH_4 emissions in LG and LL were higher than expected based on their respective trophic states, as detailed by Deemer et al. (2016). Moreover, emissions observed in LG are within the higher range of fluxes from Brazilian reservoirs (0.62 to $83.5 \text{ mmol m}^{-2} \text{ d}^{-1}$; de Mello et al., 2018; dos Santos et al., 2006) and are even comparable to those reported for dairy and swine farm wastewater lagoons (6.25 to $3,125 \text{ mmol m}^{-2} \text{ d}^{-1}$; Grant and Boehm, 2015; Leytem et al., 2017; Sharpe and Harper, 1999).

Notably, C_{CO_2} was subject to a narrower range than C_{CH_4} (Figure 7.2.2B), from 84.2 to $593.5 \text{ mmol m}^{-3}$ in LG and from 5.9 to $197.5 \text{ mmol m}^{-3}$ in LL. In LG, the mean C_{CO_2} over the entire column was about 25 times higher than the atmospheric equilibrium concentration, while in LL

the mean C_{CO_2} was 4 times above equilibrium. In terms of emissions, the mean total CO_2 flux was $107.70 \pm 78.60 \text{ mmol m}^{-2} \text{ d}^{-1}$ in LG, which is within the range previously reported from other subtropical reservoirs (Table 7.2.S2) and eutrophic aquatic ecosystems, i.e. -27 to 76 $\text{mmol CO}_2 \text{ m}^{-2} \text{ d}^{-1}$ (Deemer et al., 2016). In LL, despite observing an overall supersaturation of CO_2 in the water column, the surface waters were often undersaturated, resulting in predominantly negative CO_2 fluxes, at $-9.5 \pm 13.6 \text{ mmol m}^{-2} \text{ d}^{-1}$. The latter is also in accordance with emissions previously reported from oligotrophic and mesotrophic reservoirs, i.e. -6.99 – 15.10 $\text{mmol m}^{-2} \text{ d}^{-1}$ (Deemer et al., 2016). Thus, LL can be considered as a CO_2 sink and a dominantly autotrophic ecosystem, whereas LG is a source of CO_2 and a dominantly heterotrophic ecosystem.

In LG, the eutrophic/hypereutrophic conditions promoted respiratory processes and DO depletion, as shown in the C_{DO} contour maps (Figure 7.2.2C). Throughout the three campaigns, most of the LG water column was characterized by C_{DO} values that were below the detection limit of the method, while mean seasonal C_{DO} were within the dysoxic range (Tyson and Pearson, 1991), i.e. from 10.68 ± 25.36 to $26.45 \pm 65.8 \text{ mmol m}^{-3}$, which corresponds to 5.59–13.85% saturation. These low C_{DO} are below survival levels for regular macrobiota (U.S. EPA, 2000) and are an additional indicator of the polluted state of LG. Contrastingly, all year-round, a fully oxygenated water column was observed in LL with mean seasonal C_{DO} levels ranging from 198.53 to 272.24 mmol m^{-3} , which corresponds to 93–127% saturation. The oversaturation commonly observed in LL confirms the dominant autotrophic nature of the reservoir. In LG, the observed DO undersaturation was partly compensated by positive influxes from the atmosphere, with seasonal means ranging from -23.65 to -137.93 $\text{mmol m}^{-2} \text{ d}^{-1}$. In contrast, LL was a source of O_2 to the atmosphere with mean seasonal fluxes ranging from 4.94

to $23.92 \text{ mmol m}^{-2} \text{ d}^{-1}$. Although diffusive O_2 fluxes are not extensively reported in the literature, our measurements are within the range previously reported by Gelda and Effler (2002; -300 to $60 \text{ mmol m}^{-2} \text{ d}^{-1}$) in a hypereutrophic lake and close to an overall estimation for lakes published by Koschorreck et al. (2017; -90 to $90 \text{ mmol m}^{-2} \text{ d}^{-1}$).

7.2.3.3 *Bioprocesses rates*

Microbial activity profiles were determined for each season at LG-6 and LL-4, which had mean depths of 10.7 ± 4.2 and 16.5 ± 0.5 m, respectively (Figure 7.2.S3). Regarding CH_4 , as standardly observed in most lakes and reservoirs, a clear methanotrophic activity was observed in both lakes. However, irregular trends were observed in LG, while a relatively smooth and constant pattern was observed in LL. Since the standard deviations of the triplicate measurements were smaller than the observed variations, experimental noise was discarded as a possible explanation of that observed behavior. Irregular patterns of methanotrophic activity with drastic variations within short depth intervals have been previously observed (Thalasso et al., 2020) and hypothesized to be the result of complex transitions between aerobic and anaerobic CH_4 production/oxidation along the water column. It is noteworthy that during the dry cold season, a minimum methanotrophic rate of $-13.55 \text{ mmol-CH}_4 \text{ m}^{-3} \text{ d}^{-1}$ was found at the bottom of the water column in LG which is a clear indication of methanogenesis. Equally noticeable is the maximum methanotrophic rate of $30.08 \text{ mmol-CH}_4 \text{ m}^{-3} \text{ d}^{-1}$ found during the same season, 7 m below the oxycline and 6 m below the photic depth, as estimated from SD (4 m; French et al., 1982). Since incubations were done under dark and anaerobic conditions (no O_2 added, DO concentration undetectable), the methanotrophic rates observed below 5 m

strongly suggest anaerobic oxidation of methane (AOM). The latter has been previously reported to naturally occur in lakes (Martinez-Cruz et al., 2018).

In terms of CO₂, the production rates found in LG were higher than those observed in LL but were limited to the oxic epilimnion. Notably, a negative CO₂ production rate was observed at the depth where AOM was found, which suggests the presence of reverse methanogenesis driven by archaea (Kellermann et al., 2012) or other autotrophic processes, such as acetogenesis or iron oxidation (Bryce et al., 2018; Lay et al., 1998). Conversely, a significant CO₂ production rate was found in the water column where methanogenesis was observed, which is an indicator of dominant acetoclastic methanogenesis. In LL, CO₂ production was found at almost all depths of the water column over the three seasons but was highly variable. It is worth reiterating that these tests were performed under dark conditions and reflect respiration, i.e. they do not account for primary production. In terms of DO, a respiration rate was observed only at the oxic epilimnion of LG, as expected from the DO profiles. In LL, respiration was found along the entire water column with a distinctive local minimum at 10 m over the three seasons.

7.2.3.4 Spatiotemporal variations and overall metabolism

A global mass balance was established from measurements at LG-6 and LL-4, which considered a limited number of dominant processes expressed per unit of lake area, i.e. methanotrophy, methanogenesis, respiration, primary production, and emissions from/to the atmosphere. The magnitude of each process is listed in Table 7.2.1 along with the parameters of spatiotemporal distribution of C_{CH4}, C_{CO2}, and C_{DO}, the total mass of each dissolved gas present in the water column (M_x), and their corresponding turnover time (θ_x). It should be noted that the steady-state

condition assumed during the model development was confirmed by experimental data, i.e. the variation of M_x between seasons represented on average $1.69 \pm 1.13\%$ of r_x^{TOT} .

All of the determined parameters listed in Table 7.2.1 were also included in a graphical representation (Figure 7.2.3), facilitating the overall appraisal of the carbon cycle at first glance. This Figure shows drastic differences between the two reservoirs: (i) the magnitude of the CH₄ cycle in LG was significantly higher than that of LL ($p<0.01$); (ii) despite differences in magnitude, the distribution of the processes linked to the CH₄ cycle were similar in both reservoirs; (iii) the magnitude of the DO cycle was lower in LG than in LL ($p<0.02$) ; (iv) the flux components were more important in LG than in LL; (v) $r_{CO_2}^{MG}$ was negative in LG and positive in LL; (vi) GPP was a relatively minor component of the carbon cycle in LG and a dominant component in LL; and (vii) the CO₂ and O₂ cycles were more balanced in LL than in LG (as evidenced by similitude in size and processes share). The same exercise was done regarding seasonality (illustrated in Fig S4), which indicates that the variation among seasons was moderate. Meanwhile, large variations were observed between the two ecosystems, not only in terms of magnitude but also in the contribution of each bioprocess. This observation suggests that the impact of the trophic state on the carbon cycle is greater than that of seasonality.

A closer analysis of the parameters listed in Table 7.2.1 and illustrated in Figure 7.2.3 shows that $r_{CH_4}^{MG}$ was about 15 times higher in LG than in LL and that LG contained 30 to 60 times more CH₄ in the water column than LL. This shows that LG stores significantly more CH₄ than LL, which suggests

Table 7.2.1. Seasonal and mean parameters (A); metabolic rates and mass balance summary (B) for LG and LL. CV is the coefficient of variation (%). * indicates a significant difference between the means of the reservoirs ($p<0.05$).

	LG			LL				
	Dry cold	Dry hot	Wet	Mean (CV)	Dry cold	Dry hot	Wet	Mean (CV)
Lake parameters								
Temperature (°C)	16.83	20.38	19.64	18.95 (9.88)	10.82	16.64	13.04	13.5 (21.76)
Max. Depth (m)	15.00	8.25	15.00	12.75 (30.57)	18.00	17.00	17.00	17.33 (3.33)
h_{CH_4} (%)	54.88	42.00	56.00	50.96 (15.27)	55.00	74.00	57.77	62.26 (16.49)
ω_{CH_4} (°)	28.23	4.25	18.82	17.1 (70.66)	4.18	0.65	3.32	2.72 (67.76)
h_{CO_2} (%)	87.00	81.30	81.00	83.1* (4.07)	69.58	62.62	73.44	68.55* (8)
ω_{CO_2} (°)	32.45	-11.72	14.38	11.7 (189.74)	29.85	28.54	13.79	24.06 (37.07)
h_{O_2} (%)	21.77	31.73	22.00	25.17* (22.59)	88.87	91.59	88.60	89.69* (1.84)
ω_{O_2} (°)	41.86	21.98	35.24	33.03 (30.65)	31.33	-6.90	32.13	18.85 (118.32)
Metabolism and mass balance								
Rates (mmol m ⁻² d ⁻¹)								
$r_{CH_4}^{MG}$	67.06	105.19	81.29	84.51* (22.8)	4.39	4.69	8.01	5.7* (35.28)
$r_{CH_4}^{*MT}$	-50.94	-46.92	-61.16	-53.01* (13.85)	-1.21	-2.86	-7.30	-3.79* (83.14)
$F_{CH_4}^*$	-16.12	-58.27	-20.13	-31.5* (73.84)	-3.19	-1.83	-0.72	-1.91* (64.72)
$r_{CO_2}^{GPP}$	-14.65	-26.00	-108.87	-49.84* (103.20)	-168.94	-236.66	-299.58	-235.06* (27.80)
$r_{CO_2}^R$	201.08	233.50	161.24	198.61* (18.22)	105.55	92.70	79.28	92.51* (14.20)
$r_{CO_2}^{MG}$	-83.08	-45.32	-32.95	-53.78* (48.56)	59.09	115.60	221.58	132.09* (62.45)
F_{CO_2}	-103.34	-162.18	-19.42	-94.98 (75.54)	4.30	28.36	-1.28	10.46 (150.60)
$r_{O_2}^{GPP}$	17.59	31.20	130.64	59.81* (103.20)	202.72	284.00	359.50	282.07* (27.80)
$r_{O_2}^{*R}$	-66.64	-64.89	-120.32	-83.95* (37.53)	-201.63	-260.11	-355.92	-272.55* (28.58)
F_{O_2}	49.06	33.70	-10.33	24.14 (127.68)	-1.09	-23.88	-3.58	-9.52 (131.36)

Table 7.2.1. (continued)

Total mass (mmol m^{-2}) and residence time (d^{-1})								
M_{CH_4}	706.57	543.94	990.71	747.07* (30.27)	7.51	15.17	6.74	9.81* (47.55)
M_{CO_2}	3390	2724	4663	3593* (27)	1327	716	979	1008* (30)
M_{O_2}	309	318	495	373* (28)	3281	3602	3067	3317* (8)
θ_{CH_4}	10.54	5.17	12.19	9.30* (39.45)	1.71	3.23	0.84	1.93* (62.82)
θ_{CO_2}	16.86	11.67	28.92	19.15* (46.23)	7.86	3.03	3.27	4.72* (57.67)
θ_{O_2}	4.64	4.89	3.79	4.44 (13.02)	16.18	12.68	8.53	12.47 (30.72)

that flux and methanotrophy did not completely compensate for the higher CH₄ production observed in LG. This is certainly a result of the low DO availability for aerobic methanotrophy. The higher CH₄ storage is also reflected by a higher turnover time in LG than in LL, with θ_{CH_4} being 9.3 ± 3.7 d in LG and 1.9 ± 1.2 d in LL. The opposite trend to CH₄ was observed regarding DO, with $M_{O_2}^*$ 10 times higher in LL than LG, as a result of the relatively high photosynthetic DO production observed in LL, above the relatively low respiration. As a result of the latter, the DO cycle was more dynamic in LG than in LL, with a θ_{O_2} of 4.4 ± 0.6 and 12.5 ± 3.8 d, respectively. In terms of CO₂, an important contrast between LG and LL was also observed. Indeed, $M_{CO_2}^*$ was three times higher in LG than in LL. In LL, a deficit of CO₂ production compared to CO₂ uptake by primary production was compensated by a CO₂ input from the atmosphere, while in LG a large CO₂ production and relatively low primary production resulted in important emissions. Despite these drastic disparities, a relatively small difference in terms of θ_{CO_2} was observed, at 19.2 ± 8.9 and 10.1 ± 3.6 d for LG and LL, respectively.

Notably, Figure 7.2.3 and Table 7.2.1 also indicate a depleted GPP in LG despite higher concentration of nutrients and trophic level than LL. Photosynthesis is known to be inhibited by compounds that could potentially be present in the wastewater discharged into LG, such as NH₃, herbicides, sulfide, and humic substances (Chen et al., 2020; Choi et al., 2012; Godos et al., 2010; Leusch et al., 2014; Misaki et al., 2019). Chlorophyll a concentrations confirmed the hypothesis of depleted GPP in LG as it ranged 0.59 to 52.64 µg m⁻³ (CONAGUA, 2019), which is in the lower range of hypereutrophic ecosystems, i.e. 9.5–275 µg m⁻³ (Wetzel, 2001). The combination of depleted GPP and high respiration in LG suggests that allochthonous carbon was the main substrate for respiration in LG (Cole et al., 2000); meanwhile, autochthonous carbon input from GPP always

exceeded R in LL. The dominance of autotrophic over heterotrophic activity is further evidenced by the mean GPP/R ratio, which was 3.17 ± 1.31 in LL and 0.34 ± 0.40 in LG.

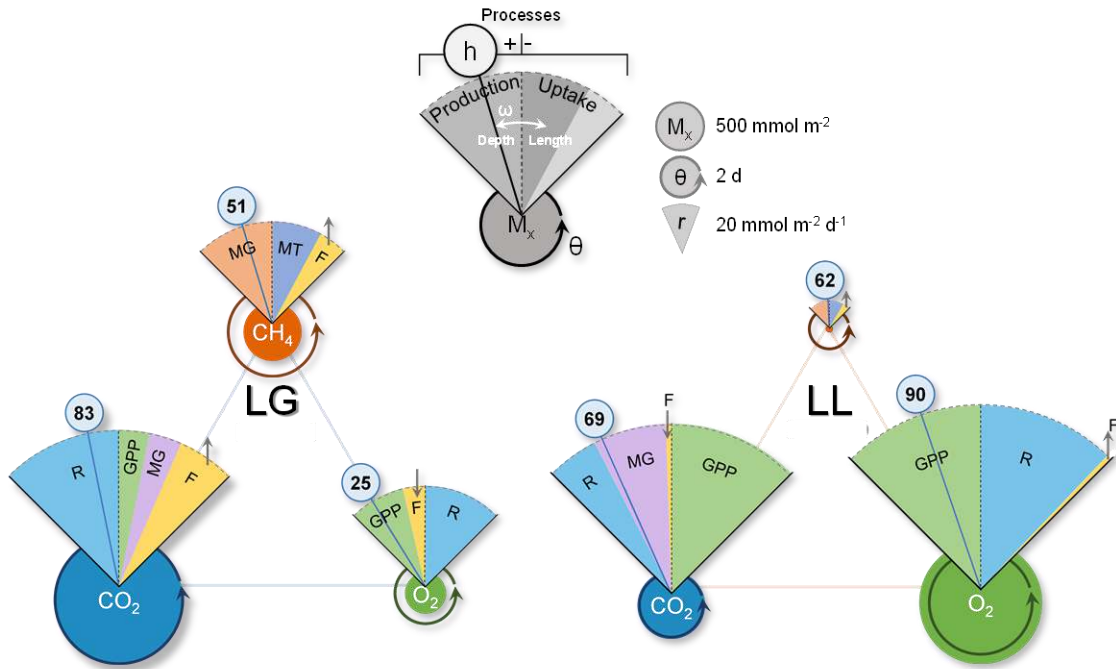


Figure 7.2.3. Graphical representation of the carbon mass balance components in LG and LL. Grey picture is for explanatory and scaling purposes. Each quarter-pie chart, where areas are scaled to magnitude, represents the proportional share of each process: MG, methanogenesis; MT, methanotrophy; F, flux; R, respiration; GPP, and gross primary production, for CH₄, CO₂ and O₂. Rates located on the left side are positive (input/production) and those on the right side are negative (output/uptake). Inferior solid-color circles represent the scaled total mass of the compound (M_x ; mmole m⁻²) and the circle arrows represent the scaled turnover time (θ_x). The superior circle represents the homogeneity factor of dissolved gases distribution (h) and the anisotropic factor (ω).

In addition to these observations, Figure 7.2.3 also indicates a negative $r_{CO_2}^{MG}$ in LG, which is in direct contrast to that observed in LL. This suggests acetoclastic methanogenesis in LL while the hydrogenotrophic pathway would be dominant in LG. This is surprising since methanogenesis in the water column of LG was observed along with a net CO₂ production, which is usually indicative of acetoclastic methanogenesis. This would suggest a shift of the dominant pathway between the

sediments and the water column, although it bears repeating that $r_{CO_2}^{MG}$ was considered as a buffer compartment in our model. Therefore, $r_{CO_2}^{MG}$ consists primarily of the CH₄ produced in the sediments and transferred to the water column, but also any other unidentified biological or abiotic process, including potentially autotrophic processes.

Aside from the main bioprocesses rates, the spatiotemporal distribution of C_{CH4}, C_{CO2}, and C_{DO} offers an additional scope on the carbon cycle. For instance, C_{DO} was the parameter most heterogeneously distributed in LG ($h_{DO} = 25\%$), while, in the same reservoir, C_{CO2} was the most homogeneously distributed parameter ($h_{CO_2} = 83\%$). As suggested by Gonzalez-Valencia et al. (2019), the comparison of the h values of several compounds is an indicator of which compounds are in excess and/or deficit. An overabundant compound is more likely to be evenly distributed, which seems to be confirmed here. Indeed, the low h observed for C_{DO} in LG appears to be caused by the dominant anoxic conditions, reflecting a DO limitation, while the homogeneous distribution of C_{CO2} suggests that respiration surpassed primary production, causing an abundant CO₂ concentration. Based on that premise, the order of the dissolved gases, from excess to deficit, was CO₂/CH₄/O₂ in LG and O₂/CO₂/CH₄ in LL, which is in line with the dominant heterotrophic and autotrophic overall metabolism in LG and LL, respectively. Together with h , the NHM also provides the anisotropic dominant direction. In this case, it was mostly depthward (positive ω_p ; Figure 7.2.S4), which is in accordance with the concept of water column stratification. Notably, in LG, ω_{CH_4} , ω_{CO_2} , and ω_{CDO} were linearly correlated to the Schmidt stability, with a $R^2 > 0.998$ ($p < 0.01$, $n = 4$), unlike LL, where no clear correlation was observed. Thus, stratification is not the dominant factor that influences the anisotropy of dissolved gas distribution in LL. In general, the predominant direction of anisotropy in LL was slighter and more stable across seasons than that of LG.

7.2.4 Conclusion

As shown in the present work, a large number of overall parameters were determined from a relatively reduced number of field measurements, including flux, dissolved concentration, and several bioprocess rates of CH₄, CO₂, and O₂, which were integrated in a mass balance model. Among these, a total of 22 parameters were arbitrarily selected to exhaustively describe the carbon cycling in two reservoirs over three seasons. All of these parameters were included in a single graphical representation, which allows for an overall appraisal of the carbon cycle at first glance. This approach revealed the share of each major process in the CH₄, CO₂, and O₂ cycles, as well as several spatiotemporal attributes of their distribution and turnover. The combination of a comprehensive study and an integrative graphical representation facilitates seasonal comparisons between the ecosystems. In the present study, this approach vividly showed how allochthonous pollution deeply modifies the global functioning of subtropical reservoirs. The same approach could be applied to draw comparisons among other aquatic ecosystems and their respective characteristics, locations, and/or seasons.

Author contribution

T. A.-C. and F.T. conceived the study, analyzed the data, and wrote the manuscript. T. A.-C. conducted the fieldwork. F. T. provided funding. R. G.-V. and F.J. C. analyzed the data and contributed to the manuscript editing. All authors have approved the final version of the manuscript.

Acknowledgements

We gratefully acknowledge the SEP-Cinvestav fund (Project #203) as well as the Consejo Nacional de Ciencia y Tecnología (Conacyt) for financial support (project #255704) and grants to T. A.-C. (#531383) and R. G.-V (#266244). We also thank Victoria Teresita Velázquez Martínez,

Juan Corona Hernández, and Francisco Silva-Olmedo for their technical assistance. The authors declare that they have no conflicts of interest.

7.2.5 References

APHA, AWWA, WEF, 2012. Standard Methods for the Examination of Water and Wastewater, 22nd ed. American Public Health Association, Washington, D.C.

<https://doi.org/10.2105/SMWW.2882.093>

Bryce, C., Blackwell, N., Schmidt, C., Otte, J., Huang, Y.-M., Kleindienst, S., Tomaszewski, E., Schad, M., Warter, V., Peng, C., Byrne, J.M., Kappler, A., 2018. Microbial anaerobic Fe(II) oxidation - Ecology, mechanisms and environmental implications. Environ. Microbiol. 20, 3462–3483. <https://doi.org/10.1111/1462-2920.14328>

Carlson, R.E., 1977. A trophic state index for lakes. Limnol. Oceanogr. 22, 361–369. <https://doi.org/10.4319/lo.1977.22.2.0361>

Chen, J., Wei, J., Ma, C., Yang, Z., Li, Z., Yang, X., Wang, M., Zhang, H., Hu, J., Zhang, C., 2020. Photosynthetic bacteria-based technology is a potential alternative to meet sustainable wastewater treatment requirement? Environ. Int. 137, 105417. <https://doi.org/10.1016/j.envint.2019.105417>

Choi, C.J., Berges, J.A., Young, E.B., 2012. Rapid effects of diverse toxic water pollutants on chlorophyll a fluorescence: Variable responses among freshwater microalgae. Water Res. 46, 2615–2626. <https://doi.org/10.1016/j.watres.2012.02.027>

Cole, J.J., Bade, D.L., Bastviken, D., Pace, M.L., Van de Bogert, M., 2010. Multiple approaches to estimating air-water gas exchange in small lakes. Limnol. Oceanogr. Methods 8, 285–293. <https://doi.org/10.4319/lom.2010.8.285>

Cole, J.J., Pace, M.L., Carpenter, S.R., Kitchell, J.F., 2000. Persistence of net heterotrophy in lakes during nutrient addition and food web manipulations. *Limnol. Oceanogr.* 45, 1718–1730.
<https://doi.org/10.4319/lo.2000.45.8.1718>

CONAGUA, 2019. Calidad del agua en México, Comisión Nacional del Agua. URL
<https://www.gob.mx/conagua/articulos/calidad-del-agua> (accessed 7.11.20).

de Mello, N.A., Brighenti, L.S., Barbosa, F.A.R., Staehr, P.A., Bezerra Neto, J.F., 2018. Spatial variability of methane (CH_4) ebullition in a tropical hypereutrophic reservoir: silted areas as a bubble hot spot. *Lake Reserv. Manage.* 35, 105–114.
<https://doi.org/10.1080/10402381.2017.1390018>

Deemer, B.R., Harrison, J.A., Li, S., Beaulieu, J.J., Delsontro, T., Barros, N., Bezerra-Neto, J.F., Powers, S.M., Santos, M.A. Dos, Vonk, J.A., 2016. Greenhouse Gas Emissions from Reservoir Water Surfaces: A New Global Synthesis. *BioScience* 66, 949–964.
<https://doi.org/10.1093/biosci/biw117>

dos Santos, M.A., Rosa, L.P., Sikar, B., Sikar, E., dos Santos, E.O., 2006. Gross greenhouse gas fluxes from hydro-power reservoir compared to thermo-power plants. *Energy Policy* 34, 481–488.
<https://doi.org/10.1016/j.enpol.2004.06.015>

French, R.H., Cooper, J.J., Vigg, S., 1982. Secchi Disc Relationships. *J. Am. Water Resour. Assoc.* 18, 121–123. <https://doi.org/10.1111/j.1752-1688.1982.tb04538.x>

Gelda, R.K., Effler, S.W., 2002. Estimating oxygen exchange across the air-water interface of a hypereutrophic lake, *Hydrobiologia* 487, 243–254. <https://doi.org/10.1023/A:1022994217578>

Godos, I. de, Vargas, V.A., Blanco, S., González, M.C.G., Soto, R., García-Encina, P.A., Becares,

E., Muñoz, R., 2010. A comparative evaluation of microalgae for the degradation of piggery wastewater under photosynthetic oxygenation. *Bioresour. Technol.* 101, 5150–5158. <https://doi.org/10.1016/j.biortech.2010.02.010>

Gonzalez-Valencia, R., Magaña-Rodriguez, F., Gerardo-Nieto, O., Sepulveda-Jauregui, A., Martinez-Cruz, K., Walter Anthony, K., Baer, D., Thalasso, F., 2014. In Situ Measurement of Dissolved Methane and Carbon Dioxide in Freshwater Ecosystems by Off-Axis Integrated Cavity Output Spectroscopy. *Environ. Sci. Technol.* 48, 11421–11428. <https://doi.org/10.1021/es500987j>

Gonzalez-Valencia, R., Magaña-Rodriguez, F., Sepulveda-Jauregui, A., Aguirre-Zabala-Campano, T., Gerardo-Nieto, O., Thalasso, F., 2019. A simple model for the numerical characterization of spatiotemporal variability in aquatic ecosystems. *Aquat. Sci.* 81. <https://doi.org/10.1007/s00027-019-0652-1>

Grant, R.H., Boehm, M.T., 2015. Inhomogeneity of methane emissions from a dairy waste lagoon. *J. Air Waste Manage. Assoc.* 65, 1306–1316. <https://doi.org/10.1080/10962247.2015.1083912>

Holgerson, M.A., Raymond, P.A., 2016. Large contribution to inland water CO₂ and CH₄ emissions from very small ponds. *Nat. Geosci.* 9, 222–226. <https://doi.org/10.1038/ngeo2654>

Jähne, B., Münnich, K.O., Bösinger, R., Dutzi, A., Huber, W., Libner, P., 1987. On the parameters influencing air-water gas exchange. *J. Geophys. Res.* 92, 1937–1949. <https://doi.org/10.1029/JC092iC02p01937>

Kellermann, M.Y., Wegener, G., Elvert, M., Yoshinaga, M.Y., Lin, Y.-S., Holler, T., Mollar, X.P., Knittel, K., Hinrichs, K.-U., 2012. Autotrophy as a predominant mode of carbon fixation in anaerobic methane-oxidizing microbial communities. *Proc. Natl. Acad. Sci.* 109, 19321–19326.

<https://doi.org/10.1073/pnas.1208795109>

Koschorreck, M., Hentschel, I., Boehrer, B., 2017. Oxygen Ebullition From Lakes. *Geophys. Res. Lett.* 44, 9372–9378. <https://doi.org/10.1002/2017GL074591>

Lay, J.J., Li, Y.Y., Noike, T., 1998. Interaction between homoacetogens and methanogens in lake sediments. *J. Ferment. Bioeng.* 86, 467–471. [https://doi.org/10.1016/S0922-338X\(98\)80153-0](https://doi.org/10.1016/S0922-338X(98)80153-0)

Leusch, F.D.L., Khan, S.J., Gagnon, M.M., Quayle, P., Trinh, T., Coleman, H., Rawson, C., Chapman, H.F., Blair, P., Nice, H., Reitsema, T., 2014. Assessment of wastewater and recycled water quality: A comparison of lines of evidence from in vitro, in vivo and chemical analyses. *Water Res.* 50, 420–431. <https://doi.org/10.1016/j.watres.2013.10.056>

Leytem, A.B., Bjorneberg, D.L., Koehn, A.C., Moraes, L.E., Kebreab, E., Dungan, R.S., 2017. Methane emissions from dairy lagoons in the western United States. *J. Dairy Sci.* 100, 6785–6803. <https://doi.org/10.3168/jds.2017-12777>

Li, Z., Sun, Z., Chen, Y., Li, C., Pan, Z., Harby, A., Lv, P., Chen, D., Guo, J., 2020. The net GHG emissions of the China Three Gorges Reservoir: I. Pre-impoundment GHG inventories and carbon balance. *J. Clean. Prod.* 256, 120635. <https://doi.org/10.1016/j.jclepro.2020.120635>

Lovett, G.M., Cole, J.J., Pace, M.L., 2006. Is Net Ecosystem Production Equal to Ecosystem Carbon Accumulation? *Ecosystems* 9, 152–155. <https://doi.org/10.1007/s10021-005-0036-3>

Martinez-Cruz, K., Sepulveda-Jauregui, A., Casper, P., Anthony, K.W., Smemo, K.A., Thalasso, F., 2018. Ubiquitous and significant anaerobic oxidation of methane in freshwater lake sediments. *Water Res.* 144, 332–340. <https://doi.org/10.1016/j.watres.2018.07.053>

McMahon, P.B., Chapelle, F.H., 2008. Redox Processes and Water Quality of Selected Principal Aquifer Systems. *Ground Water* 46, 259–271. <https://doi.org/10.1111/j.1745-6584.2007.00385.x>

Misaki, K., Morita, Y., Kobayashi, K., Sugawara, Y., Shimizu, Y., Kusakabe, T., 2019. Evaluation of algal photosynthesis inhibition activity for dissolved organic matter with the consideration of inorganic and coloring constituents. *Chemosphere* 224, 333–342. <https://doi.org/10.1016/j.chemosphere.2019.02.106>

Sander, R., 2017. Henry's Law Constants, in: Linstrom, P.J., Mallard, W.G. (Eds.), NIST Chemistry WebBook, NIST Standard Reference Database Number 69. National Institute of Standards and Technology, Gaithersburg, p. 20899. <https://doi.org/10.18434/T4D303>

Santoso, A.B., Hamilton, D.P., Schipper, L.A., Ostrovsky, I.S., Hendy, C.H., 2020. High contribution of methane in greenhouse gas emissions from a eutrophic lake: a mass balance synthesis. *New Zeal. J. Mar. Freshw. Res.* 54, 1–20. <https://doi.org/10.1080/00288330.2020.1798476>

Sepulveda-Jauregui, A., Hoyos-Santillan, J., Gutierrez-Mendieta, F.J., Torres-Alvarado, R., Dendooven, L., Thalasso, F., 2013. The impact of anthropogenic pollution on limnological characteristics of a subtropical highland reservoir Lago de Guadalupe, Mexico. *Knowl. Manag. Aquat. Ecosyst.* 410. <https://doi.org/10.1051/kmae/2013059>

Sharpe, R.R., Harper, L.A., 1999. Methane emissions from an anaerobic swine lagoon. *Atmos. Environ.* 33, 3627–3633. [https://doi.org/10.1016/S1352-2310\(99\)00104-1](https://doi.org/10.1016/S1352-2310(99)00104-1)

St-Pierre, A.P., Shikon, V., Schneider, D.C., 2018. Count data in biology—Data transformation or model reformation? *Ecol. Evol.* 8, 3077–3085. <https://doi.org/10.1002/ece3.3807>

Thalasso, F., Sepulveda-Jauregui, A., Gandois, L., Martinez-Cruz, K., Gerardo-Nieto, O., Astorga-España, M.S., Teisserenc, R., Lavergne, C., Tananaev, N., Barret, M., Cabrol, L., 2020. Sub-oxycline methane oxidation can fully uptake CH₄ produced in sediments: case study of a lake in Siberia. *Sci. Rep.* 10, 3423. <https://doi.org/10.1038/s41598-020-60394-8>

Tranvik, L.J., Downing, J.A., Cotner, J.B., Loiselle, S.A., Striegl, R.G., Ballatore, T.J., Dillon, P., Finlay, K., Fortino, K., Knoll, L.B., Kortelainen, P.L., Kutser, T., Larsen, S., Laurion, I., Leech, D.M., McCallister, S.L., McKnight, D.M., Melack, J.M., Overholt, E., Porter, J.A., Prairie, Y., Renwick, W.H., Roland, F., Sherman, B.S., Schindler, D.W., Sobek, S., Tremblay, A., Vanni, M.J., Verschoor, A.M., Wachenfeldt, E. Von, Weyhenmeyer, G.A., 2009. Lakes and reservoirs as regulators of carbon cycling and climate. *Limnol. Oceanogr.* 54, 2298–2314.

Tyson, R. V., Pearson, T.H., 1991. Modern and ancient continental shelf anoxia: an overview. *Geol. Soc. London, Spec. Publ.* 58, 1–24. <https://doi.org/10.1144/GSL.SP.1991.058.01.01>

U.S. EPA, 2000. Ambient aquatic life water quality criteria for dissolved oxygen (saltwater): Cape Cod to Cape Hatteras.

Wanninkhof, R., 2014. Relationship between wind speed and gas exchange over the ocean revisited. *Limnol. Oceanogr. Methods* 12, 351–362. <https://doi.org/10.4319/lom.2014.12.351>

Wetzel, R. G. (2001). Limnology: Lake and River Ecosystems (3rd ed.). San Diego, California: Academic Press.

Wetzel, R.G., Likens, G.E., Wetzel, R.G., Likens, G.E., 2000. Primary Productivity of Phytoplankton, in: Limnological Analyses. Springer New York, pp. 219–239. https://doi.org/10.1007/978-1-4757-3250-4_14

Whiting, G.J., Chanton, J.P., 1993. Primary production control of methane emission from wetlands. *Nature* 364, 794–795. <https://doi.org/10.1038/364794a0>

Wickham, H., François, R., Henry, L., Müller, K., 2020. dplyr: A Grammar of Data Manipulation. R package dplyr version 1.0.2. URL <https://cran.r-project.org/package=dplyr> (accessed 9.24.20).

Willmott, C.J., Matsuura, K., 2006. On the use of dimensioned measures of error to evaluate the performance of spatial interpolators. *Int. J. Geogr. Inf. Sci.* 20, 89–102.
<https://doi.org/10.1080/13658810500286976>

Winslow, L., Read, J., Woolway, R., Brentrup, J., Zwart, J., Albers, S., Collinge, D., 2019. rLakeAnalyzer: Package for the analysis of lake physics.

7.3 Dinámica estacional de gases de efecto invernadero y oxígeno sobre un gradiente de salinidad de una laguna costera tropical

Artículo por someter a Estuarine and Coastal Ecosystems o Limnology & Oceanography

Resumen

En este trabajo, se presenta la caracterización exhaustiva de la dinámica de metano, dióxido de carbono y oxígeno de la laguna costera tropical “La Mancha”, ubicada en el estado de Veracruz, en tres estaciones características. Se realizaron mediciones en los sedimentos y columna de agua, y se cuantificaron las emisiones de gases de efecto invernadero. El ciclo del metano fue caracterizado en dos transectos: (i) longitudinal norte-sur, abarcando el gradiente de salinidad ocasionado por el mezclado de agua dulce, proveniente de un río (Caño Grande) en el extremo sur de la laguna, y agua marina, en el lado norte de la laguna y (ii) transversal oeste-este, abarcando la zona noroeste dominada por manglar hasta la salida de La Mancha al mar del lado este. Se observó una fuerte regulación estacional que a su vez influyó sobre la entrada de agua dulce a La Mancha. En particular, la temporada de lluvias, en la que aumenta la descarga del río, la materia orgánica y la entrada de agua del mar se observó la mayor variabilidad y magnitud de emisiones. A nivel global, se estima que La Mancha contribuye 191 kg de metano y 184 Mg de dióxido de carbono a la atmósfera por año. Los resultados presentados resaltan la importancia de realizar estudios que caractericen con alta resolución espaciotemporal los cuerpos de agua costeros.

Seasonal dynamics of greenhouse gases and oxygen over the saline gradient of a tropical coastal lagoon

Teresa Aguirrezabala-Campano¹, Frédéric Thalasso¹

¹Biotechnology and Bioengineering Department, Cinvestav, Avenida IPN 2508, Mexico City, San Pedro Zacatenco, 07360, Mexico.

Abstract

This work presents the exhaustive characterization of the methane, carbon dioxide and oxygen dynamics of the tropical coastal lagoon “La Mancha”, located in the State of Veracruz, Mexico. We performed measurements in the sediments and water column, and we quantified the greenhouse gas emissions of the lagoon in three characteristic seasons. The methane cycle was characterized in two transects: (i) North-South longitudinal, including the salinity gradient caused by the mixing of freshwater streaming from a river in the southernmost part of the lagoon and the seawater incoming from the North of the lagoon, and (ii) West-East transversal, including the northwest area dominated by mangrove up to the opening of the lagoon. We observed a strong seasonal regulation which in turn influenced the inflow of freshwater into La Mancha. The rainy season in particular, during which the river discharge, organic matter, and water input from the sea increases, we observed the highest variability and magnitude of emissions. Globally, we estimate that La Mancha contributes 191 kg of methane and 184 Mg of carbon dioxide per year. Our results highlight the importance of performing studies that characterize with high spatiotemporal resolution the coastal water bodies.

7.3.1 Introduction

Methane (CH_4) is a greenhouse gas (GHG) known to be the second most abundant in the atmosphere. It also possesses a global warming potential 28 times higher than carbon dioxide (CO_2) on a 100-year horizon (Saunois et al., 2016). Input of CH_4 to the atmosphere comes from both anthropogenic activities and natural sources, the latter includes aquatic ecosystems such as wetlands, freshwater, geological sources, and oceans. Oceanic sources are estimated to emit up to 10 Tg of CH_4 per year (Saunois et al., 2019) and may arise from different sources, i.e. lateral transport, geological CH_4 seepage, marine hydrates, groundwater discharge, plant-facilitated transport, or *in situ* production in the water column and sediments. Coastal ecosystems are particularly important as they account for 75% of oceanic emissions (Osudar et al., 2015). Mangroves, tidal flats, salt marshes, and coastal lagoons all comprise coastal environments and, as such, they represent valuable transition zones between the ocean and terrestrial ecosystems. Their value lies in the broad spectrum of essential services they provide, e.g. coast protection from erosion and mitigation of hurricanes, or nursery and breeding sites for marine species and birds.

Despite being active sites of mixing and exchange of nutrients and organic carbon, CH_4 emissions are relatively low compared to freshwater ecosystems. However, as more studies are performed, the complexity of the CH_4 cycle in these ecosystems unravels. For instance, some studies have shown that high sulfate and salinity concentrations, which is a characteristic of these ecosystems, negatively impacts CH_4 -producing (methanogenic) archaea and CH_4 -oxidation (methanotrophic) bacteria (Liu et al., 2016; Osudar et al., 2015). Other studies have provided evidence that have shown that methanogenesis and sulfate reduction coexist in diverse ecosystems (Dupraz et al., 2009; Sela-Adler et al., 2017; Wu et al., 2014; Yuan et al., 2009), despite previous evidence that relatively high sulfate concentration hinders methanogenesis due to substrate competition with

sulfate-reducing bacteria (SRB). Sela-Adler et al. (2007) showed that although sulfate reduction will control the rate of methanogenesis under limiting substrate concentrations, both processes can coexist in sites with excess substrate. Other studies, focused on deep marine sediment, have shown that the main substrate for methanogenesis in these sites is methylated compounds (Oremland and Polcin, 1983; Zhuang et al., 2016), thus avoiding competition with SRB, since these microorganisms are unable to process methylated compounds. A paradoxical methane supersaturation that has been observed in the surface of some marine ecosystems (Oremland, 1979; Reeburgh, 2007; Repeta et al., 2016) has been recently explained by alternative pathways for CH₄ release through bacterial aerobic degradation of methyl phosphonates (Karl et al., 2008; Repeta et al., 2016). Furthermore, anaerobic methane oxidation (AOM) could be masking methanogenesis in saline ecosystems due the readily availability of alternative electron acceptors, resulting in low methane concentration in the water column and low net methane production in sediments (Valenzuela et al., 2020, 2017; Zhuang et al., 2018). Chuang et al. (2017), observed relatively high CH₄ concentration and fluxes in mangrove-dominated coastal lagoons, attributed to strong methanogenesis in the sediments and the inability of methanotrophic bacteria to consume the produced CH₄, while no relation was found between CH₄ and salinity. Hence, it becomes apparent that methane-related activity is site-specific and further studies are required to both have a better understanding of the CH₄ cycle and improve emission estimations in coastal ecosystems.

The uncertainties associated to global oceanic emissions may be reduced by improving the quantification and representation of CH₄ emissions worldwide (Bange, 2006; Saunois et al., 2019). However, it is difficult to adequately represent coastal ecosystems given the complexity and spatiotemporal variability associated to CH₄ dynamics. Mexico is a particularly privileged country given that it possesses one of the largest coastlines worldwide, extending over 11,122 km with a

continental shelf of 288,000 km² (CONABIO-CONANP-TNC-PRONATURA, 2007), which has been scarcely studied in terms of the CH₄ cycle. In this work, high-resolution methods were used for the full characterization of the CH₄ dynamics of a coastal lagoon with riverine input located in the Atlantic coast of Mexico. Our aim was to characterize all the aspects of the CH₄ cycle, encompassing production, storage, and emissions. As such, this is the first study to report all the aspects of the methane cycle using a high-resolution approach, providing a valuable insight into the dynamics of methane of the coastal lagoon La Mancha, located in the Veracruz State (Gulf of Mexico).

7.3.2 Materials and methods

7.3.2.1 Site description and sampling campaigns

La Mancha (LM) is a coastal lagoon located in the State of Veracruz, Mexico, its climate is equatorial tropical savanna climate (Aw; Kottke et al., 2006), characterized by mean annual temperature above 22 °C. As depicted in Figure 7.3.1, LM has a length of 3 km, and area of 1.32 km², the main water inflows come from the “Caño Grande” stream, located at the southernmost edge of the lagoon, and, ephemerally, the Gulf of Mexico. The connection to the sea depends on the season and the local fishing community, the latter according to their necessity for a certain salinity to ensure oyster survival, which are collected and commercialized. The site is characterized for having three distinctive seasons: dry, i.e. February through May, rainy, i.e. June through September, and north wind season, i.e. October through January. During the dry season, the temperature rises, and it has a low accumulated precipitation (<60 mm), whereas during the rainy season LM becomes connected to the sea and experiences the most precipitation (224 ± 25 mm) along with an increase in turbidity and discharge from the Caño Grande stream into the lagoon.

During the north wind season, hereafter referred to as the northern season, LM typically loses connection to the sea, and polar winds reach a mean velocity of 10 km h^{-1} with frequent storms and relatively low temperatures (Torres Alvarado et al., 2016). Three sampling campaigns were performed towards the end of each characteristic season to account for seasonal variation. Figure 7.3.1 shows the monitoring and sampling stations (MSS), designed to provide measurements along two transects: T1, from the south (stream inflow) to the sea connection (northwest), with increasing salinity, and T2, from the northwestern section to the sea connection.

7.3.2.2 *Limnological characteristics*

Water depth was measured at over 200 locations for each season using a portable sounder (Depthmate Portable Sounder, Speedtech, USA) and a global positioning system (eTrex 20, Garmin, USA) to produce bathymetric maps. The surface area (A_w) was estimated through image analysis of satellite photographs obtained from Google Earth Pro (v.7.3), while the seasonal volumes (V) were interpolated from the bathymetric maps. Temperature, pH, oxidation-reduction potential (ORP), and salinity (sal) were measured continuously from the surface to the bottom at each MSS with a multi-parametric probe (HI 9828, Hanna Instruments, Mexico and YSI 556 MPS, Xylem Analytics, USA). Mid-column water samples were taken from selected MSS with a horizontal 2.2-L Van Dorn bottle (Wildco, Mexico), handled according to standard methods (APHA, 1985) and used for determination of ammonia, nitrates and nitrites, and total phosphorus. Secchi depth was determined with a 0.2 m Secchi disk in each MSS. The halocline depth determination was obtained by calculating the density of water, corrected by salinity and temperature, from the surface to the sediments and obtaining the highest difference in density.

7.3.2.3 Greenhouse gases fluxes

Fluxes of greenhouse gases, CH₄ and CO₂, were determined *in situ* using a floating static chamber (SC) method connected to an ultraportable greenhouse gas analyzer (UGGA, Los Gatos Research, USA) in a closed circuit. Triplicate determination of fluxes were calculated as:

$$F = \frac{\Delta C}{\Delta t} \cdot \frac{V_{sc}}{A_{sc}} \quad (1)$$

where F is the flux (mg m⁻² d⁻¹), ΔC is the change of CH₄ or CO₂ concentration (mg m⁻³) observed in the SC over the total sampling time (Δt; d), V_{SC} is the SC volume (7.8×10^{-3} m³), and A_{SC} is the area of the SC in contact with the water surface (9.6×10^{-3} m²). The UGGA has a data acquisition frequency of 1 Hz, providing high-resolution CH₄ and CO₂ concentration measurements. The SC method allows to distinguish diffusive and ebullitive fluxes, but only the former were detected. Diffusive flux measurements were validated using a linear model fit, fluxes with a linear correlation coefficient (R²) superior to 0.80 and a p-value lower than 0.05 were considered diffusive. Despite the large number of flux measurements (215 total), no ebullition events were observed during our measurements.

7.3.2.4 Dissolved gas concentration

The M-ICOS method (Gonzalez-Valencia et al., 2014) was used to determine the dissolved CH₄ (C_{CH4}) and CO₂ (C_{CO2}) concentrations in the water column. This method consisted of a gas-liquid exchange membrane (PDMSXA-1000, Medarray Inc., USA) composed of an array of silicone hollow fibers, with a total exchange area of 1000 cm². The water extracted at the desired depth of the reservoir was constantly flowing outside of the hollow fibers, while a CH₄- and CO₂-free nitrogen was counterflowing inside the hollow fibers at a constant rate. Due to diffusive forces,

the dissolved CH₄ and CO₂ contained in the water were transferred to the gas phase, where they were detected by an ultraportable greenhouse gas analyzer (UGGA, Los Gatos Research, USA). The water was continuously extracted at the desired depth with a peristaltic pump (12 V, Solinst, Mexico), at a flow rate of 1.2 L min⁻¹, while the CH₄- and CO₂-free nitrogen was flowing at a constant flow rate of 0.75 L min⁻¹, controlled by a mass flow controller (GFC 17, Aalborg, Mexico). According to the M-ICOS method, the setup was calibrated at the beginning and at the end of each measurement day, with a standard headspace equilibration technique (Gonzalez-Valencia et al., 2014a). In order to obtain the C_{CH₄} and C_{CO₂} profiles, the extraction probe was maintained just below the water surface for about 60 s, the probe was then allowed to descend steadily at a rate of 1 m min⁻¹ until it reached the bottom where it was kept for an additional 30 s. Additionally a flow-through oxygen optode (FTC-PSt3, PreSens, Germany) was included in the water extraction line, allowing the simultaneous determination of dissolved oxygen concentration (C_{DO}). Using this procedure, about 60 data points on dissolved gases were acquired for each meter of water column depth. The lower detection limit of the M-ICOS method under the present configuration was 0.08 µg L⁻¹ for C_{CH₄} and 176 µg L⁻¹ for C_{CO₂}, while the lower detection limit of the C_{DO} optode was 20 µg L⁻¹.

7.3.2.5 Methane production/oxidation rates

Water samples were taken to measure the CH₄ production/oxidation rates following the salinity gradient and, in some cases, C_{CH₄} and C_{DO} profiles. The water samples, taken with a Van Dorn bottle were carefully transferred to 50-mL glass syringes that included an optical oxygen Sensor Spot (PSt-3 or PSt-6, PreSens, Germany) previously fixed to the inside wall. Avoiding the presence of any bubble, these syringes were transferred as soon as possible to the laboratory, typically within

one hour, for incubation at constant temperature, similar to water temperature of the lagoon. Then, at time intervals, dissolved oxygen concentration was determined by querying the Sensor Spots, and 2 mL of sub-samples were taken in a 5-mL plastic syringe, in which 3 mL of CH₄- and CO₂-free nitrogen were further added. The sub-sample syringe was then vigorously shaken for 30 s, to allow for gas/liquid equilibration. The liquid volume of the sub-sample syringes was evacuated, and the 3 mL gas content of the syringe was then injected through a septum, in a continuous flow of nitrogen passing through the UGGA circuit, i.e., open circuit. The presence of CH₄ in the sample injected was detected as a peak response, that was integrated, after proper calibration with known volumes of CH₄. The CH₄ concentration in the original samples were determined according to the Bunsen coefficient (Liotta and Martelli, 2012). These incubations were sustained from five to seven days, during which a total of five to six triplicate measurements of C_{CH₄} were done to establish the CH₄ production/oxidation rates. That protocol allowed for the determination of combined CH₄ and C_{DO} production/uptake rates without headspace addition, thus under the C_{DO} and C_{CH₄} conditions prevailing in LM.

7.3.2.6 *Sediment CH₄ and CO₂ concentration*

Sediment samples were taken at each MSS using a dredge and transferred into 60-mL plastic syringes with the piston removed using a spoon, until approximately 20 mL were obtained. Then, 10 mL of surface water were added, as well as a glass bead and the syringe was assembled carefully to avoid losing water and sediment. Atmospheric air was taken into the syringe to reach 60 mL and closed using a three-way valve. The CH₄ input from the water and air are negligible considering the high C_{CH₄} present in the sediments. In the laboratory, the syringes were shaken and centrifuged, which allowed to visualize and record the actual sediment volume. Finally, 3 mL

of headspace sample were transferred into a 3-mL plastic syringe and then injected into the UGGA. The peak response was integrated as described in section 2.5 and translated into headspace concentration of CH₄, which was then used to back calculate the CH₄ content of the sediment samples.

7.3.2.7 Sediment CH₄ production rates

Sediment samples were collected using an Eckman dredge at each MSS and transferred into double Ziploc bags. Once in the laboratory, using a 60-mL syringe, 30 mL of sediment were transferred into borosilicate glass serological bottles (120 mL), sealed with butyl-rubber septa and aluminum crimp, and then flushed with N₂ to ensure anaerobic conditions. The CH₄ concentration was performed by taking 1 mL of N₂ in a 3-mL plastic syringe, the syringe was then inserted through the septa using a needle and the volume of N₂ was injected into the bottles. After allowing mixing without removing the syringe, the same volume was withdrawn from the headspace and injected into the closed circuit of the UGGA. The peak response was integrated as described in section 2.5 and translated into headspace concentration of CH₄, allowing the calculation of CH₄ production rate from each MSS. This procedure was repeated approximately every 24 h, always ensuring that anaerobic conditions were preserved. After the first measurement, the bottles accumulated pressure from gas production, which was registered using a pressure transducer (PSI-30, Centrepoint Electronics, Ireland).

7.3.2.8 Data treatment and statistics

Data collected during the campaigns were processed using MATLAB (MathWorks, 2015a), the dissolved gas concentration profiles were smoothed by weighted linear least squares and a Savitzky-Golay filter. The contour maps were generated by interpolation of the high-resolution

data using Surfer 11.0 software (Golden Software, USA). The Surfer Software provides 10 interpolation methods, from which the best was chosen by evaluating their mean absolute error (MAE) and the mean bias error (MBE ;Willmott and Matsuura, 2006).

We used the numerical homogeneity model (NHM; Gonzalez-Valencia et al., 2019) to examine the spatial distribution of the salinity, fluxes, and dissolved gas concentrations. The NHM assigned a numerical value to the distribution. In brief, the model yields a homogeneity index of parameter P (h_p , %) along two dimensions, which can be length and length for surface fluxes, or length and depth for dissolved gases or salinity. A nonhomogeneous distribution contains values $0 \leq h_p < 100\%$, while for a homogeneous distribution, $h_p = 100\%$. Similarly, the NHM allows the calculation of homogeneity in one dimension ($h_{P,x}$), with x being either length or depth, depending on the parameter. Using the NHM we can also calculate an anisotropic factor (ω_P , °), which indicates the angle of the heterogeneities in the two-dimensional space. This value ranges from -45°, when heterogeneities are observed only in the x dimension (length), to 45° for heterogeneities only in the y dimension (length or depth).

All statistical procedures were performed using the packages *stats*, *rstatix*, *dplyr*, and *tidyverse* of R software version 3.6.2 (Kassambara, 2020; Team, 2019; Wickham et al., 2020, 2019). Plots were generated using the *ggplot2* package (Wickham, 2016). Two-way ANOVA were performed to examine river and seasonal influence over physicochemical parameters and dissolved gas concentrations. The assumptions of the two-way ANOVA over model residual were reviewed using the Shapiro-Wilk test for normality and the Bartlett's test for homogeneity of variances. Most variables had a positive skew due to the nature of LM, which were log-transformed to achieve normality of the ANOVA residuals. In some instances, the homogeneity of variances assumption

was not met; consequently, two Welch one-way ANOVA were performed. If a significant effect was observed, multiple pairwise comparisons were then performed to determine which effect was different.

7.3.3 Results and discussion

7.3.3.1 Physicochemical and limnological characteristics

LM is a relatively shallow lagoon, its depth ranges 0.3 to 3.3 m depending on the season (Figure 7.3.1). The shallowest overall depth was observed during the rainy season with a mean of 0.89 ± 0.46 m (mean \pm one standard deviation of the mean), whereas the deepest mean depth of 1.24 ± 0.43 m was measured during the northern season. The mean depth of LM was 1.03 ± 0.36 m during the dry season. A halocline was consistently observed in the southern section of the lagoon, and stratified LM due to the density difference caused by freshwater and seawater salinity with a depth and length that fluctuated across seasons. During the rainy season, when LM was connected to the sea, we observed the deepest and longest halocline from R1 to LM-6 at a mean depth of 0.48 ± 0.16 m, whereas during the northern season the halocline receded to LM-2 with a mean of 0.10 ± 0.18 m. The halocline was present during the dry season from MSS R1 to LM-2, with a mean depth of 0.24 ± 0.16 m. Thus, from this point onward, when referring to river-influenced MSS it will include R1 – LM6 for the rainy season, and R1 – LM2 for the northern and dry seasons.

Table 7.3. shows clear differences between measured parameters across seasons and above and below the halocline. The temperature difference above and below the halocline indicates that the denser seawater was warmer than the freshwater streaming above it. A marked lengthwise gradient of salinity was evident in LM. The distribution of salinity was relatively homogeneous with an h_{sal} of 85 – 99% and an anisotropic factor (ω_{sal}) of -45 to -31° for both transects across seasons. Despite

the vertical stratification caused by the halocline, the latter implies that lengthwise anisotropy was predominant. Only during the northern season depth-wise anisotropy predominated with a ω_{sal} of 12.56°.

No significant effect of river influence was found in the mid-column nutrient concentration across seasons. Total phosphorus concentrations ranged from 1.68 to 23.60 µM, with a median of 6.26 µM. Ammonium was the most predominant nitrogen specie with concentrations ranging from 0.014 to 21.71 µM and a median of 5.54 µM. Nitrites and nitrates accounted from 0.29 to 11.36 µM, with a relatively low median of 1.61 µM. Our results are in agreement with previous reports of LM (Contreras-Espinosa et al., 2005; Rivera-Guzmán et al., 2014). The N:P ratios showed nitrogen limitation with relatively low seasonal medians of 1.14, 1.28, and 2.03 for the rainy, dry, and northern season, respectively. The ratio fluctuated across MSS within the same season as well, but the northern season had the highest N:P reaching a magnitude of up to 6.46.

During the rainy season, the increased river input resuspended the sediments and carried organic matter from land runoff (Torres-Alvarado et al., 2005), while the connection to the sea increased the salinity. Thus, the higher organic matter input from the river and the increased concentration of alternative electron acceptors present in the seawater input were likely responsible for the reduced ORP conditions observed for the rainy season. The northern season standed out with a lower salinity, temperature, and higher ORP compared to the rainy and dry season ($p<0.05$). The water in LM was stagnant during the dry season, given that there was lower river input and wind speed, and exchange with the sea was limited. As a result, O₂ exchange was limited as well, thus causing a predominance of other reductive processes taking place as observed by the decline of ORP.

Season	Halocline	pH	Salinity (‰)	T (°C)	ORP (mV)
Rainy	Above	7.99 ± 0.09	6.17 ± 8.96	29.14 ± 2.8	-11.05 ± 61.43
	Below	7.65 ± 0.29	27.21 ± 2.72	33.19 ± 1.5	-190.09 ± 151.94
Northern	Above	8.13 ± 0.27	3.2 ± 4.36	25.02 ± 1.02	8.51 ± 13.05
	Below	8.09 ± 0.62	17.26 ± 2.45	26.81 ± 1.43	19.01 ± 36.32
Dry	Above	7.59 ± 0.15	3.57 ± 4.67	29.34 ± 1.05	-59.91 ± 44.13
	Below	7.42 ± 0.37	20.2 ± 2.12	32.12 ± 1.16	-124.29 ± 141.53

Table 7.3.1. Mean concentrations of the measured physicochemical parameters across seasons.

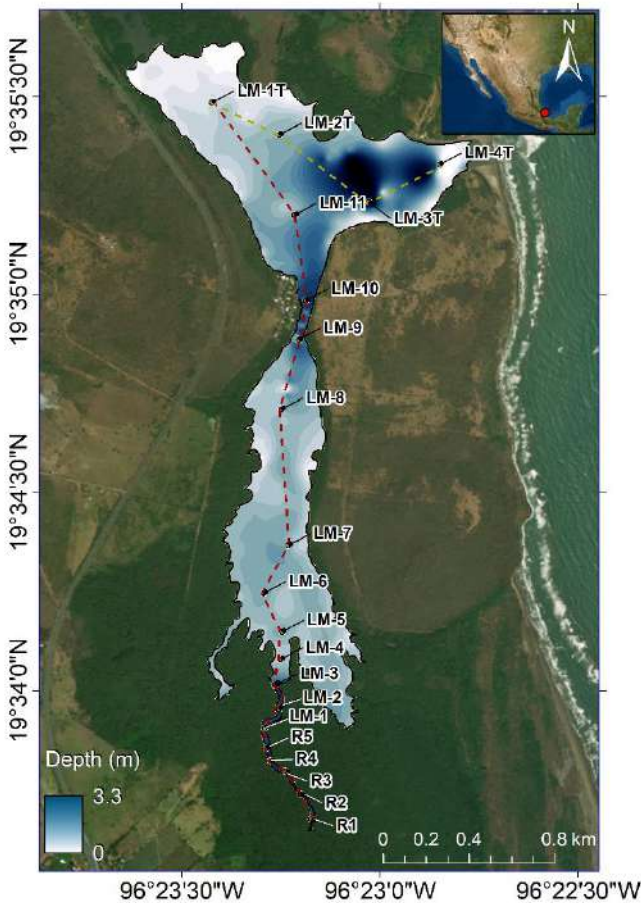


Figure 7.3.1. Bathymetric map of La Mancha during the northern season referenced for each sampling station, longitudinal transect from the river (T1, red dashed line), and longitudinal transect from the mangrove to the opening of the lagoon (T2, beige dashed line).

7.3.3.2 Sediments dynamics

The sediment CH₄ concentrations ranged from 0.002 to 55.78 mg g_{DW}⁻¹ (grams per dry-weight of sediment, Figure 7.3.2). No seasonal effect was observed, but we found significant differences between river-influenced, i.e. halocline present, and seawater-dominated samples ($p<0.05$). The median for river-influenced samples was 1.89 mg g_{DW}⁻¹, whereas the seawater-dominated samples had a median of 0.036 mg g_{DW}⁻¹. A similar trend was observed for CH₄ production rates in the sediments, with MSS samples closer to the river showing significantly higher rates of production ($p<0.05$; Figure 7.3.S1A), the mean rates of CH₄ production ranged from 0.05 to 0.88 mmol m⁻³ d⁻¹. The concentrations of CO₂ ranged from 0.003 g g_{DW}⁻¹ to 2.39 g g_{DW}⁻¹ and a significant effect of both seasons and river-influence was found in contrast to CH₄ concentrations. Dry season concentrations were significantly higher ($p<0.05$), as well as river-influenced MSS ($p<0.05$). River-influenced MSS had a median of 0.216 g g_{DW}⁻¹, while seawater-dominated had a median of 0.046 g g_{DW}⁻¹. A marked trend of CO₂ production rates decreasing with the distance from the river input (Figure 7.3.S1B). Production rates from river-influenced samples were significantly higher, as well as samples from the northern season ($p<0.05$).

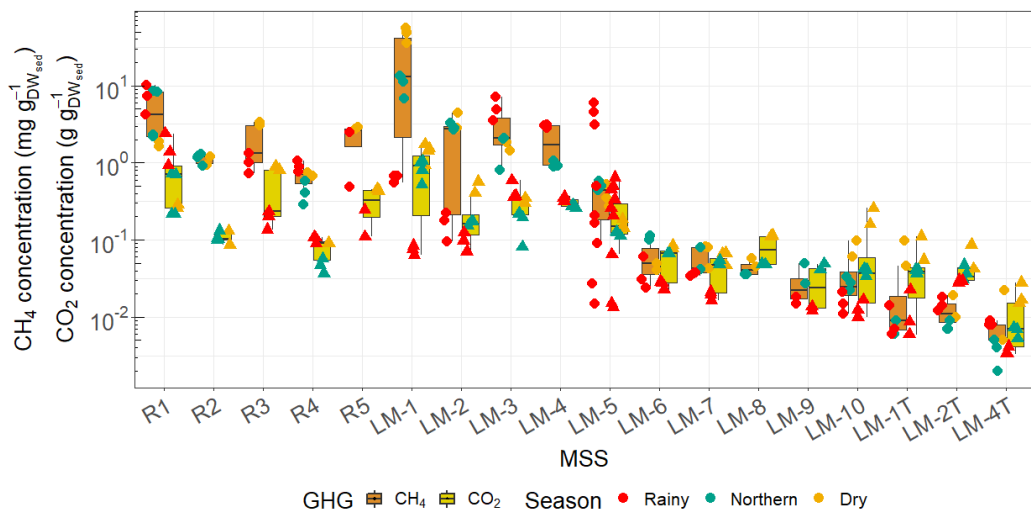


Figure 7.3.2. GHG concentration in sediment along a longitudinal transect and across seasons.

7.3.3.3 Dissolved gas concentration in the water column

An important input of GHGs coming from the river was observed (Figure 7.3.3A and Figure 7.3.S2A), dissolved GHGs concentrations in river-influenced MSS were significantly larger than the rest of LM ($p<0.05$). A difference of about one order of magnitude in the water column C_{CH_4} between river-influenced and sea-dominated MSS was observed for all seasons (Table 7.3.3). The lowest median C_{CH_4} was observed during the northern season, whereas the highest median C_{CH_4} was found during the dry season; however, only the northern season was significantly different from the others ($p<0.05$). The latter could imply there was more methanogenesis during the dry season, but storage certainly increased as there was limited exchange with the atmosphere due to the stagnant water column, as it will be described in Section 9.3.4. The range of C_{CH_4} found in LM were within the higher range of other coastal ecosystems (2.8×10^{-8} to 9.25 mg L^{-1} ; Bange, 2006; Chuang et al., 2016; Deborde et al., 2010; Huertas et al., 2018; Musenze et al., 2016; Orif et al., 2017). A relatively homogeneous distribution in the depth direction was found for C_{CH_4} , with $h_{CH_4, \text{depth}}$ ranging 90 – 93% for T1 and T2. In contrast, a more heterogeneous distribution was present for the lengthwise direction, particularly in T1 with $h_{CH_4, \text{length}}$ ranging 35 – 49%, whereas $h_{CH_4, \text{length}}$ for T2 ranged 80 – 97%. This was further observed with ω_{CH_4} showing a predominance of anisotropy in the length direction.

The highest methanotrophic activity was detected on the river-influenced MSS during the rainy and dry seasons (Table 7.3.4). A decrease in methanotrophic activity was found during the northern season, attributed to the lower temperature and C_{CH_4} concentration ($p<0.05$). The methanotrophic turnover, i.e. the time needed for methanotrophic activity to uptake the respective C_{CH_4} , of superficial CH_4 ranged between 2.59 to 341 days, whereas the bottom turnover ranged from 0.61

to 36 days. Our methanotrophic rates are within the range reported in the Mandovi and Elbe estuary, both showing the same trend of methanotrophic activity decline along their salinity gradients (Araujo et al., 2018; Matoušů et al., 2017). We also observed relatively low rates of methane production in the water column during the dry season, previously reported to exist in other seawater ecosystems (Karl et al., 2008; Repeta et al., 2016). The fact that we observed methane production only during the dry season, could be attributed to the phytoplaktonic succession that LM experiences depending on its connection to the sea (Contreras-Espinosa et al., 2005).

Similar to CH₄, there was an important input of CO₂ coming from the river exported to LM (Figure 7.3.3A and Figure 7.3.S2B), which causes a significant difference between river-influenced and seawater dominated MSS ($p<0.05$). As mentioned in the previous section, the presence of

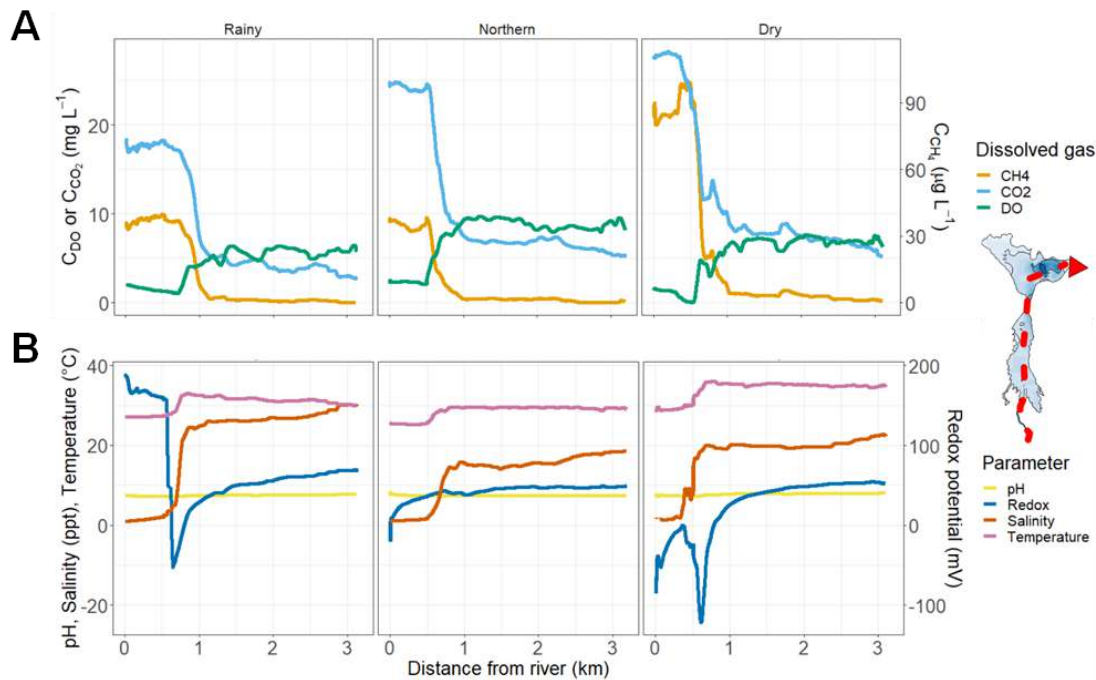


Figure 7.3.3. Seasonal continuous measurement of surface water concentration of dissolved gases (A) and physicochemical parameters (B).

Season	Section	C_{CH_4} (mg L ⁻¹)	C_{CO_2} (mg L ⁻¹)	DO (mg L ⁻¹)
Rainy	R1 to LM-6	0.052 ± 0.034	12.781 ± 3.497	0.961 ± 0.66
	LM-7 to LM-1T	0.006 ± 0.007	6.528 ± 4.431	3.577 ± 1.806
	Entire LM*	0.01	8.55	1.88
Northern	R1 to LM-2	0.028 ± 0.012	11.286 ± 1.452	0.876 ± 0.406
	LM-3 to LM-1T	0.003 ± 0.003	6.351 ± 1.298	6.138 ± 2.188
	Entire LM*	0.0016	6.79	5.96
Dry	R1 to LM-2	0.151 ± 0.061	27.854 ± 7.661	0.085 ± 0.027
	LM-3 to LM-1T	0.016 ± 0.03	10.846 ± 4.634	4.408 ± 2.306
	Entire LM*	0.0039	9.71	4.61

Table 7.3.2. Mean dissolved gas concentrations of the entire water column for the sampled seasons. *Median values are shown.

mangrove surrounding the river-dominated area contributes an important amount of organic matter into the Caño Grande stream inflow. The organic matter is then respired as it travels along T1, forming a longitudinal gradient. The high rates of riverine organic matter input and respiration, characteristic of coastal ecosystems in lower latitudes (Cai, 2011), resulted in relatively high C_{CO_2} . As expected from the latter, the distribution of CO_2 was more homogeneous compared to CH_4 . There was a predominance of lengthwise heterogeneity with $h_{CO_2, depth}$ ranging 90 – 93% while $h_{CO_2, length}$ ranged from 72 – 86% in T1 and 94 – 97% in T2. Both GHGs followed the same trend of ω development, lengthwise anisotropy dominated during the dry season, gradually equilibrating as it goes through the rainy and northern seasons. The rainy and northern seasons had similar C_{CO_2} , which could be due to the more alkaline state of LM compared to the northern and rainy seasons, i.e. inorganic carbon becomes HCO_3^- . In contrast, the highest C_{CO_2} were found during the dry season, which were significantly higher than during the northern and rainy seasons ($p < 0.05$), due to its accumulation which in turn lowers the pH of LM. The latter implies a positive feedback effect on C_{CO_2} , as it decreases pH it pushes the bicarbonate system chemical balance to free CO_2 . Further evidence of the pH impact on CO_2 equilibria was observed during our methanotrophic incubations since CO_2 net production was measured as well. Significantly lower CO_2 net

production rates were observed during the rainy and northern seasons compared to the dry season ($p<0.05$). The net CO₂ production ranged from -16.21 to 26.52 $\mu\text{mol m}^{-3} \text{d}^{-1}$, whereas during the dry season it ranged from 13.90 to 134.20 $\mu\text{mol m}^{-3} \text{d}^{-1}$. The negative rates found during the northern and rainy seasons are attributed to carbonic acid formation and its further dissociation into bicarbonate due to the higher pH.

The river input water was also clearly depleted of DO, as shown in Table 7.3.2. The respiration of the high organic matter contents of riverine water triggers the decline of DO, hence we observed a significantly lower C_{DO} in river-influence MSS compared to seawater-dominated MSS ($p<0.05$). During the northern season we observed significantly higher C_{DO} compared to the other two seasons ($p<0.05$). Contreras-Espinosa et al. (2005) showed that the fluctuation of N:P was directly related to primary productivity efficiency, as N:P increased primary productivity became more efficient. Since the highest N:P ratios were found during the northern season, we attribute the higher C_{DO} to the increased efficiency of primary production as well as the reduction of organic matter input from the river. Although no significant difference was observed between the rainy and dry season, it is worth repeating that the effect of the stagnant column during the dry season exacerbates the lack of DO as respiration proceeds in the river-influenced zone of LM (Figure 7.3.S1C). The seawater-dominated MSS of LM, during the dry season, had a relatively high C_{DO}, attributed to the excess DO leftover from the northern season and the limited atmospheric exchange. The same behavior as the GHGs was observed for C_{DO}, h_{DO} ranged 61 – 69% for T1, while T2 was relatively more homogeneous with h_{DO} ranging from 80 – 93% for T2. Lengthwise anisotropy was predominant, as ω_{DO} decreased from -17.63° during the rainy season, to -28.11° during the northern season, and reaching -31.50° in the dry season. The rainy season showed the

least homogeneous lengthwise and depthwise distribution, as expected from the limiting conditions of C_{DO}. The aerobic respiration seasonal measurements are shown in Table 7.3.3, showing a relative stability across seasons.

7.3.3.4 GHG fluxes and overall dynamics

The fluxes of CH₄ were relatively variable spanning three orders of magnitude (column in a given MSS by the quantified flux. It ranged from 0.11 to 17.05 days, with larger turnover times observed

CH4 fluxes (mg m ⁻² d ⁻¹)							
Season	Influence	Min	Max	Mean	SD	VC	Median
Rainy	River	0.47	140.30	35.12	39.67	112.96	21.69
	Lagoon	0.85	26.24	6.33	5.73	90.49	4.48
	Entire			8.43	11.49	136.30	5.04
	LM						
Northern	River	0.96	26.66	8.71	6.22	71.37	6.90
	Lagoon	0.24	16.94	3.31	3.47	104.85	2.12
	Entire			3.13	2.64	84.35	2.12
	LM						
Dry	River	4.94	77.10	22.81	19.34	84.79	14.16
	Lagoon	0.35	11.57	3.97	3.33	83.80	2.54
	Entire			5.48	6.70	122.26	3.17
	LM						
CO2 fluxes (g m ⁻² d ⁻¹)							
		Min	Max	Mean	SD	VC (%)	Median
Rainy	River	0.79	55.88	16.52	15.05	91.09	10.13
	Lagoon	0.43	18.20	4.59	3.77	82.01	2.99
	Entire			5.51	5.55	100.72	3.82
	LM						
Northern	River	2.16	24.71	9.63	5.18	53.76	8.25
	Lagoon	0.77	14.69	4.99	3.27	65.52	3.93
	Entire			5.11	2.65	51.86	4.09
	LM						
Dry	River	4.49	27.56	11.27	5.71	50.65	9.90
	Lagoon	1.55	14.40	5.09	3.37	66.24	4.14
	Entire			5.75	3.38	58.76	4.65
	LM						

in the river-influenced MSS.

The flux turnover of the dry season was comparatively lower than that of the other two seasons, further confirming that the higher CCH₄ observed during the dry season was due to the stagnant state of the water column. Our results on CH₄ dynamics are in agreement with previous reports of

Table 7.3.4. Greenhouse gas flux statistics; min: minimum, max: maximum, SD: standard deviation, VC: variation coefficient.

coastal ecosystems (Araujo et al., 2018; Chuang et al., 2017; Matoušů et al., 2017). Although the CH₄ concentration and fluxes were negatively correlated to salinity, the latter is a covariate of O₂ concentration and temperature. Thus, we cannot assert whether salinity has a negative impact on CH₄ production in LM.

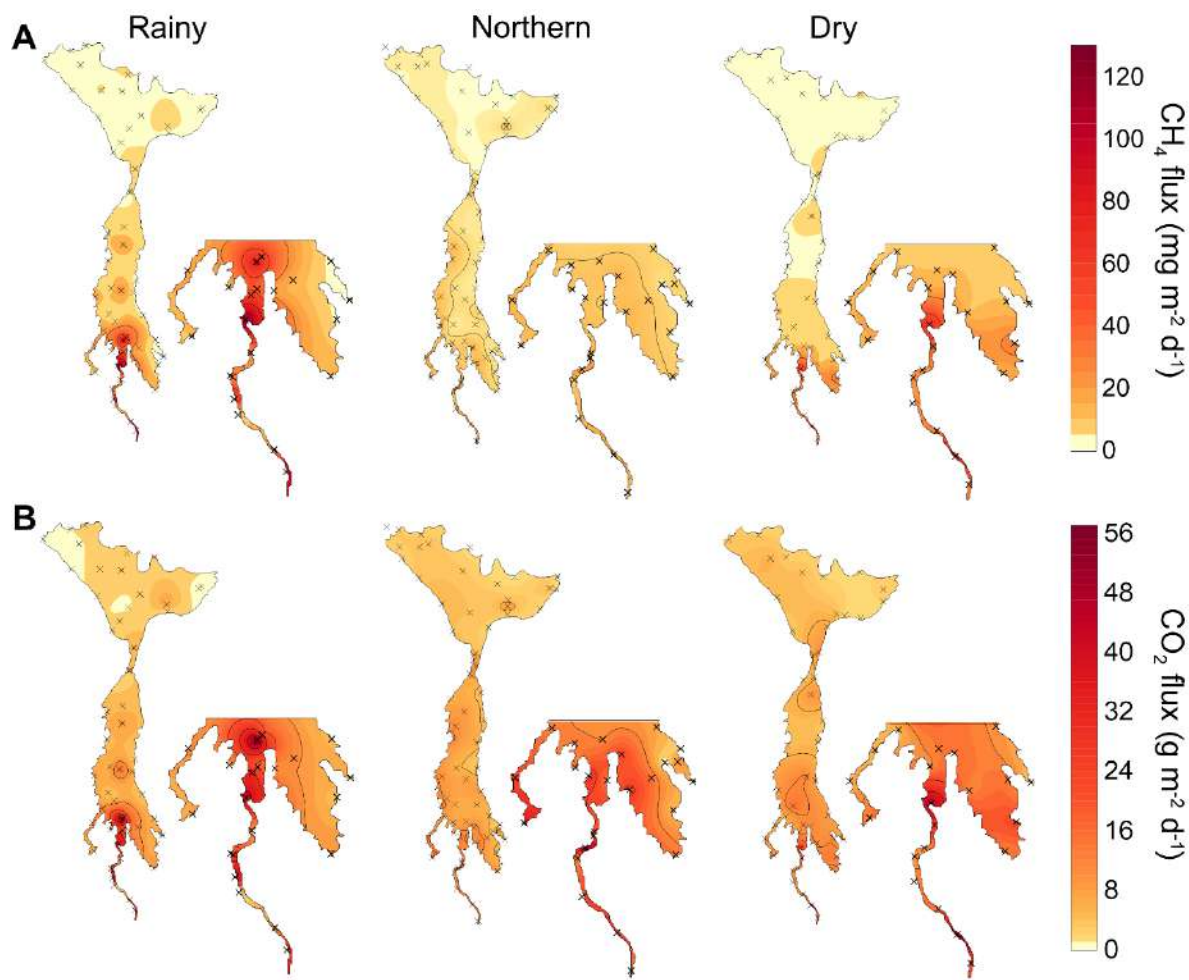


Figure 7.3.4. Contour maps of seasonal CH₄ (top) and CO₂ (bottom) fluxes for the three sampled seasons. A close-up of the river to lagoon zone is shown to the right of each map for ease of visualization. Cross symbol (×) indicates flux sampling stations.

4, Figure 7.3.4). The CH₄ fluxes showed the same trend as C_{CH₄} profiles, i.e. lower fluxes as the distance from the river input increased. Thus, the mean CH₄ fluxes from river-influenced areas were significantly higher than seawater-dominated areas ($p<0.05$). A significant seasonal effect was observed for the northern season, CH₄ fluxes were lower than those of the rainy and dry seasons ($p<0.05$).

As previously mentioned, the northern season had a higher C_{DO}, as well as lower organic matter load, and temperature. The simultaneous effect of these factors during the northern season could explain the lower CH₄ fluxes observed, being conditions more favorable to methanotrophy and less favourable to methanogenesis. The rainy season showed the highest variability of CH₄ fluxes, which is attributed to the larger area of river-influence increasing the variability of C_{CH₄}, salinity, temperature, and ORP. The spatial variability of CH₄ fluxes is further observed in Figure 7.3.A. The h_{CH₄flux} ranged from 50 – 56%, with heterogeneities predominating in the latitudinal direction, i.e. the direction of T1. Assuming a four-month duration of each season, these fluxes translate roughly to a total cumulated emission 95, 36, and 60 kg-CH₄ for the rainy, northern, and dry seasons, respectively. Yearly, we estimate that LM contributes 191 kg-CH₄. Since methanotrophic activity was not widespread in LM, evasion to the atmosphere played a major role in CH₄ turnover. To determine the turnover of CH₄ due to flux, we divided the total mass of CH₄ per area of water

MSS	Depth	Methanotrophic activity ($\mu\text{mol m}^{-3} \text{d}^{-1}$)			Respiration ($\text{mmol m}^{-3} \text{d}^{-1}$)		
		Rainy	Northern	Dry	Rainy	Northern	Dry
Season							
R1	Surface	861.69 ± 3.4	-	957.9 ± 447.8	8.29 ± 2.74	-	7.56 ± 0.64
	Bottom	n.s.	-	n.s.	-	-	-
R2	Surface	869.41 ± 14.6	-	-	7.68 ± 0.73	-	-
	Bottom	n.s.	-	-	-	-	-
LM-1	Surface	585.3 ± 430.3	84.7 ± 20.1	547.6 ± 45.1	9.91 ± 1.02	33.58 ± 2.42	16.57 ± 8.21
	Half-column	-	n.s.	-	-	51.45 ± 8.53	-
	Bottom	n.s.	-	n.s.	-	-	-
LM-5	Surface	n.s.	n.s.	-6.79 ± 14.3	27.61 ± 5.65	-	-
LM-6	Surface	4.02 ± 10.4	n.s.	n.s.	28.45 ± 5.38	-	11.73 ± 4.47
LM-7	Surface	n.s.	24.97 ± 2	n.s.	-	-	13.08 ± 0.48
LM-8	Surface	-	14.57 ± 0.6	-	-	-	-
LM-9	Surface	-	n.s.	-	-	-	-
	Bottom	-	n.s.	-	-	-	-
LM-10	Surface	n.s.	n.s.	n.s.	-	-	30.58 ± 4.38
LM-11	Surface	-	n.s.	-	-	-	-
LM-1T	Surface	-	24.97 ± 2	n.s.	-	-	-
LM-2T	Surface	n.s.	n.s.	-1.68 ± 0.8	51.79 ± 0	-	-
LM-3T	Surface	n.s.	n.s.	n.s.	23.06 ± 4.48	14.52 ± 0.83	18.8 ± 7.96
	Half-column	-	n.s.	-	-	9.77 ± 8.33	-
	Bottom	29.51 ± 31.8	5.53 ± 4.1	-	18.97 ± 1.5	23.9 ± 0.1	-
LM-4T	Surface	n.s.	n.s.	-1.73 ± 0.3	15.69 ± 1.51	12.11 ± 2.73	-

Table 7.3.3. Methanotrophic and respiration rates measured in our incubation assays. Non-significant rates are labeled as n.s. ($p>0.05$), whereas not sampled stations in certain seasons are labeled as -.

column in a given MSS by the quantified flux. It ranged from 0.11 to 17.05 days, with larger turnover times observed in the river-influenced MSS.

The flux turnover of the dry season was comparatively lower than that of the other two seasons, further confirming that the higher C_{CH4} observed during the dry season was due to the stagnant state of the water column. Our results on CH₄ dynamics are in agreement with previous reports of

CH ₄ fluxes (mg m ⁻² d ⁻¹)							
Season	Influence	Min	Max	Mean	SD	VC	Median
Rainy	River	0.47	140.30	35.12	39.67	112.96	21.69
	Lagoon	0.85	26.24	6.33	5.73	90.49	4.48
	Entire			8.43	11.49	136.30	5.04
	LM						
Northern	River	0.96	26.66	8.71	6.22	71.37	6.90
	Lagoon	0.24	16.94	3.31	3.47	104.85	2.12
	Entire			3.13	2.64	84.35	2.12
	LM						
Dry	River	4.94	77.10	22.81	19.34	84.79	14.16
	Lagoon	0.35	11.57	3.97	3.33	83.80	2.54
	Entire			5.48	6.70	122.26	3.17
	LM						
CO ₂ fluxes (g m ⁻² d ⁻¹)							
		Min	Max	Mean	SD	VC (%)	Median
Rainy	River	0.79	55.88	16.52	15.05	91.09	10.13
	Lagoon	0.43	18.20	4.59	3.77	82.01	2.99
	Entire			5.51	5.55	100.72	3.82
	LM						
Northern	River	2.16	24.71	9.63	5.18	53.76	8.25
	Lagoon	0.77	14.69	4.99	3.27	65.52	3.93
	Entire			5.11	2.65	51.86	4.09
	LM						
Dry	River	4.49	27.56	11.27	5.71	50.65	9.90
	Lagoon	1.55	14.40	5.09	3.37	66.24	4.14
	Entire			5.75	3.38	58.76	4.65
	LM						

Table 7.3.4. Greenhouse gas flux statistics; min: minimum, max: maximum, SD: standard deviation, VC: variation coefficient.

coastal ecosystems (Araujo et al., 2018; Chuang et al., 2017; Matoušů et al., 2017). Although the CH₄ concentration and fluxes were negatively correlated to salinity, the latter is a covariate of O₂ concentration and temperature. Thus, we cannot assert whether salinity has a negative impact on CH₄ production in LM.

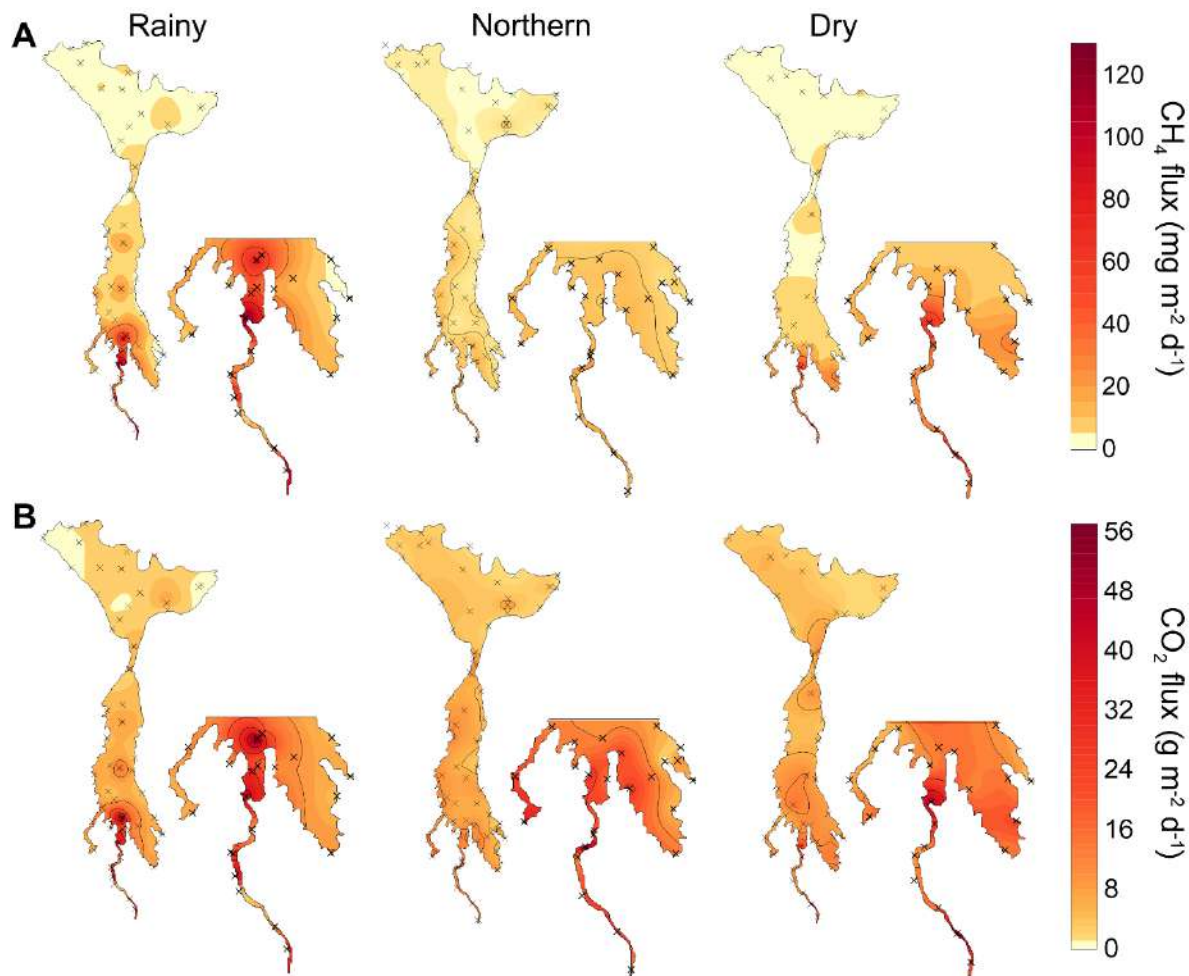


Figure 7.3.4. Contour maps of seasonal CH₄ (top) and CO₂ (bottom) fluxes for the three sampled seasons. A close-up of the river to lagoon zone is shown to the right of each map for ease of visualization. Cross symbol (×) indicates flux sampling stations.

The fluxes of CO₂ were relatively less variable, but larger in magnitude than CH₄ (column in a given MSS by the quantified flux. It ranged from 0.11 to 17.05 days, with larger turnover times observed in the river-influenced MSS.

The flux turnover of the dry season was comparatively lower than that of the other two seasons, further confirming that the higher CCH₄ observed during the dry season was due to the stagnant state of the water column. Our results on CH₄ dynamics are in agreement with previous reports of

CH4 fluxes (mg m ⁻² d ⁻¹)							
Season	Influence	Min	Max	Mean	SD	VC	Median
Rainy	River	0.47	140.30	35.12	39.67	112.96	21.69
	Lagoon	0.85	26.24	6.33	5.73	90.49	4.48
	Entire			8.43	11.49	136.30	5.04
	LM						
Northern	River	0.96	26.66	8.71	6.22	71.37	6.90
	Lagoon	0.24	16.94	3.31	3.47	104.85	2.12
	Entire			3.13	2.64	84.35	2.12
	LM						
Dry	River	4.94	77.10	22.81	19.34	84.79	14.16
	Lagoon	0.35	11.57	3.97	3.33	83.80	2.54
	Entire			5.48	6.70	122.26	3.17
	LM						
CO2 fluxes (g m ⁻² d ⁻¹)							
		Min	Max	Mean	SD	VC (%)	Median
Rainy	River	0.79	55.88	16.52	15.05	91.09	10.13
	Lagoon	0.43	18.20	4.59	3.77	82.01	2.99
	Entire			5.51	5.55	100.72	3.82
	LM						
Northern	River	2.16	24.71	9.63	5.18	53.76	8.25
	Lagoon	0.77	14.69	4.99	3.27	65.52	3.93
	Entire			5.11	2.65	51.86	4.09
	LM						
Dry	River	4.49	27.56	11.27	5.71	50.65	9.90
	Lagoon	1.55	14.40	5.09	3.37	66.24	4.14
	Entire			5.75	3.38	58.76	4.65
	LM						

Table 7.3.4. Greenhouse gas flux statistics; min: minimum, max: maximum, SD: standard deviation, VC: variation coefficient.

coastal ecosystems (Araujo et al., 2018; Chuang et al., 2017; Matoušů et al., 2017). Although the CH₄ concentration and fluxes were negatively correlated to salinity, the latter is a covariate of O₂ concentration and temperature. Thus, we cannot assert whether salinity has a negative impact on CH₄ production in LM.

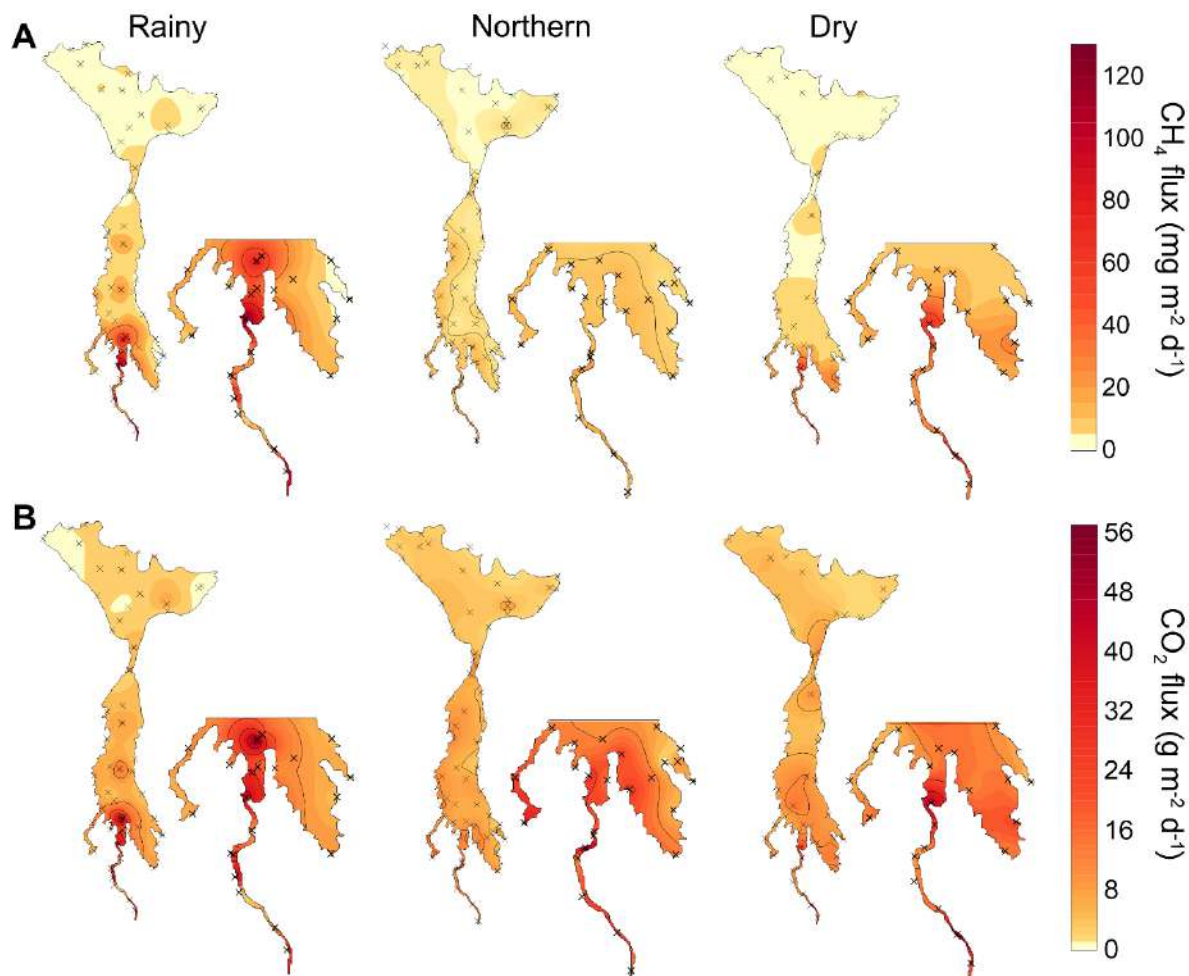


Figure 7.3.4. Contour maps of seasonal CH₄ (top) and CO₂ (bottom) fluxes for the three sampled seasons. A close-up of the river to lagoon zone is shown to the right of each map for ease of visualization. Cross symbol (×) indicates flux sampling stations.

and Figure 7.3.4B). In contrast of CH₄, no significant seasonal effect was observed for CO₂ fluxes. However, as observed for CH₄, the variability of the rainy season was comparatively higher than the other seasons. Furthermore, the significantly higher C_{CO₂} observed during the dry season did not translate to higher CO₂ fluxes, as previously mentioned, the relatively lower wind speed of the dry season decreases atmospheric exchange. Significantly higher fluxes were found in the river-influenced area of LM (p<0.05), about twice as much CO₂ was emitted per unit area in this area

CH₄ fluxes (mg m⁻² d⁻¹)

Season	Influence	Min	Max	Mean	SD	VC	Median
Rainy	River	0.47	140.30	35.12	39.67	112.96	21.69
	Lagoon	0.85	26.24	6.33	5.73	90.49	4.48
	Entire LM			8.43	11.49	136.30	5.04
Northern	River	0.96	26.66	8.71	6.22	71.37	6.90
	Lagoon	0.24	16.94	3.31	3.47	104.85	2.12
	Entire LM			3.13	2.64	84.35	2.12
Dry	River	4.94	77.10	22.81	19.34	84.79	14.16
	Lagoon	0.35	11.57	3.97	3.33	83.80	2.54
	Entire LM			5.48	6.70	122.26	3.17

CO₂ fluxes (g m⁻² d⁻¹)

		Min	Max	Mean	SD	VC (%)	Median
Rainy	River	0.79	55.88	16.52	15.05	91.09	10.13
	Lagoon	0.43	18.20	4.59	3.77	82.01	2.99
	Entire LM			5.51	5.55	100.72	3.82
Northern	River	2.16	24.71	9.63	5.18	53.76	8.25
	Lagoon	0.77	14.69	4.99	3.27	65.52	3.93
	Entire LM			5.11	2.65	51.86	4.09
Dry	River	4.49	27.56	11.27	5.71	50.65	9.90
	Lagoon	1.55	14.40	5.09	3.37	66.24	4.14
	Entire LM			5.75	3.38	58.76	4.65

compared to the rest of LM (column in a given MSS by the quantified flux. It ranged from 0.11 to 17.05 days, with larger turnover times observed in the river-influenced MSS.

The flux turnover of the dry season was comparatively lower than that of the other two seasons, further confirming that the higher CCH₄ observed during the dry season was due to the stagnant state of the water column. Our results on CH₄ dynamics are in agreement with previous reports of

Table 7.3.4. Greenhouse gas flux statistics; min: minimum, max: maximum, SD: standard deviation, VC: variation coefficient.

coastal ecosystems (Araujo et al., 2018; Chuang et al., 2017; Matoušů et al., 2017). Although the CH₄ concentration and fluxes were negatively correlated to salinity, the latter is a covariate of O₂ concentration and temperature. Thus, we cannot assert whether salinity has a negative impact on CH₄ production in LM.

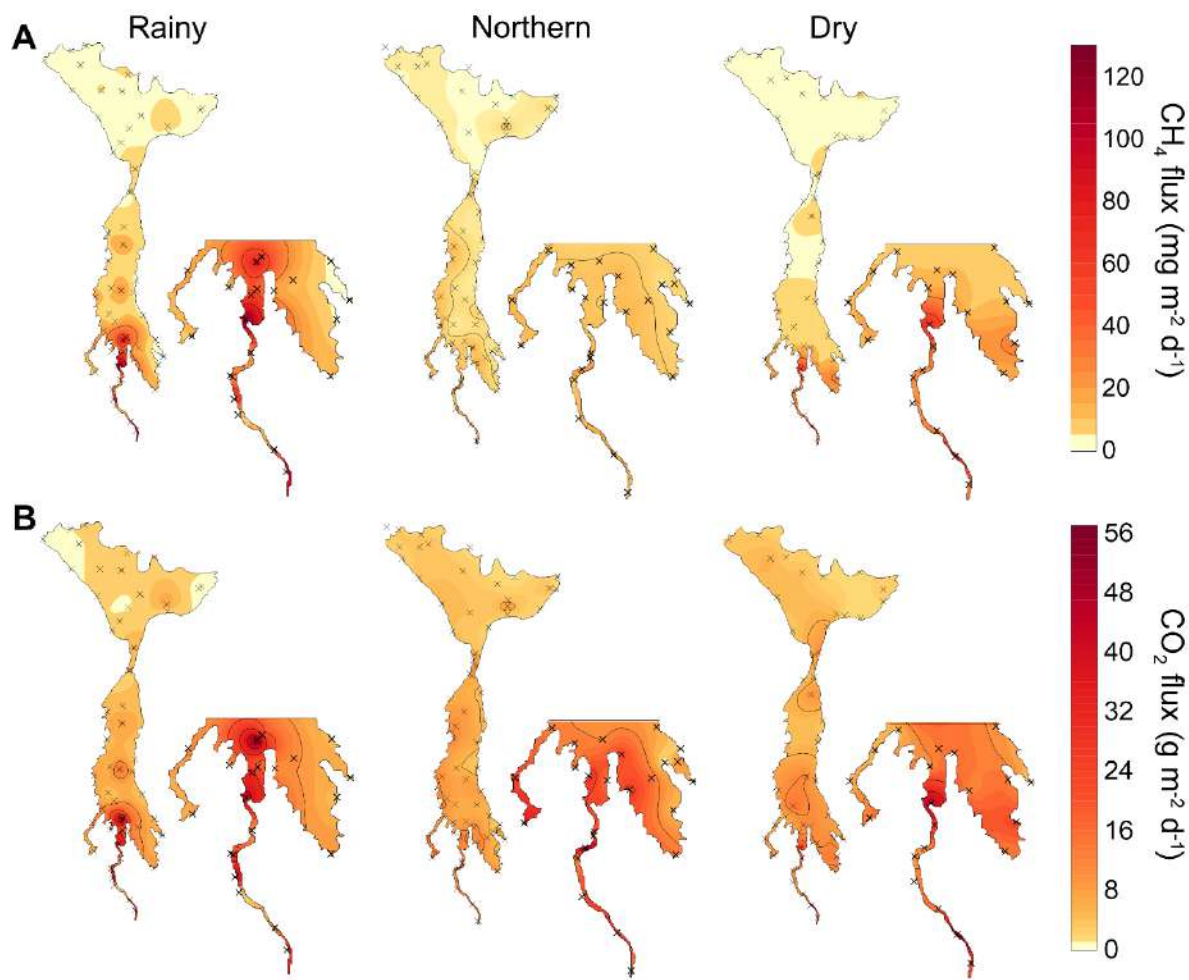


Figure 7.3.4. Contour maps of seasonal CH₄ (top) and CO₂ (bottom) fluxes for the three sampled seasons. A close-up of the river to lagoon zone is shown to the right of each map for ease of visualization. Cross symbol (×) indicates flux sampling stations.

). The fluxes of CO₂ were more homogeneously distributed than CH₄ fluxes, with h_{CO_2flux} ranging from 58 – 72%. The heterogeneities predominated in the latitudinal direction as CH₄ fluxes. The seasonal emission of LM were estimated at 59, 62, and 63 Mg-CO₂ for the northern, rainy, and dry season, respectively. Thus, we estimate that LM contributes a yearly emission of 184 Mg-CO₂.

The emissions of CO₂ from LM are within the range of previously reported ecosystems (Abril et al., 2004).

7.3.4 Conclusions

Achieving certainty of GHG fluxes from oceanic sources is highly dependent on the characterization of the GHG dynamics of coastal ecosystems across the globe. In this work, we presented a thorough report on CH₄ and CO₂ dynamic in a tropical coastal lagoon as well as relevant physicochemical parameters. The dissolved gas dynamics in LM are strongly regulated by seasonal effects driven by river and seawater inflow, temperature, and windspeed. The use of high-resolution methods allowed to further assess the influence of the river and temperature over the dynamics of the dissolved gases. The dynamics of CH₄ were particularly sensitive to temperature and river inflow, as reflected in the CH₄ concentration, consumption/uptake in the water column, and fluxes. The variability introduced by the higher input of river water and seawater increased the concentration and fluxes variability along LM. Our results indicate that the studied lagoon is a net source of GHG with an annual total emission of 189 Mg of CO₂ equivalent, of which CH₄ represents only 2.8%. We also showed that, overall and as previously reported, salinity negatively affected the emissions of both CH₄ and CO₂ as well as their dissolved concentration. Thus, the hydrologic balance between freshwater input from the surrounding ecosystems to water exchange with the sea, is a dominant feature of this lagoon.

7.3.5 References

Abril, G., Vieira Borges, A., Varfalvy, L., Roehm, C., Garneau, M., 2004. Carbon Dioxide and Methane Emissions from Estuaries, in: Tremblay, A., Varfalvy, L., Roehm, C., Garneau, M. (Eds.), Greenhouse Gas Emissions: Fluxes and Processes, Hydroelectric Reservoirs and

- Natural Environments. Springer, Berlin, Heidelberg, New York, pp. 187–207.
- Araujo, J., Pratihary, A., Naik, R., Naik, H., Naqvi, S.W.A., 2018. Benthic fluxes of methane along the salinity gradient of a tropical monsoonal estuary: Implications for CH₄ supersaturation and emission. Mar. Chem. 202, 73–85. <https://doi.org/10.1016/j.marchem.2018.03.008>
- Bange, H.W., 2006. Nitrous oxide and methane in European coastal waters. Estuar. Coast. Shelf Sci. 70, 361–374. <https://doi.org/10.1016/j.ecss.2006.05.042>
- Cai, W.-J., 2011. Estuarine and Coastal Ocean Carbon Paradox: CO₂ Sinks or Sites of Terrestrial Carbon Incineration? Ann. Rev. Mar. Sci. 3, 123–145. <https://doi.org/10.1146/annurev-marine-120709-142723>
- Chuang, P.C., Young, M.B., Dale, A.W., Miller, L.G., Herrera-Silveira, J.A., Paytan, A., 2017. Methane fluxes from tropical coastal lagoons surrounded by mangroves, Yucatán, Mexico. J. Geophys. Res. Biogeosciences 122, 1156–1174. <https://doi.org/10.1002/2017JG003761>
- Chuang, P.C., Young, M.B., Dale, A.W., Miller, L.G., Herrera-Silveira, J.A., Paytan, A., 2016. Methane and sulfate dynamics in sediments from mangrove-dominated tropical coastal lagoons, Yucatan, Mexico. Biogeosciences 13, 2981–3001. <https://doi.org/10.5194/bg-13-2981-2016>
- CONABIO-CONANP-TNC-PRONATURA, 2007. Análisis de vacíos y omisiones en conservación de la biodiversidad marina de México: océanos, costas e islas. Comisión Nacional para el Conocimiento y Uso de la Biodiversidad, Comisión Nacional de Áreas Naturales Protegidas, The Nature Conservancy- Programa México, Pronatura, A.C., México, D.F.

Contreras-Espinosa, F., Rivera-Guzmán, N.E., Segura-Aguilar, R., 2005. Nutrientes y productividad primaria fitoplanctónica en una laguna costera tropical intermitente (La Mancha , Ver .) del Golfo de México Nutrients and primary productivity on intermittent tropical coastal lagoon (La Mancha , Ver) Gulf of México. Hidrobiológica 15, 299–310.

Deborde, J., Anschutz, P., Guérin, F., Poirier, D., Marty, D., Boucher, G., Thouzeau, G., Canton, M., Abril, G., 2010. Methane sources, sinks and fluxes in a temperate tidal Lagoon: The Arcachon lagoon (SW France). Estuar. Coast. Shelf Sci. 89, 256–266.
<https://doi.org/10.1016/j.ecss.2010.07.013>

Dupraz, C., Reid, R.P., Braissant, O., Decho, A.W., Norman, R.S., Visscher, P.T., 2009. Processes of carbonate precipitation in modern microbial mats. Earth-Science Rev. 96, 141–162.
<https://doi.org/10.1016/j.earscirev.2008.10.005>

Gonzalez-Valencia, R., Magana-Rodriguez, F., Gerardo-Nieto, O., Sepulveda-Jauregui, A., Martinez-Cruz, K., Walter Anthony, K., Baer, D., Thalasso, F., 2014. In Situ Measurement of Dissolved Methane and Carbon Dioxide in Freshwater Ecosystems by Off-Axis Integrated Cavity Output Spectroscopy. Environ. Sci. Technol. 48, 11421–11428.
<https://doi.org/10.1021/es500987j>

Gonzalez-Valencia, R., Magaña-Rodriguez, F., Sepulveda-Jauregui, A., Aguirreabala-Campano, T., Gerardo-Nieto, O., Thalasso, F., 2019. A simple model for the numerical characterization of spatiotemporal variability in aquatic ecosystems. Aquat. Sci. 81.
<https://doi.org/10.1007/s00027-019-0652-1>

Huertas, I.E., Flecha, S., Navarro, G., Perez, F.F., de la Paz, M., 2018. Spatio-temporal variability

and controls on methane and nitrous oxide in the Guadalquivir Estuary, Southwestern Europe. *Aquat. Sci.* 80. <https://doi.org/10.1007/s00027-018-0580-5>

Karl, D.M., Beversdorf, L., Björkman, K.M., Church, M.J., Martinez, A., Delong, E.F., 2008. Aerobic production of methane in the sea. *Nat. Geosci.* 1, 473–478. <https://doi.org/10.1038/ngeo234>

Kassambara, A., 2020. rstatix: Pipe-Friendly Framework for Basic Statistical Tests. R Packag. version 0.6.0.

Kottek, M., Grieser, J., Beck, C., Rudolf, B., Rubel, F., 2006. World map of the Köppen-Geiger climate classification updated. *Meteorol. Zeitschrift* 15, 259–263. <https://doi.org/10.1127/0941-2948/2006/0130>

Liotta, M., Martelli, M., 2012. Dissolved gases in brackish thermal waters: an improved analytical method. *Geofluids* 12, 236–244. <https://doi.org/10.1111/j.1468-8123.2012.00365.x>

Matoušů, A., Osudar, R., Šimek, K., Bussmann, I., 2017. Methane distribution and methane oxidation in the water column of the Elbe estuary, Germany. *Aquat. Sci.* 79, 443–458. <https://doi.org/10.1007/s00027-016-0509-9>

Musenze, R.S., Fan, L., Grinham, A., Werner, U., Gale, D., Udy, J., Yuan, Z., 2016. Methane dynamics in subtropical freshwater reservoirs and the mediating microbial communities. *Biogeochemistry* 128, 233–255. <https://doi.org/10.1007/s10533-016-0206-8>

Oremland, R.S., 1979. Methanogenic activity in plankton samples and fish intestines A mechanism for in situ methanogenesis in oceanic surface waters. *Limnol. Oceanogr.* 24, 1136–1141. <https://doi.org/10.4319/lo.1979.24.6.1136>

Oremland, R.S., Polcin, S., 1983. Methanogenesis and sulfate reduction: competitive and noncompetitive substrates in estuarine sediments. Deep Sea Res. Part B. Oceanogr. Lit. Rev. 30, 470. [https://doi.org/10.1016/0198-0254\(83\)90262-5](https://doi.org/10.1016/0198-0254(83)90262-5)

Orif, M.I., Kavil, Y.N., Kelassanthodi, R., Al-Farawati, R., Al Zobidi, M.I., 2017. Dissolved methane and oxygen depletion in the two coastal lagoons, Red Sea, Indian Journal of Geo Marine Sciences.

Osudar, R., Matoušů, A., Alawi, M., Wagner, D., Bussmann, I., 2015. Environmental factors affecting methane distribution and bacterial methane oxidation in the German Bight (North Sea). Estuar. Coast. Shelf Sci. 160, 10–21. <https://doi.org/10.1016/j.ecss.2015.03.028>

Reeburgh, W.S., 2007. Oceanic methane biogeochemistry. Chem. Rev. <https://doi.org/10.1021/cr050362v>

Repeta, D.J., Ferrón, S., Sosa, O.A., Johnson, C.G., Repeta, L.D., Acker, M., DeLong, E.F., Karl, D.M., 2016. Marine methane paradox explained by bacterial degradation of dissolved organic matter. Nat. Geosci. 9, 884–887. <https://doi.org/10.1038/ngeo2837>

Rivera-Guzmán, N.E., Moreno-Casasola, P., Ibarra-Obando, S.E., Sosa, V.J., Herrera-Silveira, J., 2014. Long term state of coastal lagoons in Veracruz, Mexico: Effects of land use changes in watersheds on seagrasses habitats. Ocean Coast. Manag. 87, 30–39. <https://doi.org/10.1016/j.ocecoaman.2013.10.007>

Saunois, M., Bousquet, P., Poulter, B., Peregon, A., Ciais, P., Canadell, J.G., Dlugokencky, E.J., Etiope, G., Bastviken, D., Houweling, S., Janssens-Maenhout, G., Tubiello, F.N., Castaldi, S., Jackson, R.B., Alexe, M., Arora, V.K., Beerling, D.J., Bergamaschi, P., Blake, D.R.,

Brailsford, G., Brovkin, V., Bruhwiler, L., Crevoisier, C., Crill, P., Covey, K., Curry, C., Frankenberg, C., Gedney, N., Höglund-Isaksson, L., Ishizawa, M., Ito, A., Joos, F., Kim, H.S., Kleinen, T., Krummel, P., Lamarque, J.F., Langenfelds, R., Locatelli, R., Machida, T., Maksyutov, S., McDonald, K.C., Marshall, J., Melton, J.R., Morino, I., Naik, V., O'Doherty, S., Parmentier, F.J.W., Patra, P.K., Peng, C., Peng, S., Peters, G.P., Pison, I., Prigent, C., Prinn, R., Ramonet, M., Riley, W.J., Saito, M., Santini, M., Schroeder, R., Simpson, I.J., Spahni, R., Steele, P., Takizawa, A., Thornton, B.F., Tian, H., Tohjima, Y., Viovy, N., Voulgarakis, A., Van Weele, M., Van Der Werf, G.R., Weiss, R., Wiedinmyer, C., Wilton, D.J., Wiltshire, A., Worthy, D., Wunch, D., Xu, X., Yoshida, Y., Zhang, B., Zhang, Z., Zhu, Q., 2016. The global methane budget 2000-2012. *Earth Syst. Sci. Data* 8, 697–751.
<https://doi.org/10.5194/essd-8-697-2016>

Saunois, M., Stavert, A.R., Poulter, B., Bousquet, P., Canadell, J.G., Jackson, R.B., Raymond, P.A., Dlugokencky, E.J., Houweling, S., Patra, P.K., Ciais, P., Arora, V.K., Bastviken, D., Bergamaschi, P., Blake, D.R., Brailsford, G., Bruhwiler, L., Carlson, K.M., Carroll, M., Castaldi, S., Chandra, N., Crevoisier, C., Crill, P.M., Covey, K., Curry, C.L., Etiope, G., Frankenberg, C., Gedney, N., Hegglin, M.I., Höglund-Isakson, L., Hugelius, G., Ishizawa, M., Ito, A., Janssens-Maenhout, G., Jensen, K.M., Joos, F., Kleinen, T., Krummel, P.B., Langenfelds, R.L., Laruelle, G.G., Liu, L., Machida, T., Maksyutov, S., McDonald, K.C., McNorton, J., Miller, P.A., Melton, J.R., Morino, I., Müller, J., Murgia-Flores, F., Naik, V., Niwa, Y., Noce, S., O&Doherty, S., Parker, R.J., Peng, C., Peng, S., Peters, G.P., Prigent, C., Prinn, R., Ramonet, M., Regnier, P., Riley, W.J., Rosentreter, J.A., Segers, A., Simpson, I.J., Shi, H., Smith, S.J., Steele, P.L., Thornton, B.F., Tian, H., Tohjima, Y., Tubiello, F.N., Tsuruta, A., Viovy, N., Voulgarakis, A., Weber, T.S., van Weele, M., van der

Werf, G.R., Weiss, R.F., Worthy, D., Wunch, D., Yin, Y., Yoshida, Y., Zhang, W., Zhang, Z., Zhao, Y., Zheng, B., Zhu, Qing, Zhu, Qian, Zhuang, Q., 2019. The Global Methane Budget 2000–2017. *Earth Syst. Sci. Data Discuss.* 1–138.
<https://doi.org/10.5194/essd-2019-128>

Sela-Adler, M., Ronen, Z., Herut, B., Antler, G., Vigderovich, H., Eckert, W., Sivan, O., 2017. Co-existence of Methanogenesis and Sulfate Reduction with Common Substrates in Sulfate-Rich Estuarine Sediments. *Front. Microbiol.* 8, 1–11.
<https://doi.org/10.3389/fmicb.2017.00766>

Team, R. core, 2019. A language and environment for statistical computing. R Foundation for Statistical Computing.

Torres-Alvarado, R., Ramírez-Vives, F., Fernández, F.J., Barriga-Sosa, I., 2005. Methanogenesis and Methane Oxidation in Wetlands. Implications in the Global Carbon Cycle, Hidrobiológica.

Torres Alvarado, M.D.R., Calva-Benítez, L.G., Álvarez-Hernández, S., Trejo-Aguilar, G., 2016. Anaerobic microbiota: spatial-temporal changes in the sediment of a tropical coastal lagoon with ephemeral inlet. *Rev. Biol. Trop.* 64, 1759–1770.
<https://doi.org/10.15517/rbt.v64i4.22449>

Valenzuela, E.I., Padilla-Loma, C., Gómez-Hernández, N., López-Lozano, N.E., Casas-Flores, S., Cervantes, F.J., 2020. Humic Substances Mediate Anaerobic Methane Oxidation Linked to Nitrous Oxide Reduction in Wetland Sediments. *Front. Microbiol.* 11.
<https://doi.org/10.3389/fmicb.2020.00587>

Valenzuela, E.I., Prieto-Davó, A., López-Lozano, N.E., Hernández-Eligio, A., Vega-Alvarado, L.,

Juárez, K., García-González, A.S., López, M.G., Cervantes, F.J., 2017. Anaerobic methane oxidation driven by microbial reduction of natural organic matter in a tropical wetland. *Appl. Environ. Microbiol.* 83. <https://doi.org/10.1128/AEM.00645-17>

Wickham, H., 2016. *ggplot2: Elegant Graphics for Data Analysis*. Springer-Verlag New York.

Wickham, H., Averick, M., Bryan, J., Chang, W., McGowan, L., François, R., Grolemund, G., Hayes, A., Henry, L., Hester, J., Kuhn, M., Pedersen, T., Miller, E., Bache, S., Müller, K., Ooms, J., Robinson, D., Seidel, D., Spinu, V., Takahashi, K., Vaughan, D., Wilke, C., Woo, K., Yutani, H., 2019. Welcome to the Tidyverse. *J. Open Source Softw.* 4, 1686. <https://doi.org/10.21105/joss.01686>

Wickham, H., François, R., Henry, L., Müller, K., 2020. *dplyr: A Grammar of Data Manipulation*.

R package dplyr version 1.0.2 [WWW Document]. URL <https://cran.r-project.org/package=dplyr> (accessed 9.24.20).

Willmott, C.J., Matsuura, K., 2006. On the use of dimensioned measures of error to evaluate the performance of spatial interpolators. *Int. J. Geogr. Inf. Sci.* 20, 89–102. <https://doi.org/10.1080/13658810500286976>

Wu, Z., Zhou, H., Peng, X., Li, J., Chen, G., 2014. Rates of bacterial sulfate reduction and their response to experimental temperature changes in coastal sediments of Qi’ao Island, Zhujiang River Estuary in China. *Acta Oceanol. Sin.* 33, 10–17. <https://doi.org/10.1007/s13131-014-0458-x>

Yuan, Y., Conrad, R., Lu, Y., 2009. Responses of methanogenic archaeal community to oxygen

exposure in rice field soil. Environ. Microbiol. Rep. 1, 347–354.
<https://doi.org/10.1111/j.1758-2229.2009.00036.x>

Zhuang, G., Montgomery, A., Sibert, R.J., Rogener, M., Samarkin, V.A., Joye, S.B., 2018. Effects of pressure, methane concentration, sulfate reduction activity, and temperature on methane production in surface sediments of the Gulf of Mexico. Limnol. Oceanogr. 63, 2080–2092.
<https://doi.org/10.1002/lno.10925>

Zhuang, G.C., Elling, F.J., Nigro, L.M., Samarkin, V., Joye, S.B., Teske, A., Hinrichs, K.U., 2016. Multiple evidence for methylotrophic methanogenesis as the dominant methanogenic pathway in hypersaline sediments from the Orca Basin, Gulf of Mexico. Geochim. Cosmochim. Acta 187, 1–20. <https://doi.org/10.1016/j.gca.2016.05.005>

8. Conclusiones globales

La mayor incertidumbre en el inventario global de CH₄ proviene de los ecosistemas acuáticos, mismos que son fuentes particularmente importantes de CH₄. La dinámica del CH₄ de los ecosistemas acuáticos está sujeta a una alta variación espaciotemporal tanto por las condiciones propias del ecosistema como por variaciones climáticas y regionales. Es por ello que se requieren métodos y campañas de muestreo que permitan caracterizar la dinámica de GEI de manera representativa. Además, la literatura demuestra que la producción de GEI está fuertemente regulada por el OD. Por lo tanto, es fundamental realizar la medición simultánea de la concentración de GEI y OD. En este trabajo se demostró la importancia del continuo mejoramiento

y aplicación de métodos de alta resolución sobre ecosistemas acuáticos escasamente estudiados. Las aguas interiores salobres, sean lagos o pozas, no figuran en los inventarios globales de GEI. A pesar de la presencia de concentración relativamente alta de sulfatos, en este trabajo se demostró que las pozas subsalinas de Cuatro Ciénelas, Coahuila, son fuentes significativas de CH₄ y fuentes particularmente potentes de CO₂ por su composición química. Además, se reportó por primera vez la producción óxica de CH₄ en un ecosistema de este tipo. Nuestros resultados resaltan la importancia de estudiar estos ecosistemas subrepresentados en la literatura.

Por otra parte, el acoplamiento de la medición de O₂ mediante un sensor óptico de manera simultánea a la medición de los GEI trajo consigo claras ventajas. En concreto, determinar perfiles de concentración de O₂ y respiración aerobia con la misma resolución que los GEI, nos permitió observar de manera más detallada la relación entre estos gases disueltos. En este trabajo se demuestra el alcance que puede tener el uso de métodos de alta resolución orientados a la determinación de los componentes del ciclo del CH₄. En particular, se logró la cuantificación de los principales bioprocessos relacionados al ciclo del CH₄, incluso aquellos que no pueden ser medidos fácilmente, como la producción primaria neta y la metanogénesis, además de la identificación de respiración y metanotrofía aerobia y anaerobia. Asimismo, se propuso una representación gráfica sin precedentes que permite la visualización del impacto de la eutrofización sobre los bioprocessos y el almacenamiento de GEI de manera sencilla y directa. Finalmente, este trabajo constituye una prueba adicional de que los ecosistemas acuáticos en latitudes bajas emiten más GEI que sus contrapartes en latitudes altas.

9. Recomendaciones y perspectivas

- Los resultados del capítulo 7.1 muestran que las aguas interiores salobres pueden ser fuentes de CH₄ y CO₂ a la atmósfera. Por lo tanto, se recomienda que haya más estudios orientados a la caracterización del ciclo del CH₄ en ecosistemas salobres. México posee una gran cantidad de cuerpos de agua superficial salobres y es de interés saber si los resultados presentados en este trabajo se pueden generalizar a todos los cuerpos de agua salobres de la región. Se recomienda además caracterizar la composición química del suelo y agua, ya que la presencia de carbonatos en Cuatro Ciénegas es determinante para las emisiones de CO₂ observadas. Conforme aumente la certidumbre sobre estos ecosistemas se podrá determinar si éstos deben ser integrados a los inventarios globales de GEI. Otro aspecto interesante del capítulo 7.1 fue la producción óxica de CH₄ en la columna de agua. Existen varias rutas metabólicas propuestas en la literatura que potencialmente podrían explicar las observaciones reportadas en este trabajo. Afortunadamente, existe mucho interés en este sitio por su historial geológico, y la fauna, flora y comunidades microbianas endémicas. Estudios previos sugieren que la comunidad microbiana presente en las pozas tiene la capacidad de metabolizar fosfonatos, mismos que han sido propuestos como sustrato para la producción óxica de CH₄ en ecosistemas marinos. Futuros trabajos de investigación sobre la producción óxica de CH₄ deberían ser orientados en este sentido.
- En el capítulo 7.2 hicimos una caracterización detallada del ciclo del CH₄ en dos ecosistemas de agua dulce con estado trófico contrastante. Se logró cuantificar procesos como la producción primaria y la respiración neta de ambos sitios. Para ir más allá en este tipo de

estudio, se recomienda ampliar la caracterización detallada de la metanotrofía y respiración a todo el transecto longitudinal. Además, estos ecosistemas mostraron emisiones ebullitivas continuas, en particular el sitio contaminado. En el futuro se deberían aplicar métodos especializados para la medición de estas emisiones, pueden ser desde métodos sencillos como un embudo invertido o métodos más poderosos de alta resolución. Esta recomendación, aunque particularmente importante para mejorar futuros trabajos como el realizado para el capítulo 7.2, se extiende a todos los trabajos que pretenden caracterizar el ciclo del CH₄ en ecosistemas acuáticos.

- Se observó una emisión inesperadamente alta en comparación a otros ecosistemas del mismo estado trófico para el reservorio subtropical mesotrófico “El Llano”. En este sitio también se ha observado la presencia de macrófitas invasivas sumergidas. Se sabe que las plantas pueden facilitar el transporte de CH₄ de los sedimentos hacia la columna de agua, por lo que en el futuro podrían abordarse estudios orientados al efecto de las macrófitas sobre las emisiones en “El Llano”.
- Actualmente en la literatura existen evidencias opuestas respecto al efecto de la salinidad sobre la metanogénesis, relevante para ecosistemas costeros como el estudiado en el capítulo 7.3. Es de interés realizar estudios enfocados al efecto de la salinidad sobre el ciclo del CH₄ en LM. Nuestros resultados mostraron evidencia claras del efecto negativo de la salinidad sobre el ciclo del metano, pero no permitió determinar claramente sus causantes, en términos de bioprocessos. En el futuro podrían realizarse incubaciones de sedimento con diferentes condiciones de salinidad para evaluar el impacto de la salinidad. Además, es sumamente relevante realizar una cuantificación certera del intercambio de CH₄ entre el río, el manglar y

la laguna costera, es decir, identificar cuánto CH₄ es importado del río y manglar, cuánto es producido por la laguna y cuánto es finalmente exportado al océano.

- Finalmente, en general se recomienda que en futuros estudios se considere aumentar la resolución de otros factores importantes para el ciclo del CH₄ como los nutrientes, la calidad de la materia orgánica y la composición fitoplantónica de los ecosistemas acuáticos.

10. Bibliografía

- Aguirre-Zabala-Campano, T., Gerardo-Nieto, O., Gonzalez-Valencia, R., Souza, V., & Thalasso, F. (2019). Methane dynamics in the subsaline ponds of the Chihuahuan Desert: A first assessment. *Science of The Total Environment*, 666, 1255–1264. <https://doi.org/10.1016/j.scitotenv.2019.02.163>
- Bastin, L., Gorelick, N., Saura, S., Bertzky, B., Dubois, G., Fortin, M.-J., & Pekel, J.-F. (2019). Inland surface waters in protected areas globally: Current coverage and 30-year trends. *PLOS ONE*, 14(1), e0210496. <https://doi.org/10.1371/journal.pone.0210496>
- Bastviken, D., Tranvik, L. J., Downing, J. A., Crill, P. M., & Enrich-Prast, A. (2011). Freshwater methane emissions offset the continental carbon sink. *Science*, 331(6013), 50. <https://doi.org/10.1126/science.1196808>
- Blake, L. I., Tveit, A., Øvreås, L., Head, I. M., & Gray, N. D. (2015). Response of methanogens in arctic sediments to temperature and methanogenic substrate availability. *PLoS ONE*, 10(6), 1–18. <https://doi.org/10.1371/journal.pone.0129733>
- Bridgham, S. D., Cadillo-Quiroz, H., Keller, J. K., & Zhuang, Q. (2013). Methane emissions from wetlands: Biogeochemical, microbial, and modeling perspectives from local to global scales. *Global Change Biology*, 19(5), 1325–1346. <https://doi.org/10.1111/gcb.12131>
- Camacho, A., Picazo, A., Rochera, C., Santamans, A. C., Morant, D., Miralles-Lorenzo, J., & Castillo-Escrivà, A. (2017). Methane Emissions in Spanish Saline Lakes: Current Rates, Temperature and Salinity Responses, and Evolution under Different Climate Change Scenarios. *Water*, 9(9), 659. <https://doi.org/10.3390/w9090659>
- Casper, P., Maberly, S. C., & Hall, G. H. (2000). Fluxes of Methane and Carbon Dioxide from a Small Productive Lake to the Atmosphere Author (s): Peter Casper , Stephen C . Maberly , Grahame H . Hall and Bland J . Finlay Published by : Springer Stable URL : <http://www.jstor.org/stable/1469408> REFERENCE. *Biogeochemistry*, 49(1), 1–19.
- Chuang, P.-C., Young, M. B., Dale, A. W., Miller, L. G., Herrera-Silveira, J. A., & Paytan, A. (2017). Methane fluxes from tropical coastal lagoons surrounded by mangroves, Yucatán, Mexico. *Journal of Geophysical Research: Biogeosciences*, 122(5), 1156–1174. <https://doi.org/10.1002/2017JG003761>
- Chuang, P. C., Young, M. B., Dale, A. W., Miller, L. G., Herrera-Silveira, J. A., & Paytan, A. (2016). Methane and sulfate dynamics in sediments from mangrove-dominated tropical coastal lagoons, Yucatan, Mexico. *Biogeosciences*, 13(10), 2981–3001. <https://doi.org/10.5194/bg-13-2981-2016>
- Cole, J. J., Prairie, Y. T., Caraco, N. F., McDowell, W. H., Tranvik, L. J., Striegl, R. G., ... Melack, J. (2007). Plumbing the Global Carbon Cycle: Integrating Inland Waters into the Terrestrial Carbon Budget. *Ecosystems*, 10(1), 172–185. <https://doi.org/10.1007/s10021-006-9013-8>
- Cui, M., Ma, A., Qi, H., Zhuang, X., Zhuang, G., & Zhao, G. (2015). Warmer temperature accelerates methane emissions from the Zoige wetland on the Tibetan Plateau without changing

methanogenic community composition. *Scientific Reports*, 5(September 2014), 1–12. <https://doi.org/10.1038/srep11616>

Deborde, J., Anschutz, P., Guérin, F., Poirier, D., Marty, D., Boucher, G., ... Abril, G. (2010). Methane sources, sinks and fluxes in a temperate tidal Lagoon: The Arcachon lagoon (SW France). *Estuarine, Coastal and Shelf Science*, 89(4), 256–266. <https://doi.org/10.1016/j.ecss.2010.07.013>

Deemer, B. R., Harrison, J. A., Li, S., Beaulieu, J. J., DelSontro, T., Barros, N., ... Vonk, J. A. (2016). Greenhouse Gas Emissions from Reservoir Water Surfaces: A New Global Synthesis. *BioScience*, 66(11). <https://doi.org/10.1093/biosci/biw117>

DelSontro, T., Beaulieu, J. J., & Downing, J. A. (2018). Greenhouse gas emissions from lakes and impoundments: Upscaling in the face of global change. *Limnology and Oceanography Letters*, 3(3), 64–75. <https://doi.org/10.1002/lol2.10073>

dos Santos Furtado, L. A., Casper, P., & Esteves, F. D. A. (2002). Methanogenesis in an Impacted and Two Dystrophic Coastal Lagoons (Macaé , Brazil), 45(June), 195–202.

Duchemin, E., Lucotte, M., & Canuel, R. (1999). Comparison of Static Chamber and Thin Boundary Layer Equation Methods for Measuring Greenhouse Gas Emissions from Large Water Bodies §. *Environmental Science & Technology*, 33(2), 350–357. <https://doi.org/10.1021/es9800840>

Egger, M., Rasigraf, O., Sapart, C. J., Jilbert, T., Jetten, M. S. M., Röckmann, T., ... Slomp, C. P. (2015). Iron-mediated anaerobic oxidation of methane in brackish coastal sediments. *Environmental Science and Technology*, 49(1), 277–283. <https://doi.org/10.1021/es503663z>

Ettwig, K. F., Zhu, B., Speth, D., Keltjens, J. T., Jetten, M. S. M., & Kartal, B. (2016). Archaea catalyze iron-dependent anaerobic oxidation of methane. *Proceedings of the National Academy of Sciences*, 113(45), 12792–12796. <https://doi.org/10.1073/pnas.1609534113>

Fonseca, A. L. dos S., Minello, M., Marinho, C. C., & Esteves, F. de A. (2004). Methane concentration in water column and in pore water of a coastal lagoon (Cabiúnas lagoon, Macaé, RJ, Brazil). *Brazilian Archives of Biology and Technology*, 47(2), 301–308. <https://doi.org/10.1590/S1516-89132004000200018>

Gerardo-Nieto, O., Astorga-España, M. S., Mansilla, A., & Thalasso, F. (2017). Initial report on methane and carbon dioxide emission dynamics from sub-Antarctic freshwater ecosystems: A seasonal study of a lake and a reservoir. *Science of The Total Environment*, 593–594, 144–154. <https://doi.org/10.1016/j.scitotenv.2017.02.144>

Gerardo-Nieto, O., Vega-Peñaanda, A., Gonzalez-Valencia, R., Alfano-Ojeda, Y., & Thalasso, F. (2019). Continuous Measurement of Diffusive and Ebullitive Fluxes of Methane in Aquatic Ecosystems by an Open Dynamic Chamber Method. *Environmental Science and Technology*, 53(9), 5159–5167. <https://doi.org/10.1021/acs.est.9b00425>

Gonzalez-Valencia, R., Magana-Rodriguez, F., Gerardo-Nieto, O., Sepulveda-Jauregui, A., Martinez-Cruz, K., Walter Anthony, K., ... Thalasso, F. (2014). In Situ Measurement of Dissolved Methane and Carbon Dioxide in Freshwater Ecosystems by Off-Axis Integrated Cavity Output Spectroscopy. *Environmental Science & Technology*, 48(19), 11421–11428.

<https://doi.org/10.1021/es500987j>

Gonzalez-Valencia, R., Sepulveda-Jauregui, A., Martinez-Cruz, K., Hoyos-Santillan, J., Dendooven, L., & Thalasso, F. (2014). Methane emissions from Mexican freshwater bodies: Correlations with water pollution. *Hydrobiologia*, 721(1), 9–22. <https://doi.org/10.1007/s10750-013-1632-4>

Istvánovics, V. (2009). Eutrophication of Lakes and Reservoirs. In *Encyclopedia of Inland Waters* (pp. 157–165). Elsevier Inc. <https://doi.org/10.1016/B978-012370626-3.00141-1>

Kankaala, P., Huotari, J., Peltomaa, E., Saloranta, T., & Ojala, A. (2006). Methanotrophic activity in relation to methane efflux and total heterotrophic bacterial production in a stratified, humic, boreal lake. *Limnology and Oceanography*, 51(2), 1195–1204. <https://doi.org/10.4319/lo.2006.51.2.1195>

Martinez-Cruz, K. (2011). *Emisiones de gases con efecto invernadero en ecosistemas acuáticos de la Ciudad de México: Dinámica del metano*. CINVESTAV-IPN.

Martinez-Cruz, K., Sepulveda-Jauregui, A., Casper, P., Anthony, K. W., Smemo, K. A., & Thalasso, F. (2018). Ubiquitous and significant anaerobic oxidation of methane in freshwater lake sediments. *Water Research*, 144, 332–340. <https://doi.org/10.1016/j.watres.2018.07.053>

McMahon, P. B., & Chapelle, F. H. (2008). Redox Processes and Water Quality of Selected Principal Aquifer Systems. *Ground Water*, 46(2), 259–271. <https://doi.org/10.1111/j.1745-6584.2007.00385.x>

Murase, J., Sakai, Y., Sugimoto, A., Okubo, K., & Sakamoto, M. (2003). Sources of dissolved methane in Lake Biwa. *Limnology*, 4(2), 91–99. <https://doi.org/10.1007/s10201-003-0095-0>

Natchimuthu, S., Sundgren, I., Gålfalk, M., Klemedtsson, L., Crill, P., Danielsson, Å., & Bastviken, D. (2016). Spatio-temporal variability of lake CH₄ fluxes and its influence on annual whole lake emission estimates. *Limnology and Oceanography*, 61(S1), S13–S26. <https://doi.org/10.1002/lno.10222>

Ortiz-Llorente, M. J., & Alvarez-Cobelas, M. (2012). Comparison of biogenic methane emissions from unmanaged estuaries, lakes, oceans, rivers and wetlands. *ATMOSPHERIC ENVIRONMENT*, 59, 328–337. <https://doi.org/10.1016/j.atmosenv.2012.05.031>

Osudar, R., Matoušů, A., Alawi, M., Wagner, D., & Bussmann, I. (2015). Environmental factors affecting methane distribution and bacterial methane oxidation in the German Bight (North Sea). *Estuarine, Coastal and Shelf Science*, 160, 10–21. <https://doi.org/10.1016/j.ecss.2015.03.028>

Rolston, D. E. (1986). Gas flux. In A. Klute (Ed.), *Agronomy Monograph 9: Methods of soil analysis, Part 1. Physical and mineralogical methods*. (2nd ed., p. 17). Madison, Wisconsin, USA: American Society of Agronomy and Soil Science Society of Americ.

Romanini, D., Ventriillard, I., Méjean, G., Morville, J., & Kerstel, E. (2014). *Cavity-Enhanced Spectroscopy and Sensing* (Vol. 179). <https://doi.org/10.1007/978-3-642-40003-2>

Saunois, M., Stavert, A. R., Poulter, B., Bousquet, P., Canadell, J. G., Jackson, R. B., ... Zhuang, Q. (2019). The Global Methane Budget 2000–2017. *Earth System Science Data*

Discussions, (August), 1–138. <https://doi.org/10.5194/essd-2019-128>

Schilder, J., Bastviken, D., Van Hardenbroek, M., Kankaala, P., Rinta, P., Stötter, T., & Heiri, O. (2013). Spatial heterogeneity and lake morphology affect diffusive greenhouse gas emission estimates of lakes. *Geophysical Research Letters*, 40(21), 5752–5756. <https://doi.org/10.1002/2013GL057669>

Sepulveda-Jauregui, A., Hoyos-Santillan, J., Martinez-Cruz, K., Anthony, K. M. W., Casper, P., Belmonte-Izquierdo, Y., & Thalasso, F. (2018). Eutrophication exacerbates the impact of climate warming on lake methane emission. *SCIENCE OF THE TOTAL ENVIRONMENT*, 636, 411–419. <https://doi.org/10.1016/j.scitotenv.2018.04.283>

Serrano-Silva, N., Sarria-Guzmán, Y., Dendooven, L., & Luna-Guido, M. (2014). Methanogenesis and Methanotrophy in Soil: A Review. *Pedosphere*, 24(3), 291–307. [https://doi.org/10.1016/S1002-0160\(14\)60016-3](https://doi.org/10.1016/S1002-0160(14)60016-3)

Thalasso, Frederic, Anthony, K. W., Irzak, O., Chaleff, E., Barker, L., Anthony, P., ... Gonzalez-Valencia, R. (2020). Mobile open dynamic chamber measurement of methane macroseeps in lakes. *Hydrology and Earth System Sciences, In review*. <https://doi.org/https://doi.org/10.5194/hess-2020-420>

Thalasso, Frédéric, Sepulveda-Jauregui, A., Gandois, L., Martinez-Cruz, K., Gerardo-Nieto, O., Astorga-España, M. S., ... Cabrol, L. (2020). Sub-oxycline methane oxidation can fully uptake CH₄ produced in sediments: case study of a lake in Siberia. *Scientific Reports*, 10(1), 3423. <https://doi.org/10.1038/s41598-020-60394-8>

Thottathil, S. D., Reis, P. C. J., del Giorgio, P. A., & Prairie, Y. T. (2018). The Extent and Regulation of Summer Methane Oxidation in Northern Lakes. *Journal of Geophysical Research: Biogeosciences*, 123(10), 3216–3230. <https://doi.org/10.1029/2018JG004464>

Timmers, P. H. A., Welte, C. U., Koehorst, J. J., Plugge, C. M., Jetten, M. S. M., & Stams, A. J. M. (2017). Reverse Methanogenesis and Respiration in Methanotrophic Archaea. *Archaea*. <https://doi.org/10.1155/2017/1654237>

Valenzuela, E. I., Padilla-Loma, C., Gómez-Hernández, N., López-Lozano, N. E., Casas-Flores, S., & Cervantes, F. J. (2020). Humic Substances Mediate Anaerobic Methane Oxidation Linked to Nitrous Oxide Reduction in Wetland Sediments. *Frontiers in Microbiology*, 11. <https://doi.org/10.3389/fmicb.2020.00587>

Valenzuela, E. I., Prieto-Davó, A., López-Lozano, N. E., Hernández-Eligio, A., Vega-Alvarado, L., Juárez, K., ... Cervantes, F. J. (2017). Anaerobic methane oxidation driven by microbial reduction of natural organic matter in a tropical wetland. *Applied and Environmental Microbiology*, 83(11). <https://doi.org/10.1128/AEM.00645-17>

Verma, A., Subramanian, V., & Ramesh, R. (2002). Methane emissions from a coastal lagoon : Vembanad Lake, West Coast, India. *Chemosphere*, 47, 883–889.

Wen, X., Yang, S., Horn, F., Winkel, M., Wagner, D., & Liebner, S. (2017). Global biogeographic analysis of methanogenic archaea identifies community-shaping environmental factors of natural environments. *Frontiers in Microbiology*, 8(JUL), 1–13.

<https://doi.org/10.3389/fmicb.2017.01339>

Wen, Y., Schoups, G., & Van De Giesen, N. (2017). Organic pollution of rivers: Combined threats of urbanization, livestock farming and global climate change. *Scientific Reports*, 7. <https://doi.org/10.1038/srep43289>

Wetzel, R. G. (2001). *Limnology: Lake and River Ecosystems* (3rd ed.). San Diego, California: Academic Press.

Yuan, Y., Conrad, R., & Lu, Y. (2009). Responses of methanogenic archaeal community to oxygen exposure in rice field soil. *Environmental Microbiology Reports*, 1(5), 347–354. <https://doi.org/10.1111/j.1758-2229.2009.00036.x>

Zeikus, J. G., & Winfrey, M. R. (1976). Temperature limitations of methanogenesis in aquatic sediments. *Appl. Environ. Microbiol.*, 31(1), 99–107.

11. Anexos

11.1 Anexo 1: Material suplementario del capítulo 7.1

Methane dynamics in the subsaline ponds of the Chihuahuan Desert: a first assessment

Teresa Aguirrezabala-Campano¹, Oscar Gerardo-Nieto¹, Rodrigo Gonzalez-Valencia¹, Valeria Souza², Frederic Thalasso¹.

¹ Cinvestav, Department of Biotechnology and Bioengineering, Mexico City, Mexico.

² Universidad Nacional Autónoma de México, Departamento de Ecología Evolutiva, Mexico City, Mexico.

S1. MATERIALS AND METHODS

S1.1 Calculation of carbonate/aqueous CO₂ in equilibrium

Aqueous CO₂ concentration, [CO₂]_{aq}, as predicted by chemical equilibrium was compared to CO₂ concentration (C_{CO₂}) measured experimentally in the ponds. With that purpose, the following set of equations was used (Stumm and Morgan, 2012). The water dissociation constants (K_w), and carbonic acid (H₂CO₃) first and second dissociation constants (K₁ and K₂) were calculated from:

$$K_w = 10^{\left(-283.971 - 0.05069842T + \frac{13323.00}{T} + 102.24447\log(T) - \frac{1119669}{T^2}\right)}; \quad (\text{Eq. S1})$$

$$K_1 = 10^{\left(-356.3094 - 0.06091964T + \frac{21834.37}{T} + 126.8339\log(T) - \frac{1684915}{T^2}\right)}; \quad (\text{Eq. S2})$$

$$K_2 = 10^{\left(-107.8871 - 0.03252849T + \frac{5151.79}{T} + 38.92561\log(T) - \frac{563713.9}{T^2}\right)}; \quad (\text{Eq. S3})$$

where T is the absolute temperature (Kelvin).

Then, the bicarbonate concentration $[HCO_3^-]$ was calculated from:

$$[HCO_3^-] = \frac{Alk - K_w \times \frac{10^{-pH}}{\gamma}}{1 + 2K_2 \times 10^{pH}}; \quad (\text{Eq. S4})$$

where Alk is the alkalinity of the pond (mol L⁻¹; Table S1).

Then, the CO₂ concentration in water $[CO_2]_{aq}$ predicted from chemical equilibrium was determined from:

$$[CO_2]_{aq} = \frac{10^{pH}[HCO_3^{2-}]}{K_1} \quad (\text{Eq. S5})$$

Table S1. Parameters used for the calculation of $[HCO_3^-]$ and $[CO_2]_{aq}$, K coefficients were calculated from Eq. S1-S3 using T and pH from each pond.

ID	Alk (mmol L ⁻¹) ¹	pH	T	K _w (10 ⁻¹⁴)	K ₁ (10 ⁻⁷)	K ₂ (10 ⁻¹¹)
PB	1.67	7.10	305	1.67	4.78	5.33
LH	1.89	7.50	298	1.00	4.45	4.69
PCH	1.56	8.31	298	1.00	4.45	4.69

⁽¹⁾ Alkalinity values as CaCO₃ obtained from Escalante et al. (2008).



Figure S1. Cuatro Cienegas Valley map and photographs of each studied pond. The ponds have been numbered as 1: Poza Becerra (PB), 2: Poza Manantial (PM), 3: Poza Churince (PCH), 4: Poza Azul (PA), and 5: Poza los Hundidos (LH).

S2. RESULTS

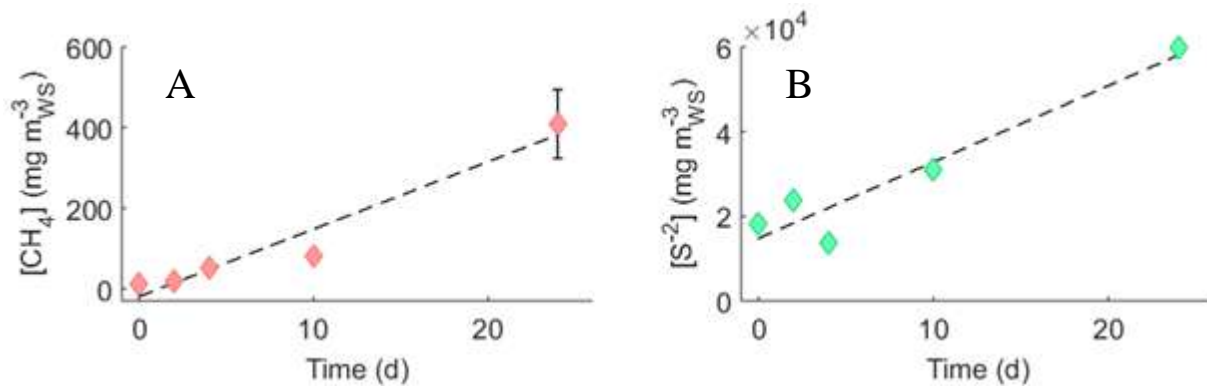


Figure S2. CH_4 (A) and S^{2-} (B) concentration observed during incubation assays of PB sediments, over a 25-day period.

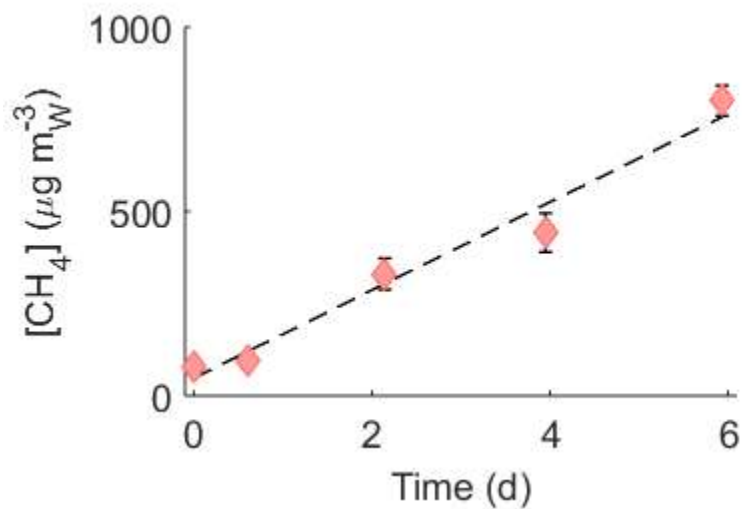


Figure S3. CH_4 concentration observed during incubations of PB water sample in 10-mL glass syringes.

Table S2. $[HCO_3^-]$ and $[CO_2]_{aq}$ calculated from chemical equilibrium using Eq. S2 and S3.

Ecosystem	$[HCO_3^-]$ (mmol L ⁻¹)	$[CO_2]_{aq}$ (mmol L ⁻¹)	$[CO_2]_{aq}$ (mg L ⁻¹)
PB	3.34	0.55	24.41
LH	3.78	0.27	11.83
PCH	3.14	0.03	1.52

References

1. Escalante, A.E., Eguiarte, L.E., Espinosa-Asuar, L., Forney, L.J., Noguez, A.M., Souza Saldivar, V., 2008. Diversity of aquatic prokaryotic communities in the Cuatro Cienegas basin. FEMS Microbiol. Ecol. 65, 50–60. <https://doi.org/10.1111/j.1574-6941.2008.00496.x>
2. Stumm, W., Morgan, J.J., 2012. Aquatic Chemistry: Chemical Equilibria and Rates in Natural Waters. Wiley.

11.2 Anexo 2: Material suplementario del capítulo 7.2

Overall spatiotemporal dynamics of greenhouse gases and oxygen in two subtropical reservoirs with contrasting trophic states

Teresa Aguirrezabala-Campano¹, Rodrigo Gonzalez-Valencia¹, Francisco J. Cervantes², and Frédéric Thalasso¹

¹ Department of Biotechnology and Bioengineering, Cinvestav, Avenida IPN 2508, Mexico City, San Pedro Zacatenco, 07360, Mexico.

² Laboratory for Research on Advanced Processes for Water Treatment, Engineering Institute, Campus Juriquilla, Universidad Nacional Autónoma de México, Blvd. Juriquilla 3001, Querétaro, 76230, Mexico

Supplementary Information

Table S1. Notations

Notation	Description	Units
C	Concentration of a given compound	mmol m ⁻³
δ	Depth section	m
F	Flux	mmol m ⁻² d ⁻¹
H	Henry's constant	mol L ⁻¹ atm ⁻¹
M	Mass of a given compound	mmol m ⁻²
r	Net rate	mmol m ⁻² d ⁻¹
Sc	Schmidt number	-
θ	Turnover time	d
Superscripts	Description	Units
*	Experimentally determined	-
GPP	Gross primary production	-
MG	Methanogenesis	-
MT	Methanotrophy	-
R	Respiration	-
Subscripts		
CH ₄	Methane	-
CO ₂	Carbon dioxide	-

DO or O ₂	Dissolved oxygen	-
x	Compound x	-

S1. Mass balance

In this work, we established a mass balance of CH₄, O₂, and CO₂, which consider the water column as a grey box containing a limited number of dominant biological processes; i.e. methanotrophy, methanogenesis, respiration and primary production. In this model, all parameters are expressed per unit of area of the lake, the black box is open to the exterior, any mass increase or entry is considered as positive, and steady state is assumed; i.e. no significant changes over time.

The CH₄ balance consists of three compartments; methanogenesis (MG), methanotrophy (MT), and emissions to/from the atmosphere (F), two of them being measured (MT and F), thus allowing the derivation of the third one (MG). It is worth noting that, on the contrary of MT and F which are limited to the water column and the lake surface, respectively, MG is not restricted to the water column and includes sediments.

MT is considered as net methanotrophy, thus being the net result of two possible antagonistic processes in the water column; i.e. methanogenesis and methanotrophy. Similarly, MG is considered as a buffer compartment as it includes mostly the methane produced in the sediments and transferred to the water column, but also any other biological or abiotic process unidentified as MT, including potential lateral transport from the surrounding ecosystem. The total CH₄ mass presents per unit of area of the water column ($M_{CH_4}^*$), can be determined from the measured dissolved CH₄ concentrations ($C_{CH_4}^*$), as follows;

$$M_{CH_4}^* = \sum_{i=1}^n C_{CH_4,i}^* \cdot \delta_i \quad (1)$$

where δ_i is the depth section of the water column corresponding to each measurement.

Assuming steady state, the CH₄ mass balance per unit of area is described by Eq. 2;

$$\frac{dM_{CH_4}^*}{dt} = 0 = r_{CH_4}^{MG} + r_{CH_4}^{*MT} + F_{CH_4}^* \quad (2)$$

Where $r_{CH_4}^{MG}$ is the methanogenic rate, $r_{CH_4}^{*MT}$ is the methanotrophic rate, determined during lab assays, and $F_{CH_4}^*$ is the measured CH₄ flux. The overall methanogenesis rate can be then determined from Eq. 2;

$$r_{CH_4}^{MG} = -(r_{CH_4}^{*MT} + F_{CH_4}^*) \quad (3)$$

In a similar way to CH₄, the O₂ mass balance includes three compartments; respiration (R), emissions to/from the atmosphere (F), and the gross primary production in the photic zone of the water column (GPP), R being measured and F estimated from the gradient between water and air concentration, thus allowing the derivation of the third one (GPP). It is worth noting that, in this case, GPP is considered as a buffer compartment as it includes mostly gross primary production but also any other unidentified process, including potential lateral transport from the surrounding ecosystem. The total O₂ mass presents per unit of area of the water column ($M_{O_2}^*$), and the mass balance between the three compartments can be determined by Eqs. 4 and 5;

$$M_{O_2}^* = \sum_{i=1}^n C_{O_2,i}^* \cdot \delta_i \quad (4)$$

$$\frac{dM_{O_2}^*}{dt} = 0 = r_{O_2}^{*R} + r_{O_2}^{GPP} + F_{O_2} \quad (5)$$

where $C_{O_2}^*$ is the DO concentration in the water column, and $r_{O_2}^{*R}$, $r_{O_2}^{GPP}$, and F_{O_2} are the respiration rate, the gross primary production rate, and the flux.

The CO₂ balance is more complex, and is considered here as a four compartments model, including methanogenesis (MG) which can result in production (acetoclastic pathway) or uptake (hydrogenotrophic pathway) of CO₂, respiration in the water column (R), gross primary production in the photic zone of the water column (GPP), and emission to/from the atmosphere (F). Two of these processes are experimentally determined (R and F), while GPP can be derived from the $R_{O_2}^{GPP}$ (see below), thus allowing to determine MG. Likewise CH₄ and O₂ balances, in this case the buffer compartment is MG, which includes mostly the CO₂ produced/consumed by methanogenesis, but also any other biological process, not identified as GPP or R, including potential lateral transport from the surrounding ecosystem or sediments heterotrophic/autotrophic activity. In this mass balance, the total CO₂ mass presents per unit of area of the water column ($M_{CO_2}^*$), and the mass balance between the three compartments can be determined by Eqs. 6 and 7;

$$M_{CO_2}^* = \sum_{i=1}^n C_{CO_2}^* \cdot \delta_i \quad (6)$$

$$\frac{dM_{CO_2}^*}{dt} = 0 = r_{CO_2}^{MG} + r_{CO_2}^{GPP} + r_{CO_2}^{*R} + F_{CO_2}^* \quad (7)$$

where $C_{CO_2}^*$ is the CO₂ concentration in the water column, and $r_{CO_2}^{MG}$, $r_{CO_2}^{GPP}$, and $r_{CO_2}^R$, are the methanogenic, the gross primary production, and the respiration rate, and $F_{CO_2}^*$ is the CO₂ flux. As previously mentioned, $r_{CO_2}^{GPP}$ is determined from $r_{O_2}^{GPP}$, according to Wetzel et al. (2000);

$$r_{CO_2}^{GPP} = r_{O_2}^{GPP} / 1.2 \quad (8)$$

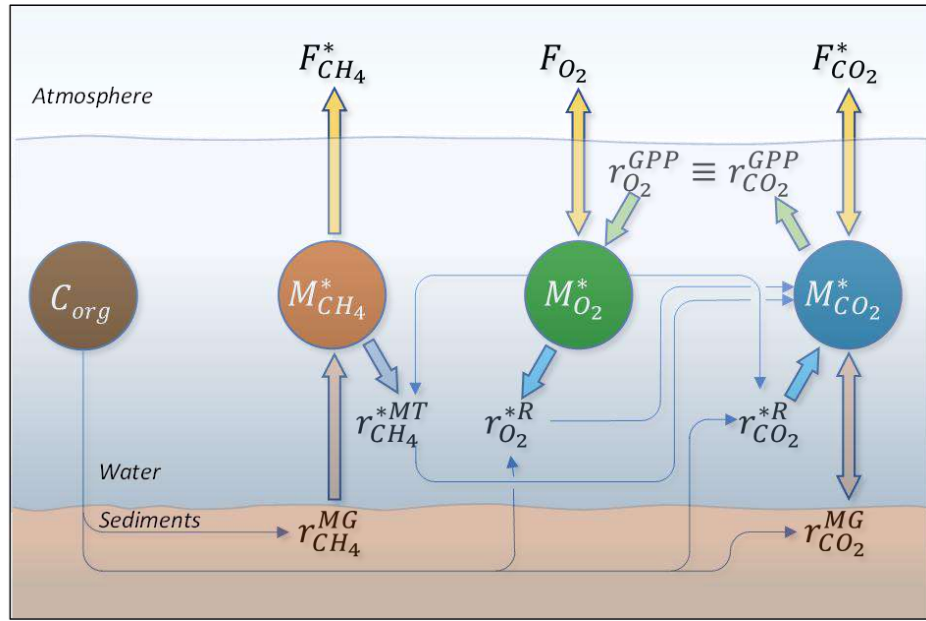


Figure S1. Mass balance conceptual diagram showing the interactions between dissolved gases through their different production and uptake processes.

Table S2. Comparative Table of surface and bottom C_{CH4} (mmol m⁻³), methanotrophic activity (mmol m⁻³ d⁻¹), diffusive and total CH₄ flux (mmol m⁻² d⁻¹), surface C_{CO2} (mmol m⁻³), CO₂ and DO flux (mmol m⁻² d⁻¹) from other subtropical (St) and tropical (T) reservoirs. Trophic states are indicated as oligotrophic (Oligo), mesotrophic (Meso), eutrophic (Eu), and hypereutrophic (Hyper). References: * This study, [1] Abril et al. (2005), [2] Abril et al. (2006), [3] Rodriguez and Casper (2018), [4] Chanudet et al. (2011), [5] Itoh et al. (2015), [6] Musenze et al. (2016), [7] Narvenkar et al. (2013), [8] Yang et al. (2019), [9] de Mello et al. (2018), [10] Zhang et al. (2019).

Site	Climate	Trophic state	Surface C _{CH4}	Bottom C _{CH4}	Methanotrophic activity	Ref.
LG	St	Eu-Hyper	12.29 ± 10.98	160.27 ± 55.92	7.34 ± 10.22	This work
LL	St	Oligo-Meso	1.24 ± 0.64	1.02 ± 0.13	0.43 ± 0.72	This work
Petit-Saut Dam	T	-	0.3 – 2.65	0.5 – 720	0.13 – 1600	1, 2
Itaparica Reservoir	T	Meso	5 ± 4	257 – 702	-	3
Laos Reservoirs	St	Oligo-Meso	0.01 – 2.1	16 – 400	-	4
Fei-Tsui Reservoir	St	Meso	0.036 ± 0.026	135.6 ± 120.1	85.08 ± 144.84	5
Australian Reservoirs	St	-	0.06 – 0.54	8 – 361	-	6
Indian Reservoirs	St	Oligo-Meso	0.0028 – 0.2629	0.05 – 140	-	7
Lianhe Reservoir	St	Oligo-Meso	-	-	-	8
Pampulha Reservoir	T	Hyper	-	-	-	9
Lake Taihu	St	Eu	-	-	-	10
Site	Climate	Trophic state	Diffusive CH ₄ flux	Total CH ₄ flux	CO ₂ flux	Ref.
LG	St	Eu-Hyper	22.22 ± 45.27	95.71 ± 180.22	107.7 ± 78.59	This work
LL	St	Oligo-Meso	2.06 ± 1.74	52.07 ± 139.04	-9.86 ± 13.71	This work
Petit-Saut Dam	T	-	0.70 ± 0.50	-	14 – 133	1, 2
Itaparica Reservoir	T	Meso	1.25 – 12.5	-	45.45 – 113.63	3
Laos Reservoirs	St	Oligo-Meso	0.04 – 11.9	-	-36 – 38	4
Fei-Tsui Reservoir	St	Meso	0 – 0.093	-	-	5
Australian Reservoirs	St	-	0.025 – 0.6	-	-	6
Indian Reservoirs	St	Oligo-Meso	-	-	-	7
Lianhe Reservoir	St	Oligo-Meso	0.002 – 0.007	-	-9.04 – 0.65	8
Pampulha Reservoir	T	Hyper	1.12 – 5.18	1.20 – 83.5	-	9
Lake Taihu	St	Eu	-	1.40 ± 0.54	37.67 – 49.09	10

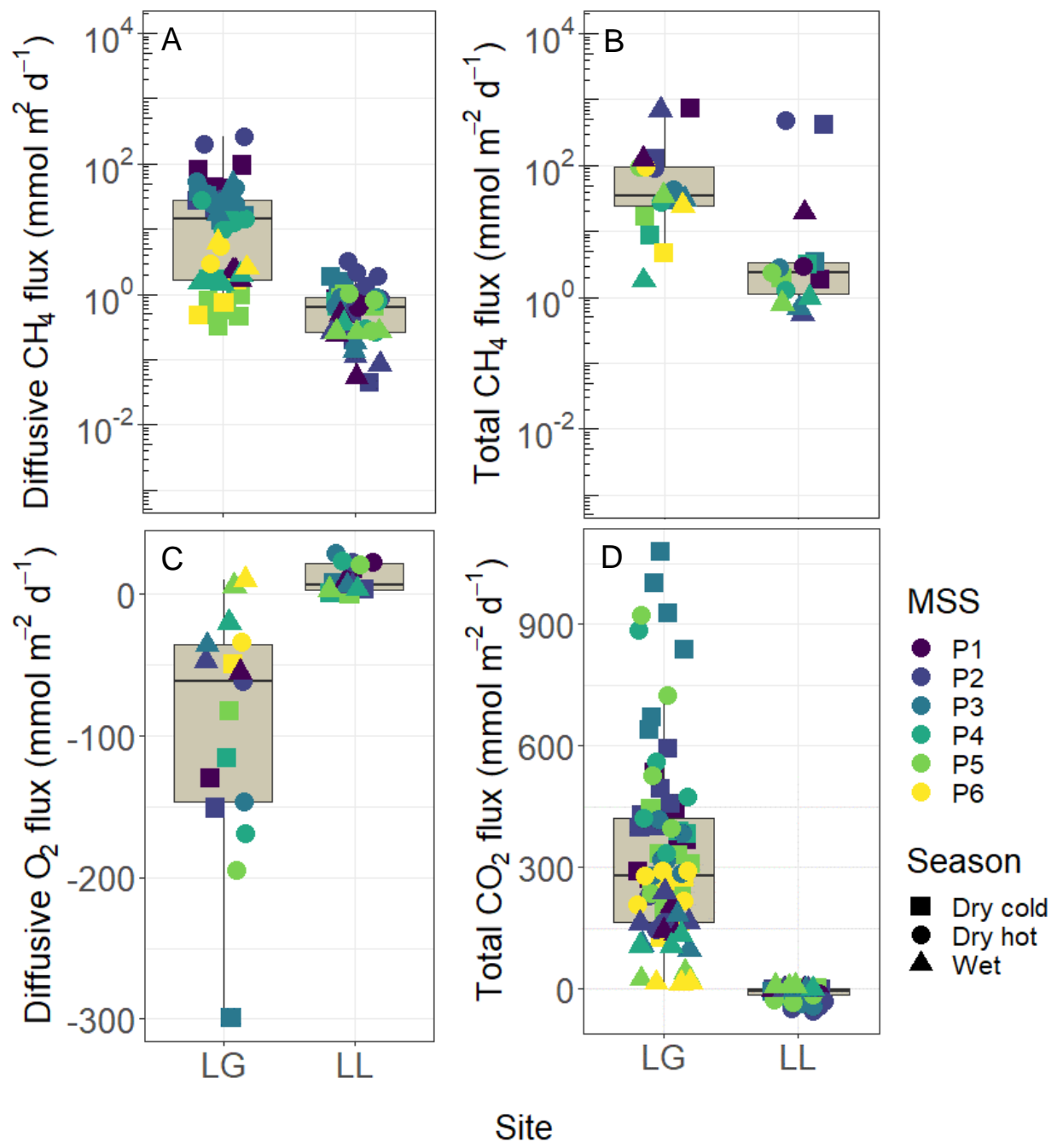


Figure S2. Diffusive and total CH_4 flux (A,B), diffusive O_2 flux (C), and total CO_2 flux (D) in LG and LL for each season and MSS. Please note the logarithmic scale in panels A and B.

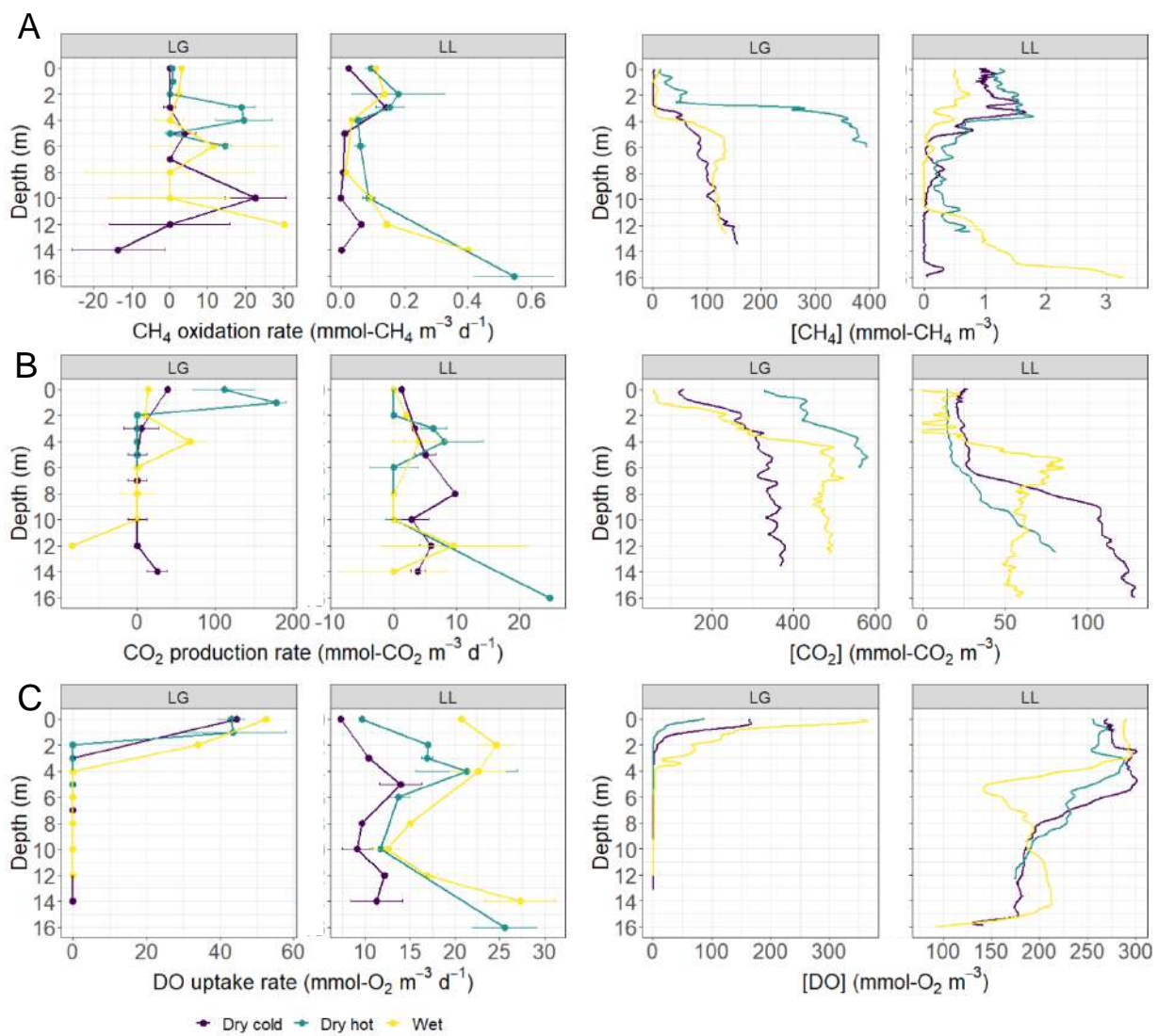


Figure S3. Net uptake rates (two left-hand panels) and dissolved gas concentration (two right-hand panels) of CH₄ (A), CO₂ (B), and DO (C).

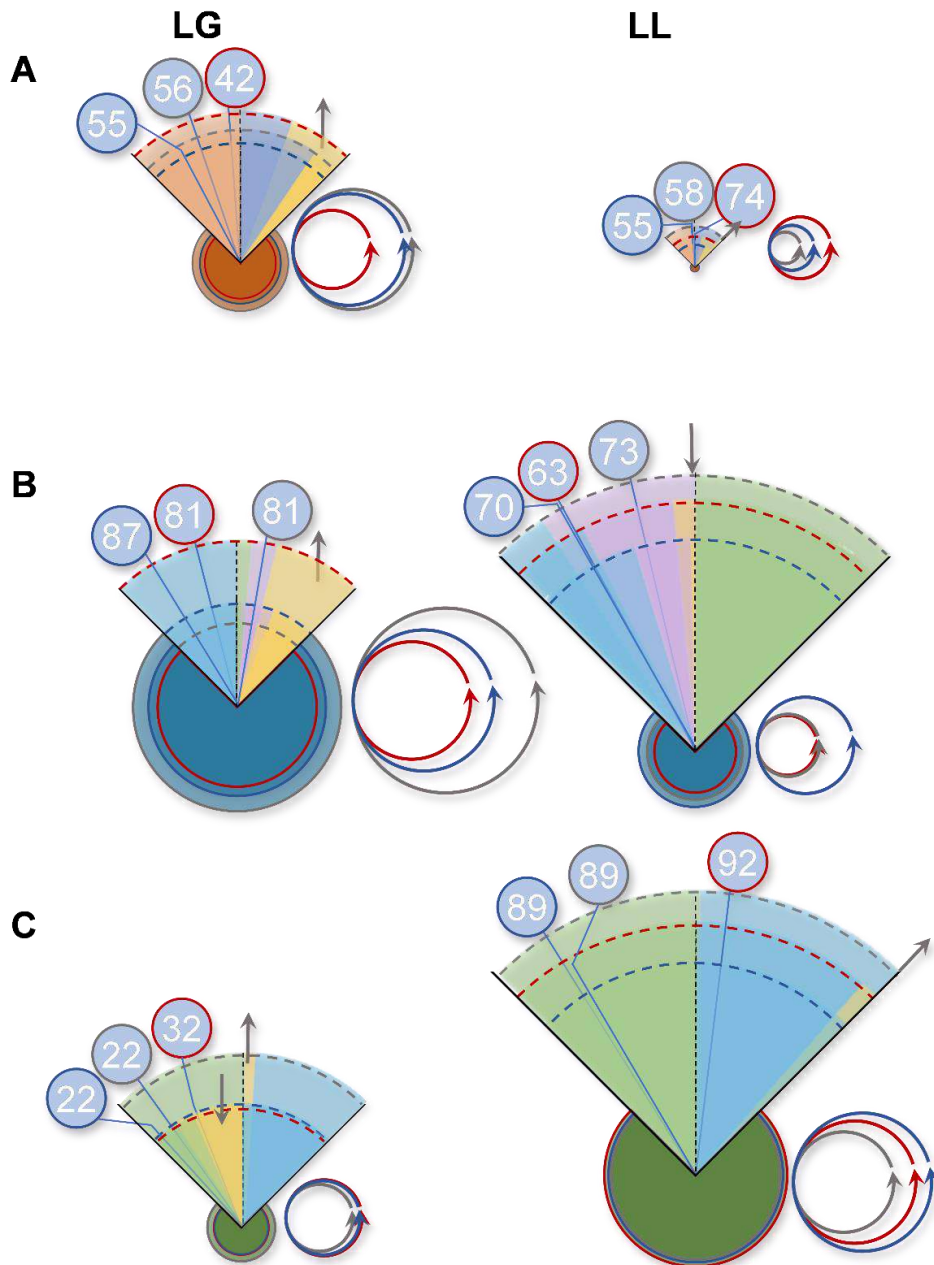


Figure S4. Graphical representation of the seasonal carbon mass balance components of (A) CH₄, (B) CO₂, and (C) O₂, in LG (left) and LL (right). Each quarter-pie chart, where areas are scaled to magnitude, represent the proportional share of each process; MG, methanogenesis; MT, methanotrophy; F, flux; R, respiration; GPP, gross primary production, for CH₄, CO₂ and O₂. Rates located on the left side are positive (input/production) and those on the right side are negative (output/uptake). Inferior solid-color circles represent the scaled total mass of the compound (M_x ; mmole m⁻²) and the circle arrows represent the scaled turnover time (θ_x). The superior circle represents the homogeneity factor of dissolved gases distribution (h) and the anisotropic factor (ω). Each season is identified by a color on the processes, mass, turnover, and h circles as blue (dry cold), red (dry hot), and grey (wet).

11.3 Anexo 3: Artículo publicado en Science of the Total Environment